

Cover Page



Universiteit Leiden



The handle <http://hdl.handle.net/1887/73614> holds various files of this Leiden University dissertation.

Author: Macedo Coelho Lima, L.

Title: Superstructures of lipids and graphene

Issue Date: 2019-05-23

Superstructures of lipids and graphene

Proefschrift

ter verkrijging van

de graad van Doctor aan de Universiteit Leiden,

op gezag van Rector Magnificus prof. mr. C. J. J. M. Stolker

volgens het besluit van het College voor Promoties

te verdedigen op 23 mei 2019

klokke 11:15 uur

door

Lia Macedo Coelho Lima

Geboren op 2 juni 1987 te Manchester, Verenigd Koninkrijk

Promotiecommissie

Promotor

Prof. dr. Alexander Kros

Copromotor

Dr. Grégory F. Schneider

Overige Leden

Prof. dr. H. S. Overkleeft, Faculty of Science, LIC (voorzitter)

Prof. dr. J. Brouwer, Faculty of Science, LIC (secretaris)

Dr. H. J. Risselada, Faculty of Science, LIC

Prof. dr. J. M van Ruitenbeek, Faculty of Science, LION

Prof. dr. T. Charitat, Institute Charles Sadron, Strasbourg, France

Dr. A. Pénicaud, Centre de Recherches Paul Pascal, Bordeaux, France

Doctor thesis, Leiden University, 2019

Cover design: José Pedro Guimarães

Printed by: Ridderprint BV | www.ridderprint.nl

ISBN: 978-94-6375-419-4

To my parents and sister,
for making me believe.

To Amedeo Bellunato,
we made it!

Table of contents

CHAPTER 1	7
Introduction	
CHAPTER 2	37
Graphene-stabilized lipid monolayer heterostructures: a novel biomembrane superstructure	
CHAPTER 3	55
Encapsulation of graphene in the hydrophobic core of a lipid bilayer	
CHAPTER 4	67
Effect of temperature on the structure of lipids in the presence of graphene	
CHAPTER 5	83
Assembly and structural characterization of lipids on graphite and on graphene	
CHAPTER 6	99
Lateral non-covalent clamping of graphene at the edges using a lipid scaffold	
CHAPTER 7	115
Conclusions, Challenges and Outlook	

Appendix I	121
Supporting Information to Chapter 2	
Appendix II	127
Supporting Information to Chapter 3	
Appendix III	133
Supporting Information to Chapter 4	
Appendix IV	137
Supporting Information to Chapter 5	
Appendix V	145
Supporting Information to Chapter 6	
Summary	151
Samenvatting	155
Curriculum Vitae	159
List of publications	161

CHAPTER 1

Introduction

1.1 Interaction between lipids and graphene

The focus of this thesis is to explore the capabilities of small amphiphilic molecules, such as lipids, to form stable assemblies on top and below a macroscopic sheet of graphene via non-covalent interactions. The first hypothesis tested during this work was that a sheet of graphene can reside, in a stable manner, in the hydrophobic core of a lipid bilayer, the main constituent of biological cell membranes.¹ Non-covalent functionalization of graphene with lipids has the advantage of not altering the intrinsic electrical properties of graphene.² Also, non-covalent interactions, as opposed to covalent modifications of the graphene basal plane, preserve the aromatic sp^2 conjugation, and do not disturb to a large extent the electronic mobility of charge carriers in graphene. Typical short range interactions involved in the functionalization of graphene include π - π stacking, hydrophobic, electrostatic and van der Waals interactions.³⁻⁴

Graphene is a two dimensional (2D) allotrope of carbon with sp^2 hybridized carbon atoms arranged in a honeycomb lattice.⁵ The exceptional electron mobility,² mechanical flexibility,⁶ and large surface/volume ratio⁷ promotes graphene as an excellent material for sensing applications, particularly through the functionalization of its surface with specific molecules. In fact, pristine graphene is relatively inert chemically, and unselective towards the binding of particular molecules. A lipid layer on the surface of graphene however can represent a sensitizing layer susceptible to integrate lipid-specific biomolecules such as olfactory proteins, receptor proteins, pore forming proteins, to name a few, allowing to electrically probe – using graphene – the activity of these proteins. Additionally, graphene can be used as a sensor to study and characterize the process of assembly of lipids onto the graphene surface, or a change in the lipid conformation.⁸⁻¹⁰ Therefore, it is vital to understand the interaction between lipids and graphene. Although a lipid coated graphene sheet resembles at first sight a simple system, several parameters influence the interactions between lipids and graphene which make it a highly complex system to study. In fact, the properties of graphene are strongly influenced by the preparation method used,¹¹ the level of contamination,¹² the transfer method¹³ and the nature of the substrate underneath.¹⁴ Also, the size and composition of the graphene sheet play a large role in determining how lipids interact with the basal plane of the 2D materials.

Furthermore, the chemical structure of the lipids and the assembly method also affect how the lipids interact with graphene.¹⁰

Recently, a growing number of publications reported on the interactions between lipids and graphene.^{8-10, 15-19} However, at the start of this PhD work, little was known about the most basic structural features of lipid-graphene assemblies, principally the orientation and conformation of the lipid layer(s). Particularly, the most widely used technique to characterize lipids – namely infrared (IR) spectroscopy – had never been applied to monitor lipid-graphene interactions.²⁰ Additionally, very few papers discuss the interaction of pristine graphene with lipids. Instead graphene oxide (GO) and reduced graphene oxide (rGO) were largely used as model graphene materials, particularly because of the ease of producing enough quantities of those. In this section of the thesis, we discuss the interactions of GO and rGO with lipids, the use of the field effect in graphene to study lipid-graphene interactions, molecular dynamic simulations, and discuss the studies involving lipids and pristine graphene.

1.1.1 Graphene oxide

GO is obtained by oxidizing graphite in the presence of sulfuric acid (H_2SO_4) and potassium permanganate (KMnO_4), i.e. the so-called Hummers method.²¹ During the chemical reaction, the aromatic sp^2 carbon in graphite are converted into sp^3 carbon atoms covalently bonded to oxygen functional groups generating structural defects on the basal plane and edges of graphene.²²⁻²³ The large fraction of oxidized carbon atoms (i.e., C-OH , $-\text{COOH}$, C-O-C and C=O) yields graphite oxide flakes highly soluble in water. Furthermore, the functional groups facilitate covalent conjugation of biomolecules onto the GO surface.²⁴

GO is negatively charged due to the presence of carboxylic acid groups favoring the adsorption of positively charged lipids. Hence, using the Langmuir-Blodgett technique²⁵ (explained in detail in section 1.1.5), the oxidized edge of GO dispersed in the aqueous sub-phase underneath a lipid monolayer, interacts in a vertical orientation with the lipid monolayer. The presence of negative charges on GO therefore allows the favorable interaction of GO with positively charged lipids, at least compared to neutral or negatively charged lipids (Figure 1.1a).²⁶ However, if instead of lipids, cationic surfactants interact with GO at the air-liquid interface, GO sheets will contact in a horizontal manner²⁷ with the basal plane of GO facing

the head groups of the cationic surfactant (Figure 1.1b). Therefore, several studies claim that positively charged lipids/surfactants have a higher affinity with GO compared to negatively charged lipids/surfactants, due to attractive electrostatic interactions.^{26, 28-29}

Alternatively, using vesicle fusion, GO can be encapsulated between lipid bilayers, sandwiched between the head groups of the lipids (Figure 1.1c) benefiting from the electrostatic attraction between the positive charge on the lipid head groups and the negative charge on GO.²⁸ GO sheets have been shown to induce the rupture of the pre-adsorbed liposomes promoting the assembly of stable lipid membranes.

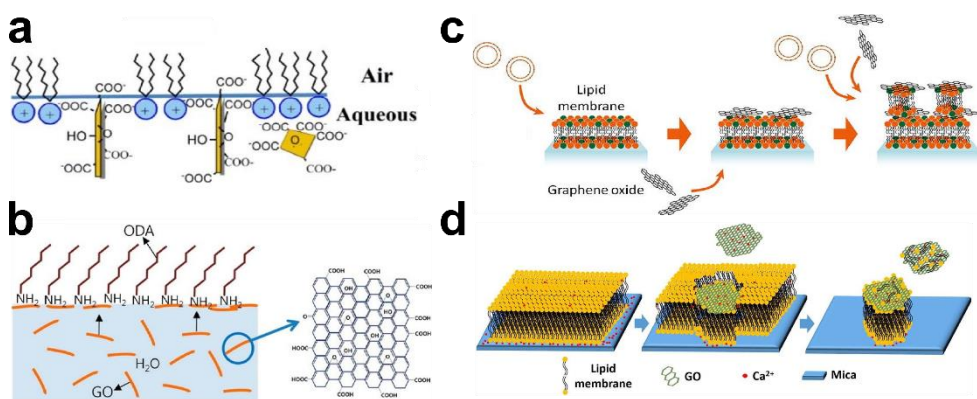


Figure 1.1. Illustrations of the interactions between graphene oxide (GO) and lipids. a) GO interacting in a vertical orientation with the cationic dioctadecyldimethylammonium bromide (DODAB) lipid at an air-liquid interface in a Langmuir trough.²⁶ b) Surface of a GO flake interacting with head groups of the cationic octadecylamine (ODA) surfactant in a Langmuir trough.²⁷ c) Rupture of lipid vesicles on a SiO₂ substrate and the formation of lipid-graphene multilayer stacks.²⁸ d) Lipid bilayer being desorbed from a mica substrate through the interaction of a GO sheet with a zwitterionic lipid bilayer in the presence of Ca²⁺ ions.³²

Studies involving quartz crystal microbalance with dissipation monitoring (QCM-D)³⁰ (explained in detail in section 1.1.5) have revealed that large GO sheets placed above supported lipid bilayers (SLBs) induce the rupture of small pre-adsorbed liposomes and the subsequent assembly of SLBs.³¹ Contrarily, a different study has revealed that zwitterionic SLBs detach from mica substrates in the

presence of GO sheets where divalent ions are used to previously stabilize the SLBs in solution (Figure 1.1d).³² Although GO is suitable to study lipid-graphene interactions, GO is by far not chemically identical to graphene. GO is an oxidized analog of graphene, and upon reduction (rGO) resembles more carbon black than graphite/graphene.³³ Studies have shown that zwitterionic liposomes do not rupture on GO and only partially on reduced graphene oxide (rGO). In contrast, full rupture is observed on pristine graphene (Figure 1.2b).³⁴ It is therefore crucial to consider the chemical nature of graphene, GO, and rGO (Figure 1.2a) to understand and/or predict how would lipids interact with the basal plane of these materials.

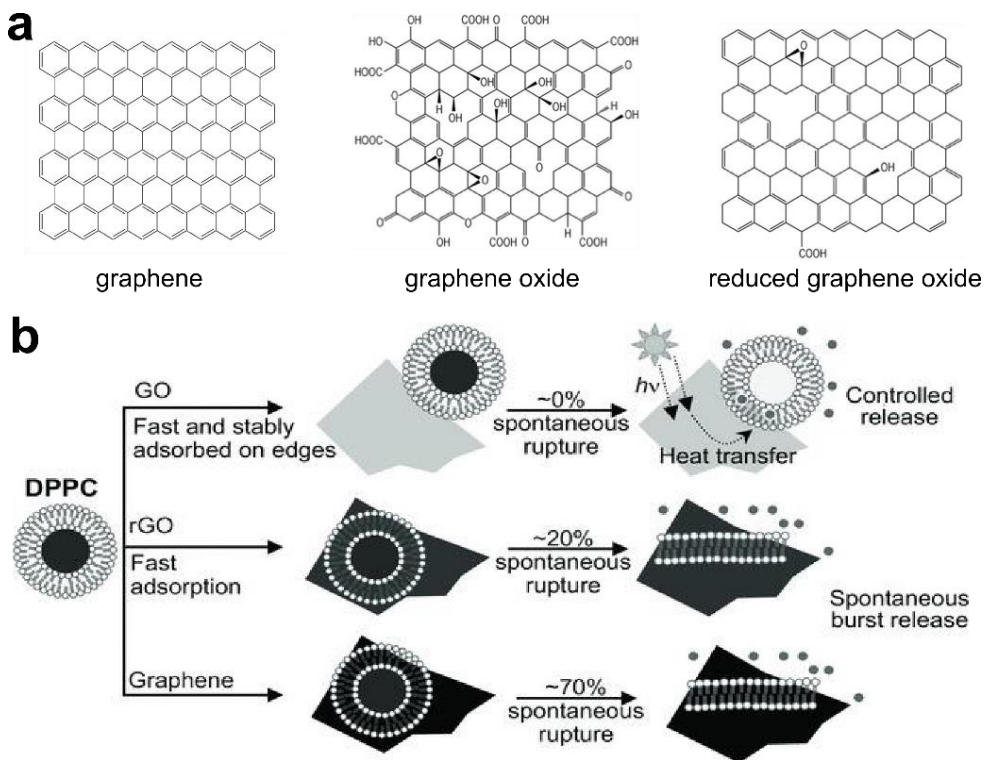


Figure 1.2. Differences in the chemical composition between graphene, graphene oxide (GO) and reduced graphene oxide (rGO) and their interactions with liposomes. a) Chemical structures of graphene, GO and rGO.⁴² b) Schematic illustration of 1,2-dipalmitoyl-*sn*-glycero-3-phosphocholine (DPPC) liposomes interacting with GO (no liposomes ruptured), with rGO (~20% liposomes ruptured), and with graphene (~70% liposomes ruptured).³⁴

1.1.2 Reduced graphene oxide

Oxygenated groups in GO can be reduced to partially recover the conjugated aromatic structure in a highly defective graphene, so called reduced graphene oxide (rGO).³⁵⁻³⁶ rGO can be obtained by treating GO with strong chemical reducing agents such as hydrazine,³⁷ other non-toxic chemicals such ascorbic acid,³⁸ thermally,³⁹ electrochemically⁴⁰ or by photo-irradiation.⁴¹ rGO has better properties compared to GO (i.e., rGO resembles more graphene compare to GO), such as increased electrical conductivity and improved carbon to oxygen ratio. Depending on the reduction method used, the properties of the rGO sheets, such as the chemical structure, thickness and electrical performance can be tuned.^{35, 37} However, rGO does not have the same properties as pristine graphene due to the large variety of basal plane chemical compositions present in rGO (particularly the presence of a large range of grain boundaries and defects, i.e. non sp^2 carbons). In addition, rGO is often prepared as a dispersion, and the obtained sheets are small (~500x500 nm) which makes the fabrication of devices cumbersome and difficult. After reduction, the initial oxygenated sp^2/sp^3 defects are converted into non-aromatic structures. This yields a poorly defined conjugation system which is by far lower than in pristine graphene.

Lipids interact differently with distinct forms of rGO, depending on the degree of reduction of GO and on the number of reduced graphene oxide layers constituting the rGO sheets. For multilayers (> 5 layers) rGO sheets, the lipids self-assemble as lipid bilayers whereas monolayer-few layers (< 5 layers) rGO sheets lead to intact vesicle structures on the surface of rGO.⁴³ In contrast, other studies have shown that lipids form a monolayer structure on rGO with the hydrocarbon chains facing the rGO sheets.⁴⁴⁻⁴⁵ Alternatively, a separate study reported the encapsulation of rGO in a lipid bilayer, with minimal perturbation of the electrical properties of rGO upon encapsulation.⁴⁶

1.1.3 Chemical vapor deposition (CVD) of graphene

Pristine graphene can be obtained by different methods such as chemical and mechanical exfoliation of graphite,⁴⁷⁻⁴⁸ epitaxial growth on SiC surfaces⁴⁹ or by CVD.⁵⁰ The most common route to produce large graphene sheets is by CVD as it yields high quality graphene samples in comparison to rGO or GO. Here, it is important to note that many parameters such as the composition of the seed gas,

temperature, cooling time and the substrate catalyst, results in graphene of different crystallinity, grain boundaries, homogeneities and defects.⁵⁰⁻⁵¹

Typically, hydrocarbon gases such as methane or ethylene are used for the CVD process where the gases are dehydrogenated at very high temperatures ($> 800^{\circ}\text{C}$) prior to graphene growth.⁵² This procedure typically consists of two steps. The chemisorption/incorporation of the decomposed hydrocarbons on the catalyst and thereafter the segregation of carbon on the surface during the cooling step to form a graphene sheet. Metal substrates are used to catalytically enforce the growth process. The catalyst substrate plays an important role during the nucleation and the growth of graphene due to the fact that different substrate catalyst have different carbon solubility and surface-carbon affinities.⁵³ The solubility of carbon on metals such as nickel⁵⁴ or ruthenium⁵⁰ is very high which typically results in carbon to dissolve and then nucleate and grow as a graphene layer on the surface of the catalyst.⁵¹ Copper, however, shows a very low solubility of carbon which enables the continuous growth of graphene on its surface. During the CVD process involving a copper surface, the carbon atoms instead of diffusing and segregating on the metal surface, adsorb and successively nucleate graphene growth via expanding local graphene-domains.⁵⁵ Graphene is deposited uniformly over the copper surface, reaching a single monolayer of graphene. To date, copper substrates are by far the most used catalysts to grow graphene.⁵⁶ The different growing procedures available to obtain single layer graphene lead to variations in graphene crystallinity which in turn affects the electrical properties of the obtained graphene. Although graphene can also be grown on non-metallic substrates such as Si/SiO₂, catalysts are important because they allow to significantly reduce the temperature needed for the growth of graphene.⁵⁰ CVD graphene on copper was used in all the projects of this PhD work.

1.1.4 Graphene field effect transistors

In its simplest architecture, a field effect transistor (FET), is generally composed of a conductive channel connected to a pair of electrodes, namely source and drain electrodes across which an electrical potential is applied (V_{sd}). In such device, the conductivity is modulated by an electric field, commonly referred to as a gate potential (V_g). This gate potential is applied on the conductive channel through

either a solid state electrode via an insulating material (Figure 1.3a), a gate electrode, or through an electrolytic solution (Figure 1.3b).⁵⁷

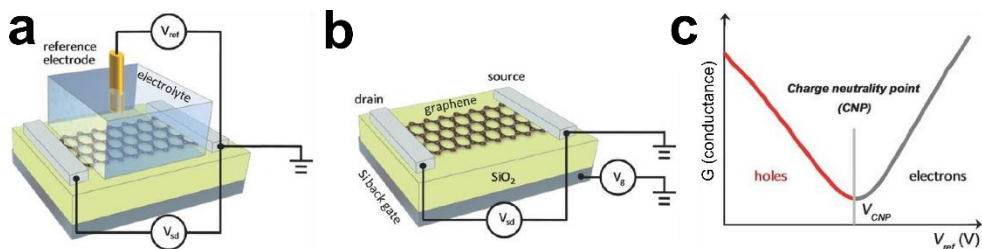


Figure 1.3. Graphene field effect transistors (GFET). a) Schematic of a liquid-gated GFET with a gate potential (V_{ref}) applied through an electrolytic solution. b) Schematic of a back-gated GFET with a gate potential applied (V_g) to SiO_2 substrate. c) Current-voltage curve of graphene with different charge carriers (holes and electrons) with a minimum at the charge neutrality point of graphene.³

Due to the linear dispersion of its electron band structure, susceptible to external gate electrical fields, graphene can be used as the conductive channel in a field effect transistor architecture. In fact, the conductivity of graphene can be modulated by a gate potential, which perturbs the density of charge carriers in its band structure, resulting in the so-called Dirac cone, with a minimum of conductance at the Dirac point (Figure 1.3c, at the charge neutrality point – CNP – the amount of electrons and holes carriers is equivalent). Notably, due to its 2D nature, the electronic band structure of graphene is extremely sensitive to external perturbations, such as molecular interactions which introduce perturbations in the band structure of graphene, and a variation of the change of its conductivity. Particularly, any small variation in the chemical composition of the environment in the vicinity of graphene primarily (dipole fluctuations) induces a change in charge carrier.^{3, 7} For instance, it has been reported that using an electrolyte-gated graphene field effect transistor (GFET), charged lipid bilayers modulate the electronic properties of graphene, yielding different responses for cationic, anionic and zwitterionic lipids. (Figure 1.4a).^{8, 10}

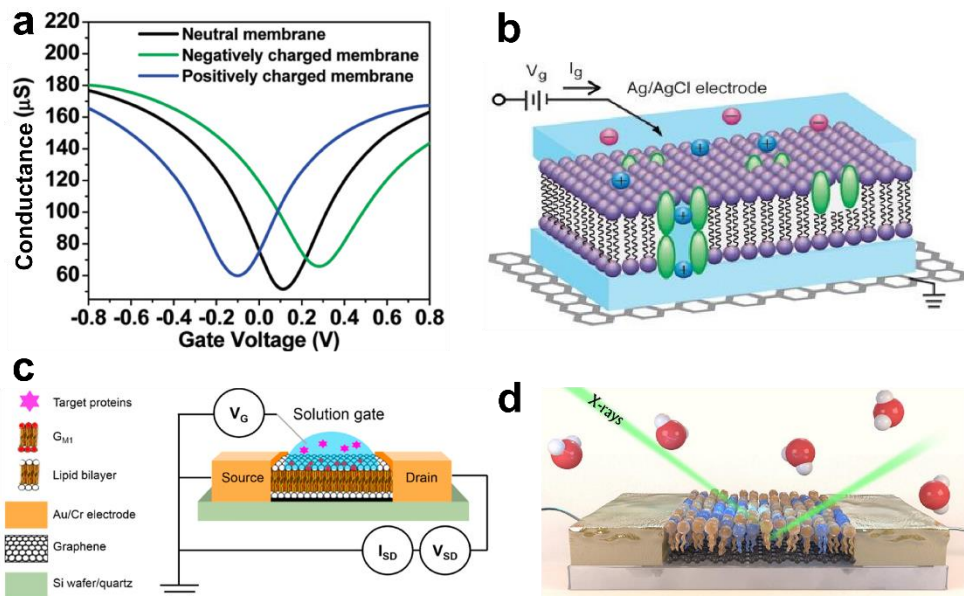


Figure 1.4. GFETs functionalized with lipids. a) Electrical properties of a GFET upon functionalization of the graphene conducting channel with neutral, negatively, positively charged lipids.¹⁰ b) Lipid bilayer membrane with a protein pore (gramicidin A) on top of a GFET used to measure the activity of an array of ion channels.⁸ c) GFET coated with a lipid bilayer for the detection of cholera toxin B.⁵⁸ d) X-ray reflectivity measurements of a lipid monolayer on a solution-gated GFET used to determine in real time the spreading and rupture of lipid vesicles (by vesicle fusion) forming a lipid monolayer.¹⁹

To fabricate a GFET, graphene is grown on a metal catalyst such as copper, and is transferred onto a Si/SiO₂ substrate. The transfer method as well as the choice of the substrate are equally important during the fabrication of GFETs. A suboptimal transfer can degrade the quality of the graphene by leaving contaminations, inducing stress or cracks. The substrate on which graphene is transferred also affects the electrical properties of graphene.⁵⁹ In Chapter 2, a lipid monolayer was proposed as a substitute to the usual hard inorganic Si/SiO₂ support for graphene. Remarkably, the lipid monolayer ameliorated the electrical properties of graphene compared to graphene on a Si/SiO₂ substrate. In addition, in Chapter 6 a clean transfer method was developed where amphiphilic lipids were used as a scaffold that clamps graphene at the edges yielding a controllable manipulation of graphene and a clean transfer to arbitrary substrates.

Graphene has been demonstrated to be sufficiently sensitive to detect changes in the properties of a lipid membrane. Particularly, the modification of a lipid membrane by a gram-negative bacteria¹⁰ or by the incorporation of individual ion channel proteins⁸ yielded changes in the electrical properties of graphene, namely fluctuations of the conductance of the conductive graphene channel (Figure 1.4b). Similarly, protein interactions with a lipid bilayer (Figure 1.4c) could also be detected by a solution-gated GFET.^{8,58}

A GFET is able to detect electrically the dynamics of vesicle rupturing on the graphene surface, in situ, and in real time (Figure 1.4d).¹⁹ While some studies claim the formation of a lipid monolayer^{16, 18-19, 60-61} (upon vesicle rupture) others report the formation of a lipid bilayer.^{8, 10, 15, 58} Typically, lipids such as 1-palmitoyl-2-oleoyl-*sn*-glycero-3-phosphocholine (POPC) or 1,2-diphytanoyl-*sn*-glycero-3-phosphocholine (DPhPC) self-assemble on graphene as a lipid bilayer while, lipids such as 1,2-dioleoyl-*sn*-glycero-3-phosphocholine (DOPC) and 1,2-dioleoyl-3-trimethylammonium-propane (DOTAP) rearrange as a monolayer on graphene. Thus, since graphene of different quality crystallinities is expected to yield a range of different interactions with lipids, in Chapter 5, the interactions of several distinct lipids with different graphene materials were systematically investigated to identify the most important parameters regulating lipid-graphene interactions.

1.1.5 Assembly of lipids on pristine graphene

Vesicle fusion (VF)

Lipids can be deposited on graphene surfaces using different experimental techniques. The most common methods used are the vesicle fusion (VF, Figure 1.5a), lipid dip-pen nanolithography (L-DPN, Figure 1.5c) and the Langmuir-Blodgett technique (LB, Figure 1.5b). In the previous section, GFET functionalized with lipids were prepared by lipid self-assembly on graphene using the VF method. The VF is the most convenient approach to form SLBs, as it does not require advanced setups such as a LB trough or an atomic force microscopy (AFM) apparatus, but only a dispersion of liposomes. This method is based on the spontaneous adsorption, spreading and rupture of vesicles on a solid support. The drawback of the VF method is that there is no precise control over the formation and assembly of the lipids on the surface of a substrate, at least if compared to the LB transfer method where any steps of the transfer method can be precisely

controlled: surface pressure of the lipids, transfer kinetics, calculation of the amount of lipids transferred, to name a few.⁶²⁻⁶³

Using the VF method, it was reported that the edges of graphene pattern were used as a geometrical barrier to study the lateral mobility of fluorescent SLBs. The SLBs were assembled on glass which was surrounded by graphene patterns (made by an electron ion beam), that restricted the spreading of the lipids (Figure 1.6a).¹⁷ Separately, in another study lipids self-assembled differently on graphene supported by a hydrophilic or hydrophobic substrate,⁶⁴ suggesting that graphene is transparent to the wetting properties of the substrates, i.e. the so-called wetting transparency of graphene.^{14, 65}

Lipid dip-pen nanolithography (L-DPN)

L-DPN uses the tip of a cantilever in an AFM setup, where the tip is coated with lipids which are directly transferred to arbitrary substrates such as SiO₂ or graphene to form micro-sized lipid patterns (Figure 1.5c).⁶⁶ This technique has emerged as a suitable platform for the rapid construction of precise patches of lipids on graphene. The patches are inked on graphene from a chloroform solution containing the lipids and these patches can be located with nanoscale precision using the imaging mode of the AFM instrument.⁹

Remarkably, it has been shown that as opposed to lipids on SiO₂ substrates, lipids on graphene spread rapidly over the graphene surface and form inverted lipid bilayers (as determined from the AFM height profiles, Figure 1.6b). Also, another study investigated lipids that were deposited using L-DPN on confined arrays of graphene patterned on Si/SiO₂ substrates. The graphene prevented and simultaneously confined the spreading of lipids to the hydrophilic SiO₂ substrate on the surroundings (Figure 1.5d).¹⁸

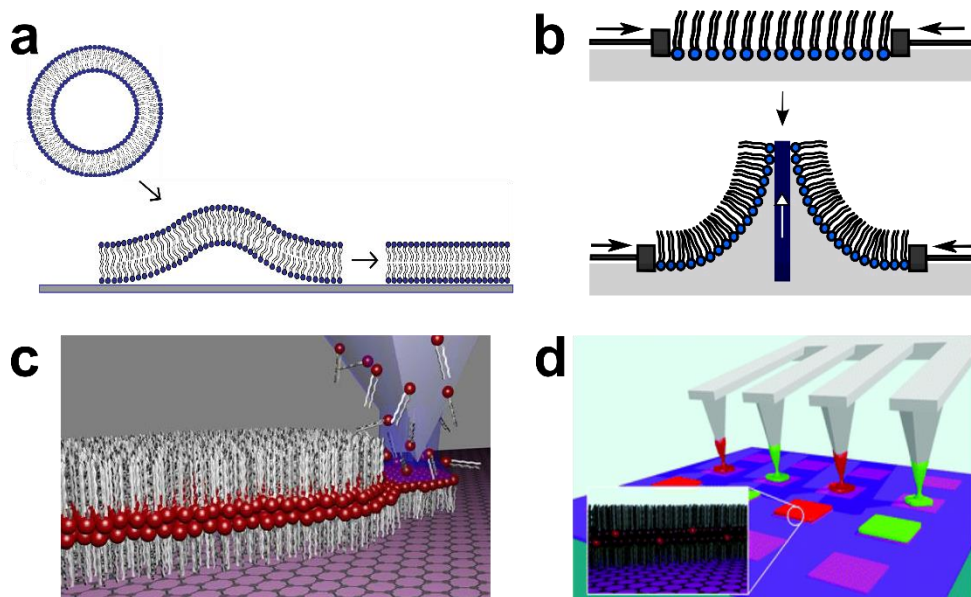


Figure 1.5. Vesicle fusion (VF), Langmuir-Blodgett (LB) and lipid dip-pen nanolithography (L-DPN) techniques used to form and study lipid-graphene interactions. a) Fusion of liposomes on a hydrophilic surface and formation of a supported lipid bilayer. b) Illustration of the LB technique where lipids are deposited at the air-liquid interface of a Langmuir trough, compressed using two lateral barriers (top) and transferred to a substrate by withdrawing the lipid monolayer from the surface of the trough (bottom). c) Artistic rendering illustrating the L-DPN method where an AFM tip coated with lipid molecules (from chloroform solution containing lipids) is used to transfer the lipids on graphene.⁹ d) Schematic design of L-DPN tips coated with lipid mixtures which were deposited on graphene squares and formed inverted lipid bilayers.¹⁸

Langmuir-Blodgett (LB) technique

Surprisingly, only few papers describe the use of the LB method to assemble a well-defined lipid structure on graphene. Most studies focus on the production and transfer of large sheets of GO or rGO using the LB method,⁶⁷⁻⁷⁰ or study the interactions between GO that is placed in the Langmuir trough sub-phase with the lipids at the interface.²⁶⁻²⁷ In a typical experiment, the LB technique is used to compress lipids at the air-water interface (hydrophilic head groups facing the water) using a Langmuir trough with two lateral barriers continuously compressing the lipids to a desired surface pressure. Next, the lipids are transferred at a constant surface pressure (pressure hold at a fix value using a feed-back loop on

the LB barriers) to a substrate (Figure 1.5b).²⁵ In Chapters 2 and 3 lipid monolayers were transferred vertically by the LB method onto hydrophilic Si/SiO₂ substrates and graphene was deposited on top of the lipid monolayer by bringing into contact with each other. The assemblies, lipids on top or below graphene were analyzed in detail by IR spectroscopy, ellipsometry, AFM and Raman spectroscopy.

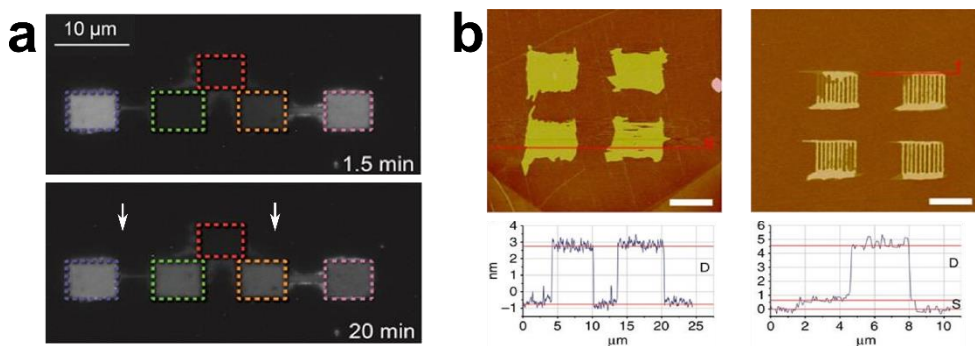


Figure 1.6. Assembly of lipid molecules on the surface of graphene. a) Fluorescence images of fluorescent SLBs (bright) deposited by vesicle fusion on glass substrates patterned with graphene (black). The SLBs spread over time through the glass channels into new reservoirs (see white arrows) that were patterned with graphene.¹⁷ b) Atomic force microscopy (AFM) images of lipid dip-pen nanolithography (L-DPN) patches of phospholipids on graphene (left panel) and on SiO₂ substrate (right panel) and the corresponding height profiles below. The lipids spread more uniformly and faster on graphene than on Si/SiO₂ substrate.⁹

Molecular dynamics (MD) simulation studies

In contrast with experimental studies, MD simulation studies allow a wide variety of conditions and situations to be tested due to the large amount of parameters that can be tested with computational approaches. With MD simulations, the interaction between lipids and graphene can be investigated at a molecular level, varying the shape of graphene, numbers of layers, sizes and oxidation degrees, all with a range of distinct lipids.

MD simulations reported that small (< 7 nm) graphene sheets can easily penetrate and be hosted within the hydrophobic core of a lipid bilayer whereas large graphene sheets (> 8 nm) tend to destabilize the membrane.⁷⁵⁻⁷⁹ In fact, large graphene sheets induce a perturbation in the lipid membrane by adsorbing on top

of the bilayer surface⁷⁶ or forming vesicles due to the contrast in size between the large graphene sheet and the small lipid molecules (Figure 1.7d).⁷⁵ For small graphene sheets (which encapsulate in the hydrophobic core of a lipid bilayer), the insertion is preferably initiated from an edge of the graphene sheet, perpendicular to the membrane.⁸⁰⁻⁸¹ Some studies demonstrate that prior to inserting into the hydrophobic core of the lipid bilayer, first a small fraction of lipids adsorb on the graphene basal plane forming a micelle in which graphene is encapsulated into. The lipid micelle then interacts with the head groups of the lipid bilayer inducing fusion where graphene enters the hydrophobic core of the lipid membrane (Figure 1.7a).⁷⁷ Additionally, the MD simulations revealed that graphene with different shapes (i.e., circle, square) and with few graphene layers can also enter and be hosted in the hydrophobic core of the lipid bilayer.^{75, 77}

Instead of sandwiching graphene in a lipid bilayer, several lipid molecules can also be extracted from the lipid membrane when interacting with graphene (Figure 1.7b). If graphene is placed perpendicularly to the lipid membrane, a large number of lipid molecules from the bilayer are withdrawn by being dragged (i.e. lipid diffusion) on both sides of the graphene surface, due to the strong van der Waals and hydrophobic interactions between the graphene and the lipids. Subsequently, the lipid membrane is then deformed, which causes a loss of its integrity.⁸²⁻⁸³ Alternately, if curved graphene sheets are inserted perpendicularly to the lipid bilayer, mainly the concave side (which is exposed to a higher amount of water) induces the extraction of the lipid molecules from the lipid membrane. This process is probably caused by the complete wetting of graphene through the lipids in water.⁸³⁻⁸⁴

Interestingly, also GO sheets tend to induce the extraction of lipid molecules from the lipid membranes.⁸² In fact, contradictory with the previous studies, different results concluded that only GO (and not pristine graphene) tends to perturb the lipid membrane by extracting several lipid molecules due to the interaction between the oxygen groups on GO surface and the hydrophilic lipid head groups,^{79, 85} or instead by lying perpendicular across the lipid bilayer.⁷⁷⁻⁷⁸ In comparison, small pristine graphene sheets can easily enter the lipid membrane without disturbing its integrity.

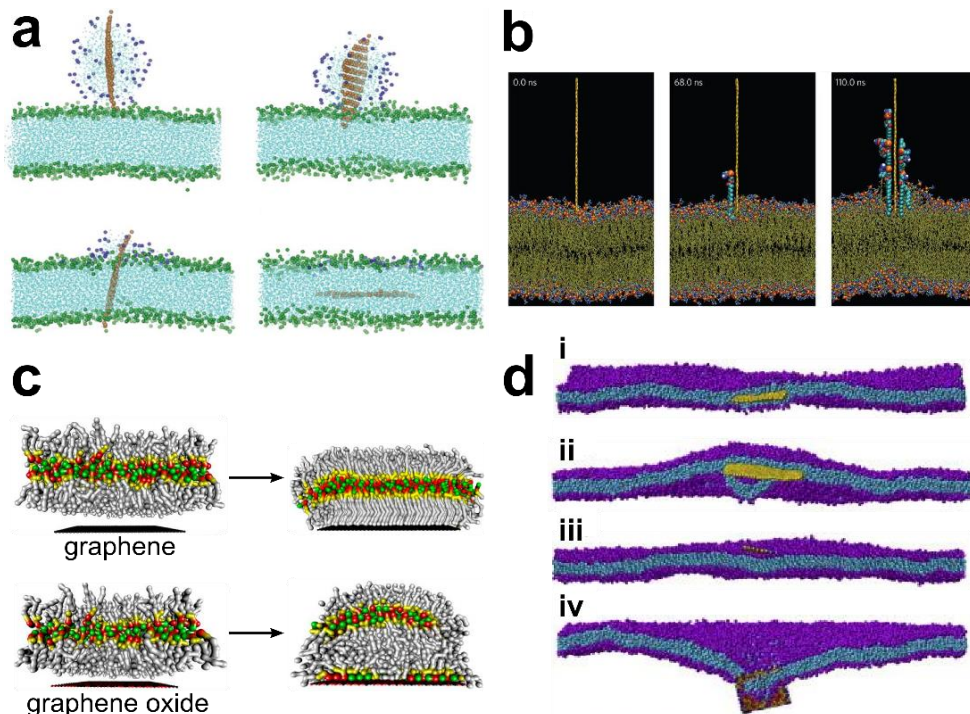


Figure 1.7. Molecular dynamic simulation studies of graphene interacting with lipids. a) Graphene sheet surrounded by a lipid micelle which enters and lies parallel to the lipid bilayer.⁷⁷ b) Lipid extraction by a graphene sheet placed perpendicular to a lipid bilayer.⁸² c) Lipids assembly by dip-pen nanolithography on graphene and graphene oxide leading to an ordered inverted bilayer and to three lipid layers structure (lipid monolayer + inverted bilayer), respectively.⁶⁰ d) Four types of graphene sheets interacting with a lipid membrane: i) small pristine graphene hosted in a lipid bilayer; ii) large graphene sheet inducing a hemisphere vesicle on its surroundings; iii) small graphene oxide sheet lying parallel on the surface of the lipid membrane; iv) large graphene oxide crossing and disturbing the lipid membrane.⁸⁵

Another set of MD simulations studies considered graphene and GO as substrates for the deposition of lipids. For GO substrates, a “1.5 lipid bilayer” (monolayer + inverted bilayer) tends to form on the GO surface due to its hydrophilic nature, whereas inverted bilayer structures – lipid tails facing graphene – are orderly arranged on the hydrophobic pristine graphene basal plane (Figure 1.7c).⁶⁰⁻⁶¹ Particularly, the interaction between lipids and pristine graphene induces ordering and rigidity of the lipid hydrocarbon chains that are close to the surface

of graphene.^{61, 86-87} These results were also confirmed experimentally in Chapter 2. The lipids showed a more ordered (extended lipid tails) and compact structure when a graphene sheet was transferred on top of the lipid monolayer supported by a Si/SiO₂ substrate, compare to a lipid monolayer without graphene on top. The heterostructure was characterized by attenuated total reflectance infrared (ATR-IR), ellipsometry, AFM, fluorescence and optical microscopy. Additionally, Chapter 3 described the complete transfer of a second lipid monolayer on top of graphene, encapsulating graphene within the hydrophobic core of the lipid membrane, confirming the MD predictions that a graphene monolayer is stable within a lipid bilayer.⁷⁷

In summary, the physicochemical properties of graphene, such as the distinct size and oxidization degree, influence how graphene interacts and disturbs a lipid membrane (Figure 1.7d and Figure 1.8b).⁸⁵ In general as described above, small pristine graphene (PG) sheets are hosted within the lipid bilayer (Figure 1.7d, i and Figure 1.8b) whereas large sheets tend to disturb the membrane by forming hemispheric vesicles surrounding the graphene sheets (Figure 1.7d,ii and Figure 1.8b). Increasing the oxidation at the edges of graphene (eGO, Figure 1.8a) shows that the GO sheets (independently of the size) preferably lie across the membrane disturbing locally the structure of the lipid bilayer (Figure 1.7d, iv and Figure 1.8b). The same behavior is observed for large sparsely (sGO, Figure 1.8a) and densely (dGO, Figure 1.8a) oxidized graphene sheets. Instead, small sGO and dGO sheets tend to horizontally adsorb on the surface of the lipid bilayer head groups (Figure 1.7d, iii and Figure 1.8b).

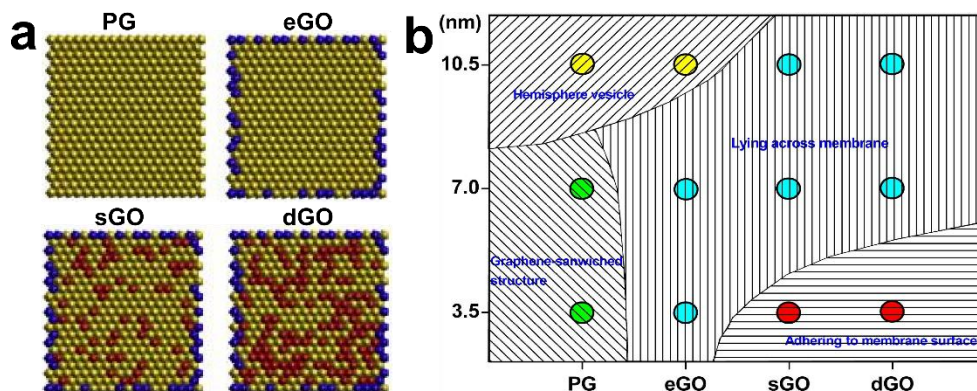


Figure 1.8. Molecular dynamic simulations of the interaction between graphene and lipid membranes. a) Illustration of different oxidation degrees of graphene: pristine graphene (PG, yellow beads of unoxidized graphene), edge oxidized graphene (eGO, blue beads of the oxidized edges), sparsely oxidized graphene (sGO, 20% of the carbon atom on the basal plane oxidized, red beads of oxidized basal plane), densely oxidized carbons (dGO, 40% of the carbon atom on the basal plane oxidized). b) Phase diagram summary of the effects of various graphene sizes and oxidation degree interacting with lipid membranes. The different colours represent the typical states written on the diagram (i.e. yellow: hemisphere vesicle; green: graphene-sandwiched structure; blue: lying across the membrane; red: adhering to membrane surface).⁸⁵

1.2 Aim and outline

The literature described in this chapter covers the main studies currently involving the interactions between lipids and graphene. A major aim of the research activities over the last 10-20 years focused on studying how lipids interact with graphene oxide (> 24), reduced graphene oxide (> 8) and with pristine graphene (> 20). This thesis aims to understand and characterize for the first time the mechanism of lipid-graphene interactions and to characterize the resulting structure using methods widely applied for studying lipids. The interactions of lipids with pristine graphene were investigated by assembling ordered lipid layers using the LB method, interfacing the hydrophobic lipid chains with the hydrophobic basal plane of CVD graphene and characterizing the assembled structures using mainly IR spectroscopy, ellipsometry, AFM, QCM and neutron reflectometry. In Chapter 2, lipids are used to replace conventional inorganic graphene substrates (such as silicon wafer). The lipids underneath graphene

presented a more ordered and organized structure compared to lipids not in contact with graphene. IR spectroscopy showed that lipids undergo a change in the lipid acyl chains conformation from *gauche* to *trans*, leading to a more compact monolayer in the presence of graphene. The heterostructure was furthermore characterized by ellipsometry, AFM, and Raman spectroscopy. In addition, lipids demonstrated to enhance the electric performances of graphene in comparison to graphene deposited on plain Si/SiO₂.

Accordingly, the lipid monolayer with graphene revealed a very stable and organized structure enabling the encapsulation of graphene in a lipid bilayer if another monolayer was transferred on top of graphene. In Chapter 3, graphene was sandwiched in between two monolayers of lipids (i. e., in the hydrophobic core of a lipid bilayer) where the lipid layers were assembled and transferred using the LB and LS techniques respectively, and characterized by IR spectroscopy, ellipsometry and neutron reflectometry.

As the stability and organization of lipid layers is also influenced by changes of temperature, in Chapter 4, the morphology and lateral organization of the lipid layers was analyzed below and above the phase transition temperature of the lipids, before and after graphene was transferred on top, by AFM. Above the phase transition, the thickness of the assembled lipid monolayer decreased adopting a fluidic state, which was confirmed by IR spectroscopy. Notably, the lipids underneath graphene remained intact and stable after the sample was rinsed with chloroform or with a hexadecyltrimethylammonium bromide (CTAB) solution, suggesting that a graphene monolayer can act as a shield protecting the lipids underneath from harsh environments.

The interactions of distinct lipids on graphene materials were systematically studied in Chapter 5. Cationic, anionic and zwitterionic lipids with different tail lengths and saturations were used and assembled with the LB or VF techniques. The structure and organization of the lipids on CVD graphene on copper and on highly oriented pyrolytic graphite (HOPG) substrates were analyzed by IR spectroscopy. QCM-D measurements monitored the dynamics and interactions of the distinct liposomes (assembled by the VF method) on graphene transferred on SiO₂ and on gold substrates. The results revealed that graphene was transparent to the substrates underneath by forming a lipid bilayer on graphene transferred to

a hydrophilic SiO₂-coated quartz crystal substrate and that the liposomes remained intact on graphene transferred to a hydrophobic gold-coated quartz crystal substrate.

Separately, a clean and continuous graphene surface is critical for the sensitivity of graphene in devices and therefore for the electrical detection of adsorbed molecules on the surface of graphene using a GFET. Chapter 6 introduced lipids as a scaffold to clamp graphene from the edges while floating at the air-water interface. Clamping graphene from the edges with lipids provided a clean graphene surface upon transfer to Si/SiO₂ substrates.

This thesis systematically analyzes the physical-chemistry of lipid-graphene interactions with the major objective of reconciling the variety of results reported in the literature. By using five major characterization techniques typically used to study lipids, namely IR spectroscopy, ellipsometry, AFM, neutron reflectivity and QCM-D, this thesis characterizes – in details – layered structures of graphene and lipids (so called superstructures) and separately studies the dynamics of the interaction between lipids and graphene. The most remarkable result is that through the systematic construction of i) a lipid monolayer on a silicon substrate; ii) the subsequent coating with graphene and iii) the deposition of a last lipid monolayer on top of the two layers stack; graphene could be encapsulated in the hydrophobic core of a lipid bilayer for the first time, promising a range of applications to sense biological processes occurring near or inside a lipid bilayer.

1.3 References

1. Titov, A. V.; Kral, P.; Pearson, R., Sandwiched graphene-membrane superstructures. *ACS Nano* **2010**, *4* (1), 229-234.
2. Castro Neto, A. H.; Guinea, F.; Peres, N. M. R.; Novoselov, K. S.; Geim, A. K., The electronic properties of graphene. *Rev. Mod. Phys.* **2009**, *81* (1), 109-162.
3. Fu, W.; Jiang, L.; Geest, E. P. v.; Lima, L. M. C.; Schneider, G. F., Sensing at the surface of graphene field-effect transistors. *Adv. Mater.* **2017**, *29* (6), 1603610.
4. Ferrari, A. C.; Bonaccorso, F.; Fal'ko, V.; Novoselov, K. S.; Roche, S.; Boggild, P.; Borini, S.; Koppens, F. H. L.; Palermo, V.; Pugno, N.; Garrido, J. A.; Sordan, R.; Bianco, A.; Ballerini, L.; Prato, M.; Lidorikis, E.; Kivioja, J.; Marinelli, C.; Ryhanen, T.; Morpurgo, A.; Coleman, J. N.; Nicolosi, V.; Colombo, L.; Fert, A.; Garcia-Hernandez, M.; Bachtold, A.; Schneider, G. F.; Guinea, F.; Dekker, C.; Barbone, M.; Sun, Z.; Galiotis, C.; Grigorenko, A. N.; Konstantatos, G.; Kis, A.; Katsnelson, M.; Vandersypen, L.; Loiseau, A.; Morandi, V.; Neumaier, D.; Treossi, E.; Pellegrini, V.; Polini, M.; Tredicucci, A.; Williams, G. M.; Hee Hong, B.; Ahn, J.-H.; Min Kim, J.; Zirath, H.; van Wees, B. J.; van der Zant, H.; Occhipinti, L.; Di Matteo, A.; Kinloch, I. A.; Seyller, T.; Quesnel, E.; Feng, X.; Teo, K.; Rupesinghe, N.; Hakonen, P.; Neil, S. R. T.; Tannock, Q.; Lofwander, T.; Kinaret, J., Science and technology roadmap for graphene, related two-dimensional crystals, and hybrid systems. *Nanoscale* **2015**, *7*, 4598-4810.
5. Meyer, J. C.; Geim, A. K.; Katsnelson, M. I.; Novoselov, K. S.; Booth, T. J.; Roth, S., The structure of suspended graphene sheets. *Nature* **2007**, *446*, 60-63.
6. Gomez De Arco, L.; Zhang, Y.; Schlenker, C. W.; Ryu, K.; Thompson, M. E.; Zhou, C., Continuous, highly flexible, and transparent graphene films by chemical vapor deposition for organic photovoltaics. *ACS Nano* **2010**, *4* (5), 2865-2873.

7. Schedin, F.; Geim, A. K.; Morozov, S. V.; Hill, E. W.; Blake, P.; Katsnelson, M. I.; Novoselov, K. S., Detection of individual gas molecules adsorbed on graphene. *Nat. Mater.* **2007**, *6*, 652-655.
8. Wang, Y. Y.; Pham, T. D.; Zand, K.; Li, J.; Burke, P. J., Charging the quantum capacitance of graphene with a single biological ion channel. *ACS Nano* **2014**, *8* (5), 4228–4238.
9. Hirtz, M.; Oikonomou, A.; Georgiou, T.; Fuchs, H.; Vijayaraghavan, A., Multiplexed biomimetic lipid membranes on graphene by dip-pen nanolithography. *Nat. Commun.* **2013**, *4*, 2591.
10. Ang, P. K.; Jaiswal, M.; Lim, C. H. Y. X.; Wang, Y.; Sankaran, J.; Li, A.; Lim, C. T.; Wohland, T.; Barbaros, Ö.; Loh, K. P., A bioelectronic platform using a graphene–lipid bilayer interface. *ACS Nano* **2010**, *4* (12), 7387-7394.
11. Tour, J. M., Top-down versus bottom-up fabrication of graphene-based electronics. *Chem. Mater.* **2014**, *26* (1), 163-171.
12. Li, Z.; Wang, Y.; Kozbial, A.; Shenoy, G.; Zhou, F.; McGinley, R.; Ireland, P.; Morganstein, B.; Kunkel, A.; Surwade, S. P.; Li, L.; Liu, H., Effect of airborne contaminants on the wettability of supported graphene and graphite. *Nat. Mater.* **2013**, *12*, 925-931.
13. Suk, J. W.; Kitt, A.; Magnuson, C. W.; Hao, Y.; Ahmed, S.; An, J.; Swan, A. K.; Goldberg, B. B.; Ruoff, R. S., Transfer of cvd-grown monolayer graphene onto arbitrary substrates. *ACS Nano* **2011**, *5* (9), 6916-6924.
14. Rafiee, J.; Mi, X.; Gullapalli, H.; Thomas, A. V.; Yavari, F.; Shi, Y.; Ajayan, P. M.; Koratkar, N. A., Wetting transparency of graphene. *Nat. Mater.* **2012**, *11*, 217–222.
15. Connelly, L. S.; Meckes, B.; Larkin, J.; Gillman, A. L.; Wanunu, M.; Lal, R., Graphene nanopore support system for simultaneous high-resolution afm imaging and conductance measurements. *ACS Appl. Mater. Interf.* **2014**, *6* (7), 5290-5296.

16. Tabaei, S. R.; Ng, W. B.; Cho, S.-J.; Cho, N.-J., Controlling the formation of phospholipid monolayer, bilayer, and intact vesicle layer on graphene. *ACS Appl. Mater. Interf.* **2016**, *8* (18), 11875-11880.
17. Li, W.; Chung, J. K.; Lee, Y. K.; Groves, J. T., Graphene-templated supported lipid bilayer nanochannels. *Nano Lett.* **2016**, *16* (8), 5022-5026.
18. Hirtz, M.; Oikonomou, A.; Clark, N.; Kim, Y.-J.; Fuchs, H.; Vijayaraghavan, A., Self-limiting multiplexed assembly of lipid membranes on large-area graphene sensor arrays. *Nanoscale* **2016**, *8* (33), 15147-15151.
19. Blaschke, B. M.; Böhm, P.; Drieschner, S.; Nickel, B.; Garrido, J. A., Lipid monolayer formation and lipid exchange monitored by a graphene field-effect transistor. *Langmuir* **2018**, *34* (14), 4224-4233.
20. Tamm, L. K.; Tatulian, S. A., Infrared spectroscopy of proteins and peptides in lipid bilayers. *Q. Rev. Biophys.* **1997**, *30* (4), 365-429.
21. Hummers, W. S.; Offeman, R. E., Preparation of graphitic oxide. *J. Am. Chem. Soc.* **1958**, *80* (6), 1339-1339.
22. Chen, D.; Feng, H.; Li, J., Graphene oxide: Preparation, functionalization, and electrochemical applications. *Chem. Rev.* **2012**, *112* (11), 6027-6053.
23. Compton, O. C.; Nguyen, S. T., Graphene oxide, highly reduced graphene oxide, and graphene: Versatile building blocks for carbon-based materials. *Small* **2010**, *6* (6), 711-723.
24. Dreyer, D. R.; Park, S.; Bielawski, C. W.; Ruoff, R. S., The chemistry of graphene oxide. *Chem. Soc. Rev.* **2010**, *39* (1), 228-240.
25. Pichot, R.; Watson, L. R.; Norton, T. I., Phospholipids at the interface: Current trends and challenges. *Int. J. Mol. Sci.* **2013**, *14* (6), 11767-11794.
26. Li, S. H.; Stein, A. J.; Kruger, A.; Leblanc, R. M., Head groups of lipids govern the interaction and orientation between graphene oxide and lipids. *J. Phys. Chem. B* **2013**, *117* (31), 16150-16158.

27. Kim, H.; Jang, Y. R.; Yoo, J.; Seo, Y. S.; Kim, K. Y.; Lee, J. S.; Park, S. D.; Kim, C. J.; Koo, J., Morphology control of surfactant-assisted graphene oxide films at the liquid-gas interface. *Langmuir* **2014**, *30* (8), 2170-2177.
28. Frost, R.; Jonsson, G. E.; Chakarov, D.; Svedhem, S.; Kasemo, B., Graphene oxide and lipid membranes: Interactions and nanocomposite structures. *Nano Lett.* **2012**, *12* (7), 3356-3362.
29. Huang, P.-J. J.; Wang, F.; Liu, J., Liposome/graphene oxide interaction studied by isothermal titration calorimetry. *Langmuir* **2016**, *32* (10), 2458-2463.
30. Cho, N.-J.; Frank, C. W.; Kasemo, B.; Höök, F., Quartz crystal microbalance with dissipation monitoring of supported lipid bilayers on various substrates. *Nat. Protoc.* **2010**, *5*, 1096-1106.
31. Frost, R.; Svedhem, S.; Langhammer, C.; Kasemo, B., Graphene oxide and lipid membranes: Size-dependent interactions. *Langmuir* **2016**, *32* (11), 2708-2717.
32. Lei, H.; Zhou, X.; Wu, H.; Song, Y.; Hu, J.; Guo, S.; Zhang, Y., Morphology change and detachment of lipid bilayers from the mica substrate driven by graphene oxide sheets. *Langmuir* **2014**, *30* (16), 4678-4683.
33. Rodriguez-Perez, L.; Herranz, M. A.; Martin, N., The chemistry of pristine graphene. *Chem. Commun.* **2013**, *49* (36), 3721-3735.
34. Ip Alexander, C. F.; Liu, B.; Huang Po-Jung, J.; Liu, J., Oxidation level-dependent zwitterionic liposome adsorption and rupture by graphene-based materials and light-induced content release. *Small* **2012**, *9* (7), 1030-1035.
35. Pei, S.; Cheng, H.-M., The reduction of graphene oxide. *Carbon* **2012**, *50* (9), 3210-3228.

36. Kuila, T.; Mishra, A. K.; Khanra, P.; Kim, N. H.; Lee, J. H., Recent advances in the efficient reduction of graphene oxide and its application as energy storage electrode materials. *Nanoscale* **2013**, *5* (1), 52-71.
37. Stankovich, S.; Dikin, D. A.; Piner, R. D.; Kohlhaas, K. A.; Kleinhammes, A.; Jia, Y.; Wu, Y.; Nguyen, S. T.; Ruoff, R. S., Synthesis of graphene-based nanosheets via chemical reduction of exfoliated graphite oxide. *Carbon* **2007**, *45* (7), 1558-1565.
38. Fernández-Merino, M. J.; Guardia, L.; Paredes, J. I.; Villar-Rodil, S.; Solís-Fernández, P.; Martínez-Alonso, A.; Tascón, J. M. D., Vitamin c is an ideal substitute for hydrazine in the reduction of graphene oxide suspensions. *J. Phys. Chem. C* **2010**, *114* (14), 6426-6432.
39. McAllister, M. J.; Li, J.-L.; Adamson, D. H.; Schniepp, H. C.; Abdala, A. A.; Liu, J.; Herrera-Alonso, M.; Milius, D. L.; Car, R.; Prud'homme, R. K.; Aksay, I. A., Single sheet functionalized graphene by oxidation and thermal expansion of graphite. *Chem. Mater.* **2007**, *19* (18), 4396-4404.
40. Zhou, M.; Wang, Y.; Zhai, Y.; Zhai, J.; Ren, W.; Wang, F.; Dong, S., Controlled synthesis of large-area and patterned electrochemically reduced graphene oxide films. *Chem. – Eur. J.* **2009**, *15* (25), 6116-6120.
41. Williams, G.; Seger, B.; Kamat, P. V., TiO₂-graphene nanocomposites. Uv-assisted photocatalytic reduction of graphene oxide. *ACS Nano* **2008**, *2* (7), 1487-1491.
42. Griggs, C. S.; Medina, V. F., Graphene and graphene oxide membranes for water treatment. In *Mcgraw hill encyclopedia of science & technology*, 11th ed.; McGraw-Hill Education: 2016.
43. Imran, H.; Manikandan, P. N.; Dharuman, V., Graphene oxide supported liposomes for efficient label free electrochemical DNA biosensing. *Sens. Actuat. B-Chem.* **2018**, *260*, 841-851.

44. Rui, L.; Liu, J.; Li, J.; Weng, Y.; Dou, Y.; Yuan, B.; Yang, K.; Ma, Y., Reduced graphene oxide directed self-assembly of phospholipid monolayers in liquid and gel phases. *BBA - Biomembranes* **2015**, *1848* (5), 1203-1211.
45. Tsuzuki, K.; Okamoto, Y.; Iwasa, S.; Ishikawa, R.; Sandhu, A.; Tero, R., Reduced graphene oxide as the support for lipid bilayer membrane. *J. Phys. Conf. Ser.* **2012**, *352* (1), 012016.
46. Liu, S.-J.; Wen, Q.; Tang, L.-J.; Jiang, J.-H., Phospholipid-graphene nanoassembly as a fluorescence biosensor for sensitive detection of phospholipase d activity. *Anal. Chem.* **2012**, *84* (14), 5944-5950.
47. Novoselov, K. S.; Geim, A. K.; Morozov, S. V.; Jiang, D.; Zhang, Y.; Dubonos, S. V.; Grigorieva, I. V.; Firsov, A. A., Electric field effect in atomically thin carbon films. *Science* **2004**, *306* (5696), 666-669.
48. Feng, H. B.; Wu, Y. M.; Li, J. H., Direct exfoliation of graphite to graphene by a facile chemical approach. *Small* **2014**, *10* (11), 2233-2238.
49. Emtsev, K. V.; Speck, F.; Seyller, T.; Ley, L.; Riley, J. D., Interaction, growth, and ordering of epitaxial graphene on $\text{SiC}(0001)$ surfaces: A comparative photoelectron spectroscopy study. *Phys. Rev. B* **2008**, *77* (15), 155303.
50. Seah, C.-M.; Chai, S.-P.; Mohamed, A. R., Mechanisms of graphene growth by chemical vapour deposition on transition metals. *Carbon* **2014**, *70*, 1-21.
51. Chen, X.; Zhang, L.; Chen, S., Large area cvd growth of graphene. *Synth. Met.* **2015**, *210*, 95-108.
52. Munoz, R.; Gomez-Aleixandre, C., Review of cvd synthesis of graphene. *Chem. Vap. Depos.* **2013**, *19* (10-12), 297-322.
53. Yu, Q.; Jauregui, L. A.; Wu, W.; Colby, R.; Tian, J.; Su, Z.; Cao, H.; Liu, Z.; Pandey, D.; Wei, D.; Chung, T. F.; Peng, P.; Guisinger, N. P.; Stach, E. A.; Bao, J.; Pei, S.-S.; Chen, Y. P., Control and characterization of individual

grains and grain boundaries in graphene grown by chemical vapour deposition. *Nat. Mater.* **2011**, *10*, 443.

54. Li, X.; Cai, W.; Colombo, L.; Ruoff, R. S., Evolution of graphene growth on ni and cu by carbon isotope labeling. *Nano Lett.* **2009**, *9* (12), 4268-4272.
55. Li, X.; Colombo, L.; Ruoff, R. S., Synthesis of graphene films on copper foils by chemical vapor deposition. *Adv. Mater.* **2016**, *28* (29), 6247-6252.
56. Mattevi, C.; Kim, H.; Chhowalla, M., A review of chemical vapour deposition of graphene on copper. *J. Mater. Chem.* **2011**, *21* (10), 3324-3334.
57. Reddy, D.; Register, L. F.; Carpenter, G. D.; Banerjee, S. K., Graphene field-effect transistors. *J. Phys. D* **2011**, *44*, 313001.
58. Kuo, C.-J.; Chiang, H.-C.; Tseng, C.-A.; Chang, C.-F.; Ulaganathan, R. K.; Ling, T.-T.; Chang, Y.-J.; Chen, C.-C.; Chen, Y.-R.; Chen, Y.-T., Lipid-modified graphene-transistor biosensor for monitoring amyloid- β aggregation. *ACS Appl. Mater. Interf.* **2018**, *10* (15), 12311-12316.
59. Banszerus, L.; Schmitz, M.; Engels, S.; Dauber, J.; Oellers, M.; Haupt, F.; Watanabe, K.; Taniguchi, T.; Beschoten, B.; Stampfer, C., Ultrahigh-mobility graphene devices from chemical vapor deposition on reusable copper. *Sci. Adv.* **2015**, *1* (6), e1500222.
60. Willems, N.; Urtizbera, A.; Verre, A. F.; Iliut, M.; Lelimosin, M.; Hirtz, M.; Vijayaraghavan, A.; Sansom, M. S. P., Biomimetic phospholipid membrane organization on graphene and graphene oxide surfaces: A molecular dynamics simulation study. *ACS Nano* **2017**, *11* (2), 1613-1625.
61. Rivel, T.; Yesylevskyy, S. O.; Ramseyer, C., Structures of single, double and triple layers of lipids adsorbed on graphene: Insights from all-atom molecular dynamics simulations. *Carbon* **2017**, *118*, 358-369.

62. Hardy, G. J.; Nayak, R.; Zauscher, S., Model cell membranes: Techniques to form complex biomimetic supported lipid bilayers via vesicle fusion. *Curr. Opin. Colloid Interface Sci.* **2013**, *18* (5), 448-458.
63. Schwartz, D. K.; Garnæs, J.; Viswanathan, R.; Zasadzinski, J. A. N., Surface order and stability of langmuir-blodgett films. *Science* **1992**, *257* (5069), 508-511.
64. Yamazaki, K.; Kunii, S.; Ogino, T., Characterization of interfaces between graphene films and support substrates by observation of lipid membrane formation. *J. Phys. Chem. C* **2013**, *117* (37), 18913-18918.
65. Belyaeva, L. A.; Deursen, P. M. G. v.; Barbetsea, K. I.; Schneider, G. F., Hydrophilicity of graphene in water through transparency to polar and dispersive interactions. *Adv. Mater.* **2018**, *30* (6), 1703274.
66. Lenhart, S.; Sun, P.; Wang, Y.; Fuchs, H.; Mirkin, C. A., Massively parallel dip-pen nanolithography of heterogeneous supported phospholipid multilayer patterns. *Small* **2006**, *3* (1), 71-75.
67. Zheng, Q.; Shi, L.; Ma, P.-C.; Xue, Q.; Li, J.; Tang, Z.; Yang, J., Structure control of ultra-large graphene oxide sheets by the langmuir–blodgett method. *RSC Adv.* **2013**, *3* (14), 4680-4691.
68. Jaafar, M. M.; Ciniciato, G. P. M. K.; Ibrahim, S. A.; Phang, S. M.; Yunus, K.; Fisher, A. C.; Iwamoto, M.; Vengadesh, P., Preparation of a three-dimensional reduced graphene oxide film by using the langmuir–blodgett method. *Langmuir* **2015**, *31* (38), 10426-10434.
69. Li, X.; Zhang, G.; Bai, X.; Sun, X.; Wang, X.; Wang, E.; Dai, H., Highly conducting graphene sheets and langmuir–blodgett films. *Nat. Nanotechnol.* **2008**, *3*, 538–542.
70. Zheng, Q.; Ip, W. H.; Lin, X.; Yousefi, N.; Yeung, K. K.; Li, Z.; Kim, J.-K., Transparent conductive films consisting of ultralarge graphene sheets produced by langmuir–blodgett assembly. *ACS Nano* **2011**, *5* (7), 6039-6051.

71. Lewis, R. N. A. H.; McElhaney, R. N., Membrane lipid phase transitions and phase organization studied by fourier transform infrared spectroscopy. *BBA-Biomembranes* **2013**, *1828* (10), 2347-2358.
72. Blume, A.; Kerth, A., Peptide and protein binding to lipid monolayers studied by ft-irra spectroscopy. *BBA-Biomembranes* **2013**, *1828* (10), 2294-2305.
73. Keller, C. A.; Kasemo, B., Surface specific kinetics of lipid vesicle adsorption measured with a quartz crystal microbalance. *Biophys. J.* **1998**, *75* (3), 1397-1402.
74. Melendrez, D.; Jowitt, T.; Iliut, M.; Verre, A. F.; Goodwin, S.; Vijayaraghavan, A., Adsorption and binding dynamics of graphene-supported phospholipid membranes using the qcm-d technique. *Nanoscale* **2018**, *10* (5), 2555-2567.
75. Guo, R.; Mao, J.; Yan, L.-T., Computer simulation of cell entry of graphene nanosheet. *Biomaterials* **2013**, *34* (17), 4296-4301.
76. Dallavalle, M.; Calvaresi, M.; Bottoni, A.; Melle-Franco, M.; Zerbetto, F., Graphene can wreak havoc with cell membranes. *ACS Appl. Mater. Interf.* **2015**, *7* (7), 4406-4414.
77. Wang, J.; Wei, Y.; Shi, X.; Gao, H., Cellular entry of graphene nanosheets: The role of thickness, oxidation and surface adsorption. *RSC Adv.* **2013**, *3* (36), 15776-15782.
78. Dallavalle, M.; Bottoni, A.; Calvaresi, M.; Zerbetto, F., Functionalization pattern of graphene oxide sheets controls entry or produces lipid turmoil in phospholipid membranes. *ACS Appl. Mater. Interf.* **2018**, *10* (18), 15487-15493.
79. Chen, J.; Zhou, G.; Chen, L.; Wang, Y.; Wang, X.; Zeng, S., Interaction of graphene and its oxide with lipid membrane: A molecular dynamics simulation study. *J. Phys. Chem. C* **2016**, *120* (11), 6225-6231.

80. Li, Y.; Yuan, H.; von dem Bussche, A.; Creighton, M.; Hurt, R. H.; Kane, A. B.; Gao, H., Graphene microsheets enter cells through spontaneous membrane penetration at edge asperities and corner sites. *Proc. Natl. Acad. Sci.* **2013**, *110* (30), 12295-12300.
81. Yi, X.; Gao, H., Cell interaction with graphene microsheets: Near-orthogonal cutting versus parallel attachment. *Nanoscale* **2015**, *7* (12), 5457-5467.
82. Tu, Y.; Lv, M.; Xiu, P.; Huynh, T.; Zhang, M.; Castelli, M.; Liu, Z.; Huang, Q.; Fan, C.; Fang, H.; Zhou, R., Destructive extraction of phospholipids from escherichia coli membranes by graphene nanosheets. *Nat. Nanotechnol.* **2013**, *8* (8), 594-601.
83. Luo, Z.; Li, S.; Xu, Y.; Ren, H.; Zhang, X.; Hu, G.; Huang, F.; Yue, T., Extracting pulmonary surfactants to form inverse micelles on suspended graphene nanosheets. *Environ. Sci. Nano* **2018**, *5* (1), 130-140.
84. Luan, B.; Huynh, T.; Zhou, R., Complete wetting of graphene by biological lipids. *Nanoscale* **2016**, *8* (10), 5750-5754.
85. Mao, J.; Guo, R.; Yan, L.-T., Simulation and analysis of cellular internalization pathways and membrane perturbation for graphene nanosheets. *Biomaterials* **2014**, *35* (23), 6069-6077.
86. Yue, T.; Wang, X.; Zhang, X.; Huang, F., Molecular modeling of interaction between lipid monolayer and graphene nanosheets: Implications for pulmonary nanotoxicity and pulmonary drug delivery. *RSC Adv.* **2015**, *5* (38), 30092-30106.
87. Song, Z.; Wang, Y.; Xu, Z., Mechanical responses of the bio-nano interface: A molecular dynamics study of graphene-coated lipid membrane. *Theor. Appl. Mech. Lett.* **2015**, *5* (6), 231-235.

CHAPTER 2

Graphene-stabilized lipid monolayer heterostructures: a novel biomembrane superstructure

Chemically defined and electronically benign interfaces are attractive substrates for graphene and other two-dimensional materials. Here, lipid monolayers are introduced as an alternative, structurally ordered, and chemically versatile support for graphene. Deposition of graphene on the lipids resulted in a more ordered monolayer than regions without graphene. The lipids also offered graphene a more uniform and smoother support, reducing graphene hysteresis loop and the average value of the charge neutrality point under applied voltages. Our approach promises to be effective towards measuring experimentally biochemical phenomena within lipid monolayers and bilayers.

This chapter was published as a full article: Lia M. C. Lima, Wangyang Fu, Lin Jiang, Alexander Kros and Grégory F. Schneider, *Nanoscale*, **2016**, 8, 18646-8653

2.1 Introduction

Graphene¹ is typically supported – sometimes sandwiched – with other two-dimensional (2D) materials to promote higher mobility,² to ensure the reproducibility in electrical performances,³ and to prevent environmental contamination.⁴ Frequently composed of inorganic, hard and crystalline materials, the so called van der Waals heterostructures have emerged as a route to design new and remarkably complex layer-by-layer films of 2D materials, including graphene.⁵ For example, the atomically flat hexagonal boron nitride (hBN) is frequently used as a support for graphene yielding a very high graphene electron mobility, in comparison with a Si/SiO₂ substrate which has a high surface roughness.⁶ Alternatively, removing the hard substrates underneath graphene, i.e., suspending graphene, also improves the electron mobility of graphene, although the architecture and the methods of characterization are still limited.⁷

Nevertheless, one challenge associated with 2D materials as supporting and sandwiching layers is their limited chemical diversity, functions, and inherent inorganic nature. The possibility of combining graphene with soft, dynamic and molecular self-assembled monolayers is therefore of high interest as an organic alternative to inorganic 2D materials and could provide a versatile platform for applications, such as biosensors, drug delivery systems or cellular devices.⁸

Lipids – the main constituents of cell membranes – are amphiphilic molecules that can self-assemble and form stable quasi two dimensional fluidic membrane structures.⁹ Lipids can spread on graphene,¹⁰ however little is known on the formation, stability and molecular structure of lipid molecules surrounding graphene.¹⁰⁻¹⁷ Mainly, studies focused on graphene oxide (GO), as both lipid vesicles and GO form stable suspensions in aqueous environments.¹⁸ GO is an easily accessible form of graphene, suitable to study the influence of oxidation states on the chemical characteristics of GO-lipid assemblies, at the cost of lower electron mobility, higher chemical reactivity, oxygen doping, and surface/edge inhomogeneities. Being negatively charged, GO has a particular affinity with positively charged lipid head groups,¹⁹ highlighting the importance of electrostatic interactions in the assembly process.²⁰ Pristine graphene, however, does not contain charges on the basal plane therefore minimizing electrostatic interactions and favoring hydrophobic interactions between lipid tails and graphene at the

interface.²¹ To understand and quantify the interactions between lipid tails and graphene, an approach is that graphene crowd surfs directly on the lipid chains, and measure at the same time the electrical properties of graphene and the molecular structure of the lipids, for example, using infrared spectroscopy.

In this chapter we investigate the stability and structure of the lipid monolayer placed underneath graphene and report that graphene affects the conformation of a lipid monolayer, yielding a rearrangement of the lipids into a more ordered and more compact supramolecular conformation. Remarkably, attenuated transmission reflectance infrared spectroscopy (ATR-IR) and ellipsometry demonstrate an increase of the absorbance intensity and of the thickness of the lipid monolayer in presence of graphene, respectively. Our finding suggests a high affinity between the lipid tails and the graphene basal plane promoting a favorable heterostructure for biosensing applications, and represents the first step towards embedding graphene experimentally into the hydrophobic core of a lipid bilayer as proposed by recent molecular dynamics simulations reporting the favorable stabilization of such sandwiched structure.²²⁻²³

2.2 Results and discussion

One straightforward approach to form and study a graphene-lipid monolayer interface is to pre-form a well-packed monolayer of lipids on a known substrate, such as Si/SiO₂ and transfer a graphene layer on top. A well-established route to build an ordered lipid monolayer is by applying the Langmuir-Blodgett technique²⁴ using 1,2-dipalmitoyl-*sn*-glycero-3-phosphocholine (DPPC) and 1% of 1,2-dipalmitoyl-*sn*-glycero-3-phosphoethanolamine-N-(lissamine rhodamine B sulfonyl) (Liss Rhod PE) (Figure 2.1). First, the mixture of lipids is dissolved in an organic solution of chloroform/methanol (3:1) and is subsequently deposited dropwise at the air-water interface of the Langmuir trough. By further compressing this unordered lipid phase (i.e. in a gas phase (G), Figure 2.1a) to specific surface pressures, a very compact lipid monolayer can be formed and transferred to any arbitrary substrate.²⁵ In this study, the lipids were compressed to a surface pressure (π) of 30 mN/m – to form a compact and stable monolayer – and thereafter transferred to a Si/SiO₂ substrate by retracting the substrate out of the trough at maximum compression. A chemical vapor deposition (CVD) graphene layer was then transferred above the lipid film by bringing into contact the lipid

film with graphene floating on ammonium persulfate solution (APS, 0.5 M). The sample was immediately rinsed with ultrapure water to remove traces of APS (see Appendix I).

Figure 2.1a shows the surface pressure (π) – area isotherm of DPPC:Liss Rhod PE (99:1) (solid line) on a pure water sub-phase and the subsequent decompression of the Langmuir film (dashed line) after the transfer of the lipid monolayer onto the Si/SiO₂ substrate.

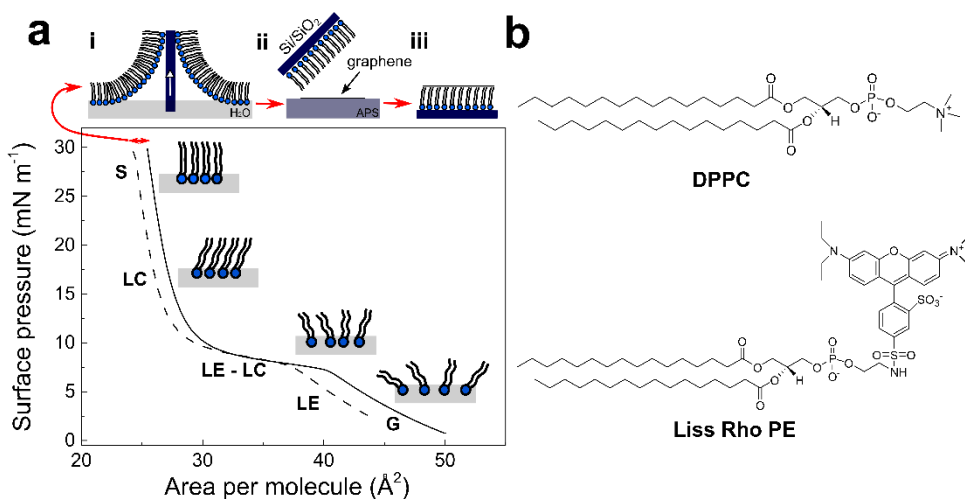


Figure 2.1. Lipid monolayer assembly and transfer of graphene. a) Surface pressure – area (π -A) compression isotherm of DPPC:Liss Rhod PE (99:1) monolayer (solid line) and the subsequent decompression (dashed line) after the transfer of the lipid monolayer on a Si/SiO₂ substrate (see top inset, step i). The different lipidic phases are: G, gaseous state; LE, liquid expanded state; LC, liquid condensed state; and S, solid state. In a last step graphene is transferred on top of the lipid monolayer from an ammonium persulfate solution (APS) (see top inset, step ii-iii). b) Molecular structure of the two lipids used in this work: 1,2-dipalmitoyl-*sn*-glycero-3-phosphocholine (DPPC) and 1,2-dipalmitoyl-*sn*-glycero-3-phosphoethanolamine-N-(lissamine rhodamine B sulfonyl) (Liss Rhod PE).

The lipid monolayer was compressed until a π of 30 mN/m passing through distinct separate phases characteristic of phospholipid molecules. In the first step, the lipids spread at the air-water interface yielding a gaseous state (G) due to the small intermolecular forces between the individual lipid molecules resulting from the large distance between molecules. As the mobile barriers of the Langmuir

trough start to compress, the available area per molecule and the intermolecular distance between the lipids decreases, resulting in the transition from the gaseous to a liquid expanded state (LE). After further compression, the molecules undergo a phase transition from a fluidic to a condensed phase. This liquid expanded (LE) – liquid condensed (LC) phase transition is characterized by a different aggregation state where the lipids present a strong lateral cohesion and a well-defined orientation. Finally, when the available area of the monolayer is further reduced, the lipid molecules self-organize in a perfectly ordered and stable monolayer, called the solid state (S).²⁶ At this stage, the well-packed lipid monolayer is transferred to the Si/SiO₂ substrate, resulting in a shift in the compression isotherms from which the transfer ratio of the lipids on the substrate is determined (Figure 2.1a, dashed line, red arrow; see Appendix I).

Optical and fluorescence microscopy measurements of the lipid monolayer and the subsequent lipid-graphene assembly are shown in Figure 2.2. A homogenous and continuous fluorescence layer is observed on Si/SiO₂ substrate (Figure 2.2a). Next, graphene was transferred onto the lipid monolayer resulting in a strong fluorescence quenching of the rhodamine B dye.²⁷ Note that millimeter sized graphene domains are observed, even without the need of a polymer such as PMMA for the transfer, as shown by Figure 2.2b and 2.2c.²⁸ The cracks on the basal plane of graphene are advantageous to image graphene using fluorescence quenching microscopy.²⁹ Remarkably, after rinsing with ultrapure water (to remove APS traces), the lipids underneath the graphene area remained intact, as confirmed by infrared spectroscopy and ellipsometry (Figure 2.3a), suggesting that graphene acts as a shield that prevent the lipids from getting rinsed off and protecting them from the environment (Figure 2.2b).

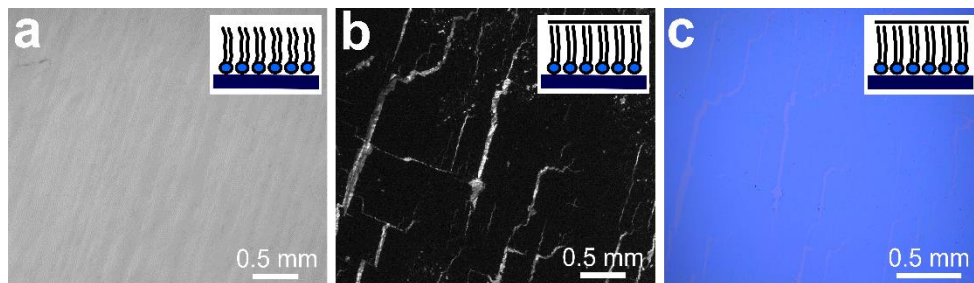


Figure 2.2. Microscopy imaging of the lipids and of the lipid-graphene heterostructure. a) Fluorescence image of DPPC:Liss Rhod PE (99:1) monolayer on Si/SiO₂ substrate. b) Fluorescence image after transferring graphene on top of the lipid monolayer. c) The corresponding optical image on the same graphene area of 2.2b.

In order to characterize the molecular structure and organization of the lipids, we performed attenuated total reflectance infrared (ATR-IR) spectroscopy measurements. Figure 2.3a shows the absorption bands characteristic for the stretching vibrations of the lipid acyl chains for the lipid monolayer (black line) and for the lipid-graphene assembly (red line).³⁰ The presence of these peaks confirms that the lipids remained underneath the graphene even after the extensive rising steps. Depending on whether the lipids are in contact or not with graphene, a shift in the wavenumber of the peak maximum is observed, characteristic for changes in the lipid conformation (i.e., a shift to lower wavenumber is often observed when the lipids within the monolayer are becoming more ordered).³¹ Additionally, a shift was observed in the asymmetric methylene vibration (CH₂) from ~2915 to 2912 cm⁻¹ and in the symmetric methylene vibration (CH₂) from ~2848 to 2844 cm⁻¹, respectively. Furthermore the intensity of the asymmetric and symmetric CH₂ bands of the lipid-graphene assembly increased. The observed shift is attributed to a change of the physical properties of the lipids film, where the frequencies of CH₂ stretching vibrations are known to decrease if lipids are well packed. An elongation of the lipid acyl chains will also yield an increase of intensity of the band. As the CH₂ frequency decreases, the lipid hydrocarbon chain order increases, suggesting a change from *gauche* to *trans* conformation of the lipid chains.³² The molecules are closer to each other, have less freedom to vibrate and therefore lead to a decrease of the wavenumber. Thus, the lipids underneath graphene present a crystalline structure with presumably very restricted diffusional mobility.³¹⁻³³ At

this stage of the experiment, we therefore considered that graphene enters into – what we call – a ‘crowd surfing’ mode, either static or dynamic.

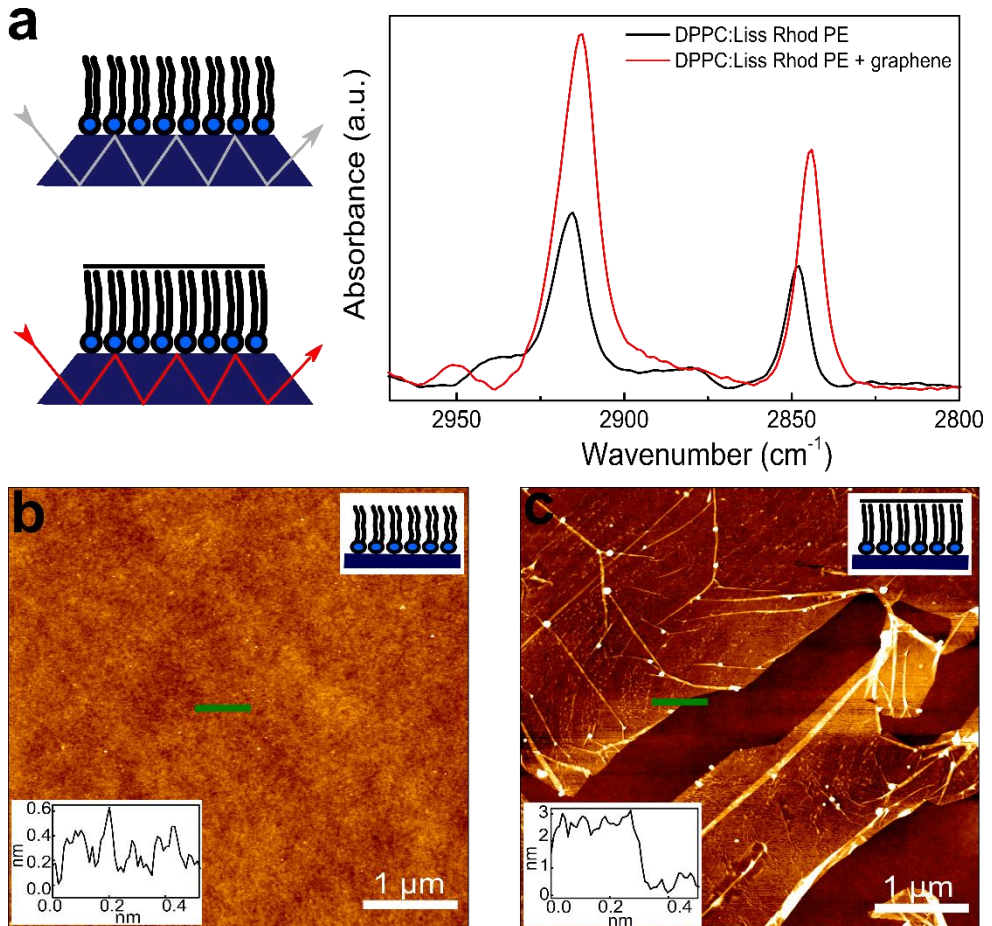


Figure 2.3. Attenuated total reflectance infrared (ATR-IR) and atomic force microscopy (AFM) characterization of the lipid-graphene heterostructure on a Si/SiO₂ substrate. a) ATR-IR absorption bands of CH₂ stretching vibrations of the lipid acyl chains before (black) and after (red) transferring graphene on top of a lipid monolayer transferred by Langmuir-Blodgett onto a Si/SiO₂ substrate. b) AFM intermittent contact mode image in air at room temperature of a DPPC:Liss Rhod PE (99:1) monolayer on Si/SiO₂ substrate and c) after transferring graphene on top of the lipid monolayer. The insets are the corresponding height profiles (green lines).

To obtain further information on the change of conformation of the lipid molecules upon their interaction with graphene, we determined the thickness of the different layers composing the thin film by ellipsometry (see Appendix I). The thickness of the SiO₂ layer was determined to be 282.9 ± 1.4 nm.³⁴ Then, after depositing the lipid monolayer, the total thickness increased by 2.5 ± 0.4 nm, as expected for a lipid monolayer.³⁵ After transferring graphene on top of the lipid monolayer, the thickness of the lipid monolayer increased to 3.9 ± 0.9 nm. This expansion of the lipid acyl chains, as confirmed previously by ATR-IR, corresponds to the formation of a more ordered structure. The interactions of the hydrophobic lipid tails with the hydrophobic graphene transferred on top are most probably remarkably favorable.^{10, 22} This increase of 1.4 nm, could also be expected if a bilayer would form, but this hypothesis is excluded as no more lipids were in contact with the sample during the sample preparation. Although an absolute increase in thickness of 1.4 nm is surprising giving the expected head-to-tail length of DPPC, it is evident that the lipids re-arrange in a more organized layer after interacting with graphene, as confirmed previously by ATR-IR. The graphene thickness measured was 0.4 ± 0.2 nm, in agreement with the transfer of a single monolayer graphene.

The atomic force microscopy (AFM) images and the corresponding height profiles of the lipid monolayer in air at room temperature before and after transferring graphene showed the presence of an homogenous monolayer of lipids (Figure 2.3b), and for this reason, no significant step height differences could be measured on the lipid monolayer. These results confirm the formation of a stable and compacted lipid layer on Si/SiO₂ substrate (Figure 2.1a). The transferred graphene sheet on top of the lipid monolayer showed very flat and continuous domains (Figure 2.3c) with only a few wrinkles and cracks, as shown by fluorescence microscopy (Figure 2.2b).³⁶

Figure 2.4a shows the averaged Raman spectra for graphene on a Si/SiO₂ substrate (black line) and for graphene transferred above the lipid monolayer in air at room temperature (red line). The sharp, symmetric and intensive 2D peak (~ 2680 cm⁻¹) and G peak (~ 1580 cm⁻¹) indicates the presence of single layer graphene.³⁷ The weak D peak at 1350 cm⁻¹ is commonly present in CVD graphene, revealing a reasonable graphene quality. Specifically, the G band has been generally considered as an important indicator of doping effect in graphene.³⁸⁻³⁹ In

Figure 2.4b, the G peak of graphene (1585.8 cm^{-1}) blue shifts if lipids are present underneath (1589.0 cm^{-1}). Such blue shift can be attributed to the known p-doping of lipids,³⁷ or due to the presence of an adsorbed water layer⁴⁰ at the interface between graphene and the substrate.

The imaging of the G peak position, its full width at half maximum (FWHM) and the intensity ratio of $I(2D)/I(G)$ are summarized in the mapping data shown in Figure 2.4c. The G peak shows a larger blue shift and a much narrower width in the presence of the lipids as seen by the overall more reddish plots. Furthermore, the ratio of $I(2D)/I(G)$ decreases for the lipid-graphene assembly compare to graphene on Si/SiO₂ substrate. All of these evidences confirm the p-doping effect from the lipids underneath graphene.⁴¹⁻⁴² It is also worth to notice that the lipid-graphene assembly presents a more evenly color distribution than those of graphene on Si/SiO₂, which demonstrates that the lipid monolayer underneath supplies a more uniform and smooth support to graphene.

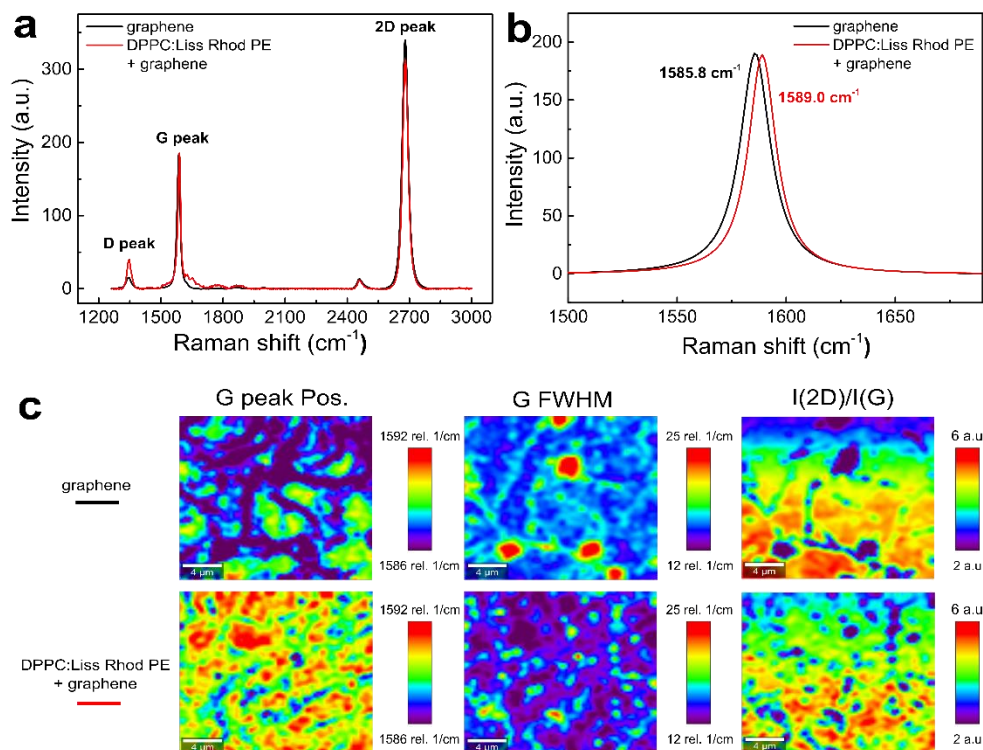


Figure 2.4. Raman spectroscopy and imaging of graphene and of lipid-graphene assembly. a) Raman spectra of graphene (black line) and of the lipid-graphene heterostructure (red line) on a Si/SiO₂ substrate. b) The Lorentz fitted G peak of the Raman spectra. c) Raman imaging of the G peak position, of its FWHM and the intensity ratio of I(2D)/I(G) for graphene (top) and for lipid-graphene heterostructure (bottom).

For electrical characterization of the lipid-graphene assembly, metal electrodes (chromium, 30 nm) were deposited on the CVD graphene above the lipid monolayer using a physical mask. As a control, we fabricated another graphene device directly on the Si/SiO₂ substrate using a PMMA assisted transfer method.²⁸

The graphene device on bare Si/SiO₂ substrate exhibits a hysteresis of 10 V with an average charge neutrality point (CNP), V_{CNP} of about +30 V (Figure 2.5a, black line). The relatively large hysteresis and V_{CNP} can be ascribed to the well-known charge trap and p-doping effect of the Si/SiO₂ substrate.⁴³ Remarkably, the lipid monolayer favored the screening of the silicon substrate (Figure 2.5a, red line). As

a result, the electrical performances of the lipid-graphene device were improved with a reduced hysteresis loop (4 V) and a smaller average V_{CNP} (23 V). We note here that the decrease of the estimated carrier mobility of graphene on the lipid monolayer ($430 \text{ cm}^2/\text{Vs}$ compared to $640 \text{ cm}^2/\text{Vs}$ on bare substrate) most likely originates from the incomplete surface coverage of graphene on the lipid monolayer. Another possible origin of this lower mobility is maybe the presence of more wrinkles as depicted in Figure 2.3c. The graphene coverage with the lipid-assisted transfer method was below 80%, whereas the graphene coverage on bare substrate was larger than 95% (observed by optical images). In addition, occasionally we also observed in our experiments that defective lipids (Langmuir-Blodgett transfer ratio < 1) degraded the performance of graphene device by introducing even more p-doping effect (with $V_{\text{CNP}} > 80 \text{ V}$) and larger hysteresis (> 25 V) (Figure 2.5a, green line). We have repeated the electrical measurements for another lipid-graphene sample. This sample exhibited a carrier mobility of $570 \text{ cm}^2/\text{Vs}$, a hysteresis of 1.5 V, and a V_{CNP} of 8 V, closely resembling what we showed in Figure 2.5a. We noted here that we tested also a few defective samples. The carrier mobility, hysteresis, and V_{CNP} of these defective samples demonstrated a wide distribution of $\sim 100\text{-}700 \text{ cm}^2/\text{Vs}$, $\sim 6\text{-}11 \text{ V}$, and $\sim 11\text{-}45 \text{ V}$, respectively.

In Figure 2.5b, the intensity ratio between the D peak and G peak $I(\text{D})/I(\text{G})$ revealed the disorder and defects on graphene, which can be ascribed to effects of the substrate. These substrate effects are primarily due to the roughness of Si/SiO₂ substrate, the strain induced by the lipid monolayer underneath, and the possible adsorbed water layer at the Si/SiO₂-lipid interface. Compare to graphene on the lipid monolayer (Figure 2.5b, middle), the $I(\text{D})/I(\text{G})$ ratio of graphene on defective lipids (Figure 2.5b, bottom) is more intense. A higher $I(\text{D})/I(\text{G})$ ratio is in line with the larger field-effect hysteresis (25 V in case of defective lipids supporting graphene compared to 4 V in case of graphene on lipid monolayer) and the higher p-doping (i.e., larger average V_{CNP} of 80 V compared to 23 V for graphene on lipid monolayer). We note here that the $I(\text{D})/I(\text{G})$ ratio of graphene on a bare Si/SiO₂ substrate (Figure 2.5b, top) was indeed less intensive than the one for graphene on a lipid monolayer (Figure 2.5b, middle). Nevertheless, we observed a less pronounced field-effect hysteresis (4 V in case of lipid monolayer supporting graphene compared to 10 V in case of graphene on the bare substrate) and a smaller average V_{CNP} (23 V compared to 30 V for graphene on the bare substrate),

which could be ascribed to the PMMA assisted transfer method we used for transferring graphene on bare substrate.

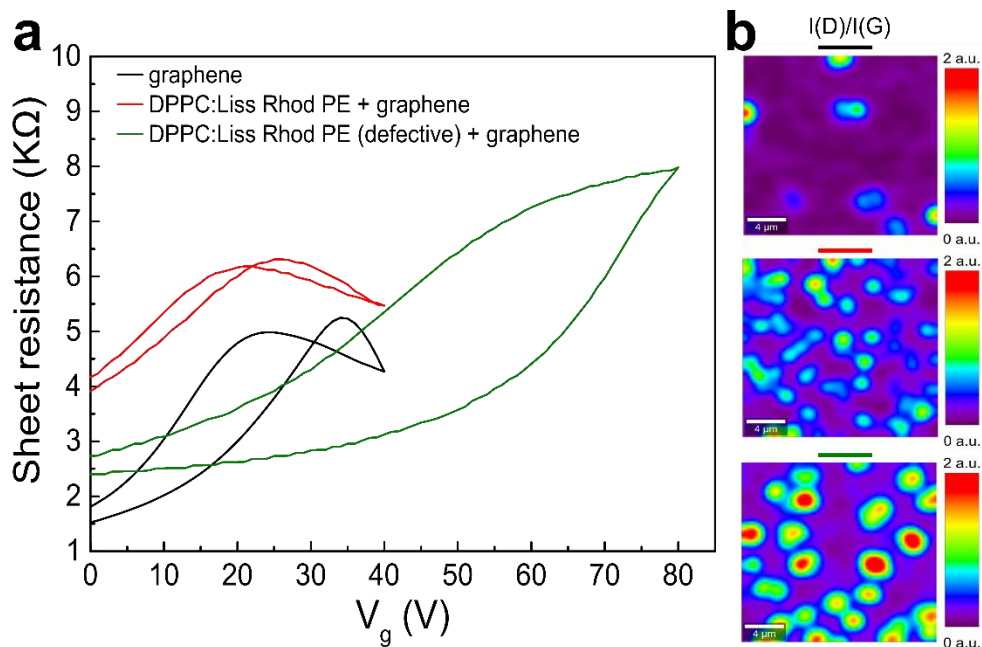


Figure 2.5. Effect of the lipid monolayer on the electrical measurements of graphene. a) The back gate voltage (V_g) dependent sheet resistance (R) of graphene on Si/SiO₂ substrate (black line), lipid-graphene assembly (red line), and on graphene with defective lipid monolayer (green line). b) Raman imaging of the intensity ratio of $I(D)/I(G)$ for graphene on Si/SiO₂ substrate (top), lipid-graphene assembly (middle), and graphene with defective lipid monolayer (bottom).

2.3 Conclusions

The observation of a unique re-ordering of lipid molecules in the presence of graphene reveals an increase in the packing of the lipid monolayer as graphene crowd surfs on the lipid monolayer. Remarkably, lipids ameliorated the electrical performances of the graphene, which is of high interest for using lipids as alternative soft substrates for graphene. Additionally, the direct contact between graphene and lipids is particularly attracting for measuring biochemical phenomena, for example in-situ a lipidic layer. Future experiments investigating

different lipids with different charges, different phase transition temperatures, and different lipid packing will be essential to elucidate the potential sensitivity of graphene to even more subtle changes in (bio)molecular conformations. A practical benefit of the lipid monolayer is also that large millimeter sized and continuous graphene domains are supported, avoiding polymers or any contaminants usually used during typical graphene transfers.

Interfacing graphene with lipid molecules will offer a new sensing platform to chemically modulate the electrical properties of graphene by varying the lipids structure and is the first step towards sandwiching graphene within the hydrophobic core of a lipid bilayer (Chapter 3).

2.4 References

1. Novoselov, K. S.; Geim, A. K.; Morozov, S. V.; Jiang, D.; Zhang, Y.; Dubonos, S. V.; Grigorieva, I. V.; Firsov, A. A., Electric field effect in atomically thin carbon films. *Science* **2004**, *306* (5696), 666-669.
2. Dean, C. R.; Young, A. F.; Meric, I.; Lee, C.; Wang, L.; Sorgenfrei, S.; Watanabe, K.; Taniguchi, T.; Kim, P.; Shepard, K. L.; Hone, J., Boron nitride substrates for high-quality graphene electronics. *Nat. Nanotechnol.* **2010**, *5* (10), 722-726.
3. Xue, J.; Sanchez-Yamagishi, J.; Bulmash, D.; Jacquod, P.; Deshpande, A.; Watanabe, K.; Taniguchi, T.; Jarillo-Herrero, P.; Leroy, B. J., Scanning tunnelling microscopy and spectroscopy of ultra-flat graphene on hexagonal boron nitride. *Nat. Mater.* **2011**, *10* (4), 282-285.
4. Wang, L.; Meric, I.; Huang, P. Y.; Gao, Q.; Gao, Y.; Tran, H.; Taniguchi, T.; Watanabe, K.; Campos, L. M.; Muller, D. A.; Guo, J.; Kim, P.; Hone, J.; Shepard, K. L.; Dean, C. R., One-dimensional electrical contact to a two-dimensional material. *Science* **2013**, *342* (6158), 614-617.
5. Geim, A. K.; Grigorieva, I. V., Van der waals heterostructures. *Nature* **2013**, *499* (7459), 419-425.
6. Xue, J.; Sanchez-Yamagishi, J.; Bulmash, D.; Jacquod, P.; Deshpande, A.; Watanabe, K.; Taniguchi, T.; Jarillo-Herrero, P.; LeRoy, B. J., Scanning tunnelling microscopy and spectroscopy of ultra-flat graphene on hexagonal boron nitride. *Nat. Mater.* **2011**, *10*, 282.
7. Du, X.; Skachko, I.; Barker, A.; Andrei, E. Y., Approaching ballistic transport in suspended graphene. *Nat. Nanotechnol.* **2008**, *3*, 491.
8. Ferrari, A. C.; Bonaccorso, F.; Fal'ko, V.; Novoselov, K. S.; Roche, S.; Boggild, P.; Borini, S.; Koppens, F. H. L.; Palermo, V.; Pugno, N.; Garrido, J. A.; Sordan, R.; Bianco, A.; Ballerini, L.; Prato, M.; Lidorikis, E.; Kivioja, J.; Marinelli, C.; Ryhanen, T.; Morpurgo, A.; Coleman, J. N.; Nicolosi, V.; Colombo, L.; Fert, A.; Garcia-Hernandez, M.; Bachtold, A.; Schneider, G. F.; Guinea, F.; Dekker, C.; Barbone, M.; Sun, Z.; Galiotis, C.; Grigorenko, A. N.; Konstantatos, G.; Kis, A.; Katsnelson, M.; Vandersypen, L.; Loiseau, A.; Morandi, V.; Neumaier, D.; Treossi, E.; Pellegrini, V.; Polini, M.; Tredicucci,

- A.; Williams, G. M.; Hee Hong, B.; Ahn, J.-H.; Min Kim, J.; Zirath, H.; van Wees, B. J.; van der Zant, H.; Occhipinti, L.; Di Matteo, A.; Kinloch, I. A.; Seyller, T.; Quesnel, E.; Feng, X.; Teo, K.; Rupesinghe, N.; Hakonen, P.; Neil, S. R. T.; Tannock, Q.; Lofwander, T.; Kinaret, J., Science and technology roadmap for graphene, related two-dimensional crystals, and hybrid systems. *Nanoscale* **2015**, *7*, 4598-4810.
9. van Meer, G.; Voelker, D. R.; Feigenson, G. W., Membrane lipids: Where they are and how they behave. *Nat. Rev. Mol. Cell. Biol.* **2008**, *9* (2), 112-124.
 10. Hirtz, M.; Oikonomou, A.; Georgiou, T.; Fuchs, H.; Vijayaraghavan, A., Multiplexed biomimetic lipid membranes on graphene by dip-pen nanolithography. *Nat. Commun.* **2013**, *4*, 2591.
 11. Wang, Y. Y.; Pham, T. D.; Zand, K.; Li, J.; Burke, P. J., Charging the quantum capacitance of graphene with a single biological ion channel. *ACS Nano* **2014**, *8* (5), 4228–4238.
 12. Ang, P. K.; Jaiswal, M.; Lim, C. H. Y. X.; Wang, Y.; Sankaran, J.; Li, A.; Lim, C. T.; Wohland, T.; Barbaros, Ö.; Loh, K. P., A bioelectronic platform using a graphene–lipid bilayer interface. *ACS Nano* **2010**, *4* (12), 7387-7394.
 13. Connelly, L. S.; Meckes, B.; Larkin, J.; Gillman, A. L.; Wanunu, M.; Lal, R., Graphene nanopore support system for simultaneous high-resolution afm imaging and conductance measurements. *ACS Appl. Mater. Interf.* **2014**, *6* (7), 5290-5296.
 14. Yamazaki, K.; Kunii, S.; Ogino, T., Characterization of interfaces between graphene films and support substrates by observation of lipid membrane formation. *J. Phys. Chem. C* **2013**, *117* (37), 18913-18918.
 15. Tabaei, S. R.; Ng, W. B.; Cho, S.-J.; Cho, N.-J., Controlling the formation of phospholipid monolayer, bilayer, and intact vesicle layer on graphene. *ACS Appl. Mater. Interfaces* **2016**, *8* (18), 11875-11880.
 16. Tu, Y.; Lv, M.; Xiu, P.; Huynh, T.; Zhang, M.; Castelli, M.; Liu, Z.; Huang, Q.; Fan, C.; Fang, H.; Zhou, R., Destructive extraction of phospholipids from escherichia coli membranes by graphene nanosheets. *Nat. Nanotechnol.* **2013**, *8* (8), 594-601.

17. Luan, B.; Huynh, T.; Zhou, R., Complete wetting of graphene by biological lipids. *Nanoscale* **2016**, *8* (10), 5750-5754.
18. Hummers, W. S.; Offeman, R. E., Preparation of graphitic oxide. *J. Am. Chem. Soc.* **1958**, *80* (6), 1339-1339.
19. Li, S. H.; Stein, A. J.; Kruger, A.; Leblanc, R. M., Head groups of lipids govern the interaction and orientation between graphene oxide and lipids. *J. Phys. Chem. B* **2013**, *117* (31), 16150-16158.
20. Frost, R.; Jonsson, G. E.; Chakarov, D.; Svedhem, S.; Kasemo, B., Graphene oxide and lipid membranes: Interactions and nanocomposite structures. *Nano Lett.* **2012**, *12* (7), 3356-3362.
21. Rodriguez-Perez, L.; Herranz, M. A.; Martin, N., The chemistry of pristine graphene. *Chem. Commun.* **2013**, *49* (36), 3721-3735.
22. Titov, A. V.; Kral, P.; Pearson, R., Sandwiched graphene-membrane superstructures. *ACS Nano* **2010**, *4* (1), 229-234.
23. Mao, J.; Guo, R.; Yan, L.-T., Simulation and analysis of cellular internalization pathways and membrane perturbation for graphene nanosheets. *Biomaterials* **2014**, *35* (23), 6069-6077.
24. Yu, Z.-W.; Jin, J.; Cao, Y., Characterization of the liquid-expanded to liquid-condensed phase transition of monolayers by means of compressibility. *Langmuir* **2002**, *18* (11), 4530-4531.
25. Hirtz, M.; Fuchs, H.; Chi, L., Influence of substrate treatment on self-organized pattern formation by langmuir–blodgett transfer. *J. Phys. Chem. B* **2008**, *112* (3), 824-827.
26. Oncins, G.; Picas, L.; Hernández-Borrell, J.; Garcia-Manyes, S.; Sanz, F., Thermal response of langmuir-blodgett films of dipalmitoylphosphatidylcholine studied by atomic force microscopy and force spectroscopy. *Biophys. J.* **2007**, *93* (8), 2713-2725.
27. Arjmandi-Tash, H.; Jiang, L.; Schneider, G. F., Rupture index: A quantitative measure of sub-micrometer cracks in graphene. *Carbon* **2017**, *118*, 556-560.

28. Li, X.; Zhu, Y.; Cai, W.; Borysiak, M.; Han, B.; Chen, D.; Piner, R. D.; Colombo, L.; Ruoff, R. S., Transfer of large-area graphene films for high-performance transparent conductive electrodes. *Nano Lett.* **2009**, *9* (12), 4359-4363.
29. Kim, J.; Cote, L. J.; Kim, F.; Huang, J., Visualizing graphene based sheets by fluorescence quenching microscopy. *J. Am. Chem. Soc.* **2010**, *132* (1), 260-267.
30. Blume, A.; Kerth, A., Peptide and protein binding to lipid monolayers studied by ft-irra spectroscopy. *BBA-Biomembranes* **2013**, *1828* (10), 2294-2305.
31. Tatulian, S. A., Attenuated total reflection fourier transform infrared spectroscopy: A method of choice for studying membrane proteins and lipids. *Biochemistry (Mosc).* **2003**, *42* (41), 11898-11907.
32. Lewis, R. N. A. H.; McElhaney, R. N., Membrane lipid phase transitions and phase organization studied by fourier transform infrared spectroscopy. *BBA-Biomembranes* **2013**, *1828* (10), 2347-2358.
33. Small, D. M., Lateral chain packing in lipids and membranes. *J. Lipid Res.* **1984**, *25* (13), 1490-1500.
34. C. M. Herzinger, W. A. J., J. A. Woollam, Ellipsometric determination of optical constants for silicon and thermally grown silicon dioxide via a multi-sample, multi-wavelength, multi-angle investigation. *J. Appl. Phys.* **1998**, *86* (6), 3323-3336.
35. Yang, X. M.; Xiao, D.; Xiao, S. J.; Wei, Y., Domain structures of phospholipid monolayer langmuir-blodgett films determined by atomic force microscopy. *Appl. Phys. A* **1994**, *59* (2), 139-143.
36. Nemes-Incze, P.; Osváth, Z.; Kamarás, K.; Biró, L. P., Anomalies in thickness measurements of graphene and few layer graphite crystals by tapping mode atomic force microscopy. *Carbon* **2008**, *46* (11), 1435-1442.
37. Das, A.; Pisana S.; Chakraborty B.; Piscanec S.; Saha, S. K.; Waghmare, U. V.; Novoselov, K. S.; Krishnamurthy, H. R.; Geim, A. K.; Ferrari, A. C.; Sood, A. K., Monitoring dopants by raman scattering in an electrochemically top-gated graphene transistor. *Nat. Nanotechnol.* **2008**, *3* (4), 210-215.

38. Pisana, S.; Lazzeri, M.; Casiraghi, C.; Novoselov, K. S.; Geim, A. K.; Ferrari, A. C.; Mauri, F., Breakdown of the adiabatic born-oppenheimer approximation in graphene. *Nat. Mater.* **2007**, *6* (3), 198-201.
39. Yan, J.; Zhang, Y.; Kim, P.; Pinczuk, A., Electric field effect tuning of electron-phonon coupling in graphene. *Phys. Rev. Lett.* **2007**, *98* (16), 166802.
40. Tsukamoto, T.; Yamazaki, K.; Komurasaki, H.; Ogino, T., Effects of surface chemistry of substrates on raman spectra in graphene. *J. Phys. Chem. C* **2012**, *116* (7), 4732-4737.
41. Bruna, M.; Ott, A. K.; Ijäs, M.; Yoon, D.; Sassi, U.; Ferrari, A. C., Doping dependence of the raman spectrum of defected graphene. *ACS Nano* **2014**, *8* (7), 7432-7441.
42. Basko, D. M.; Piscanec, S.; Ferrari, A. C., Electron-electron interactions and doping dependence of the two-phonon raman intensity in graphene. *Phys. Rev. B* **2009**, *80* (16), 165413.
43. Lafkioti, M.; Krauss, B.; Lohmann, T.; Zschieschang, U.; Klauk, H.; Klitzing, K. v.; Smet, J. H., Graphene on a hydrophobic substrate: Doping reduction and hysteresis suppression under ambient conditions. *Nano Lett.* **2010**, *10* (4), 1149-1153.

CHAPTER 3

Encapsulation of graphene in the hydrophobic core of a lipid bilayer

Theoretical simulations predicted that a lipid bilayer forms a stable superstructure when a sheet of graphene is inserted in the hydrophobic core of the bilayer. In this chapter – for the first time – a lipid-graphene-lipid assembly was experimentally constructed. By applying the Langmuir-Blodgett method, a monolayer of lipid was first deposited on a Si/SiO₂ substrate and covered with a graphene monolayer transferred on top. A second lipid monolayer was transferred with the Langmuir-Schaefer method on top of the existing lipid-graphene heterostructure, resulting in graphene sandwiched within the hydrophobic core of a lipid bilayer. The lipid-graphene-lipid assembly presented a very stable and organized structure compared to a lipid bilayer without graphene. Using infrared spectroscopy, ellipsometry and neutron reflectometry the assembly process was characterized at every step, to demonstrate the stability of the superstructure. In the future, if graphene could be electrically probed in such an architecture, this work could yield to the measurement of biochemical phenomena occurring in situ a lipid bilayer.

Publication in preparation: Lia M. C. Lima, Liubov A. Belyaeva, Hadi Arjmandi-Tash, Tetiana Mukhina, Giovanna Fragneto, Alexander Kros, Thierry Charitat, and Grégory F. Schneider.

3.1 Introduction

Lipid bilayers are stable thermodynamic structures obtained from the self-assembly between individual lipid molecules.¹⁻² The assembly process is driven by the amphiphilic behavior of the lipids that have a hydrophilic head group and hydrophobic tails. Depending on the method of preparation, a variety of lipid assemblies can be achieved, such as liposomes,³ supported lipid bilayers,⁴ or lipid monolayers.⁵

Graphene is well known for having outstanding electrical properties and for being atomically flat.⁶⁻⁷ Here, we experimentally compare the morphology of a supported lipid bilayer and its counterpart with graphene encapsulated in the hydrophobic core, with the lipid tails facing graphene on both sides. Previous studies⁸⁻¹¹ using molecular dynamic simulations predicted that graphene can be hosted in principle, inside of a lipid bilayer with no effects on the structural integrity of the bilayer.

Chapter 2 demonstrated that upon coating a lipid monolayer (on Si/SiO₂, lipid tails facing up) with graphene, the lipids underneath graphene showed a more ordered and organized structure compare to the plain lipid monolayer without graphene on top. In this Chapter, another lipid monolayer was transferred on top of the lipid-graphene structure described in Chapter 2 using the Langmuir Schaefer¹² (LS) method.

Graphene was encapsulated within the hydrophobic core of a 1,2-distearoyl-*sn*-glycero-3-phosphocholine (DSPC) bilayer using a three step protocol: i) first a DSPC monolayer is transferred on top of a Si/SiO₂ using the Langmuir-Blodgett¹³ method (LB, Figure 3.1a); ii) second, a graphene monolayer was deposited on top of the Si/SiO₂-supported DSPC monolayer (Figure 3.1b, see Appendix II for experimental details), and iii) finally a last DSPC monolayer was transferred by LS on the lipid-graphene heterostructure (Figure 3.1c). After each step of the assembly process, the construct was characterized systematically using infrared reflection absorption spectroscopy (IRRAS), ellipsometry and neutron reflectometry.

3.2 Results and discussion

The saturated lipid DSPC (Figure 3.1d) was deposited at the air-water interface of a Langmuir trough and compressed to obtain a stable monolayer with a surface pressure (π) of 40 mN/m. Next, the lipid monolayer was transferred on a Si/SiO₂ substrate by retracting the substrate from the trough at a constant π . For the transfer of graphene on top of the lipid monolayer, the ordered lipids on the substrate were brought into contact with graphene floating on an ammonium persulfate solution which was used to etch the copper substrate, as described in Chapter 2. The LS method was used to transfer a final (second) DSPC lipid layer on top of graphene by carefully and controllably lowering the graphene horizontally into contact with the compressed lipid monolayer ($\pi = 40$ mN/m) at the air-water interface, obtaining a lipid-graphene-lipid structure. By this method, graphene was successfully sandwiched into the hydrophobic core of two lipid monolayers, leading to a lipid-graphene-lipid structure.

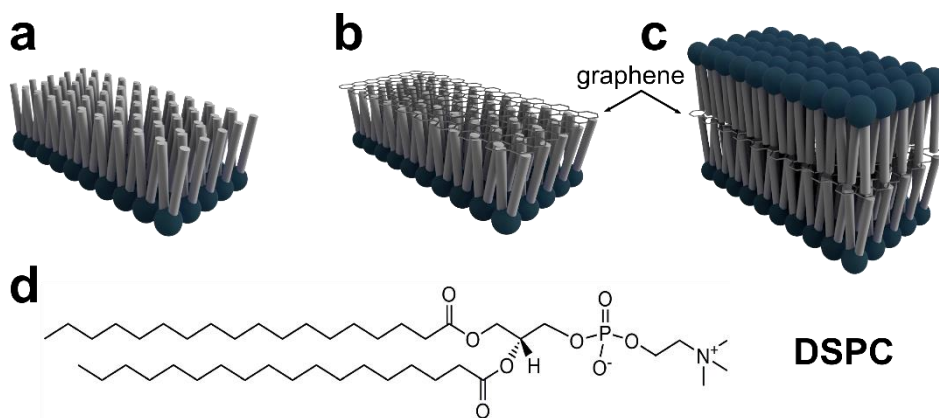


Figure 3.1. Illustration of the lipid structure and schematics of the lipids assembly with graphene. a) Lipid monolayer transferred with the Langmuir-Blodgett method. b) Lipid monolayer with graphene on top. c) Graphene encapsulated in the hydrophobic core of a lipid bilayer. d) Chemical structure of 1,2-distearoyl-*sn*-glycero-3-phosphocholine (DSPC) lipid.

After each step of the assembly process, the conformation of the lipid layers was studied using IRRAS at room temperature. Figure 3.2a shows the IRRAS spectra of the DSPC lipid monolayer deposited on a Si/SiO₂ substrate (black line), after the

deposition of graphene on top of the monolayer (red line), and after the deposition of the second DSPC monolayer (green line).

The absorption bands in Figure 3.2 correspond to the symmetric and asymmetric methylene (CH_2) stretching vibrations of the lipid acyl chains. The peaks were fitted with a Gaussian model. A shift to lower wavenumbers in the symmetric CH_2 vibration from 2911.0 ± 0.1 to $2909.3 \pm 0.1 \text{ cm}^{-1}$ and in the asymmetric CH_2 vibration from 2844.1 ± 0.1 to $2842.1 \pm 0.1 \text{ cm}^{-1}$ is observed after the deposition of graphene above the DSPC lipid monolayer (Figure 3.2a). In addition to this red shift, an increase of the absorption band intensity was observed, corresponding to an expansion of the lipid chains which, as already discussed in Chapter 2, is unexpected as no more lipids were in contact with the sample. The shift is due to an increase of the *trans* conformation within the lipid chains,¹⁴ yielding an overall re-ordering of the lipids, in line with the results described in Chapter 2. Upon the transfer of a second lipid monolayer on top of graphene, the intensity of the absorbance bands increased even further, associated to an increase of the amount of lipids, i.e., the complete transfer of a DSPC monolayer on top of graphene.

In order to understand how the second lipid monolayer structurally organizes on top of graphene and whether graphene does not destabilize two individual DSPC monolayers (i.e., the one on top and the one below graphene), a DSPC lipid bilayer on Si/SiO₂ substrate without graphene was prepared as a control and compared to the DSPC-graphene-DSPC assembly (Figure 3.2b). Compared to the DSPC bilayer, the introduction of graphene in the hydrophobic core of the lipid bilayer showed a shift of the CH_2 vibration peaks to higher wavenumbers (symmetric CH_2 vibration from 2909.8 ± 0.1 to $2911.0 \pm 0.1 \text{ cm}^{-1}$ and in the asymmetric CH_2 vibration from 2843.0 ± 0.1 to $2845 \pm 0.2 \text{ cm}^{-1}$), suggesting that the presence of graphene yields a slightly less ordered lipid bilayer than a plain lipid bilayer (Figure 3.2b). Nevertheless, according to the similarity in IRRAS spectra, graphene does not significantly disturb the IRRAS fingerprint of the lipid bilayer, suggesting the formation of a well-organized and still stable lipid-graphene-lipid structure.

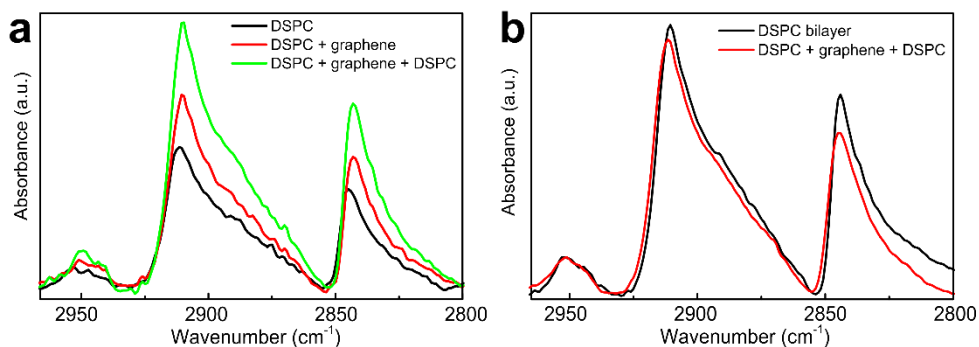


Figure 3.2. Sequential infrared reflection absorption spectroscopy (IRRAS) spectra of the stepwise assembly of DSPC monolayer and graphene yielding the encapsulation of graphene in a DSPC bilayer. a) DSPC monolayer deposited on Si/SiO₂ substrate (black line), the DSPC monolayer after the deposition of graphene on top (red line), and the subsequent transfer of the second DSPC monolayer in the DSPC-graphene stack (green line). b) DSPC bilayer (black line) and DSPC with graphene in air in the hydrophobic core of the lipid bilayer (red line).

Ellipsometry measurements were performed in order to determine the thickness of the phospholipid monolayer on Si/SiO₂ substrates both in the presence and absence of graphene. The thickness of the SiO₂ substrate was determined to be 289.2 ± 1.5 nm. Next, the first deposited DSPC monolayer had a thickness of 3.3 ± 0.3 nm (h_1 , Figure 3.3a), which is in agreement with the neutron reflectometry data for the thickness of a single DSPC monolayer with the contribution of a layer of water between the SiO₂ substrate and the lipid head groups (see Appendix II, Table II.1). After deposition of graphene on top of the DSPC monolayer, the thickness increased from 3.3 ± 0.3 to 4.8 ± 0.2 nm (h_2 , Figure 3.3a). Similar to the results obtained with DPPC (Chapter 2), this increase in thickness indicates that the lipids adopted a more compact and well-organized structure, supporting the IRRAS data (Figure 3.2a). Nevertheless, an increase to 4.8 nm is unexpected for a single DSPC monolayer, due to the head-to-tail length of DSPC. As discussed in Chapter 2 for DPPC, this unrealistic absolute value for the thickness of a lipid monolayer called for the necessity of in-depth analysis of each layer thicknesses using an alternative method, here the neutron reflectometry (see next section). The graphene layer thickness obtained was 0.4 ± 0.1 nm, proving the

successful transfer of a single graphene monolayer (see Appendix II for the details on the fitting procedure).

Finally, a second DSPC monolayer was transferred on top of the graphene-lipid monolayer assembly. Such a transfer always results in the presence of a small water layer at the surface of the assembly. After drying in air, still some water could have remained at the surface. The ellipsometry data was therefore analyzed with and without a water layer in between the lipid head groups. In the absence of a water layer, the thickness obtained for the second DSPC monolayer was 2.6 ± 0.1 nm (h_3 , Figure 3.3a), whereas adding the water layer, DSPC monolayer reached a thickness of 3.7 ± 0.1 nm (h_4 , Figure 3.3a), suggesting that the lipid head groups still retained some water in its vicinity, as the obtained value is comparable to the thickness measured for the first DSPC monolayer. Nevertheless, the neutron reflectometry data showed a thickness of 2.6 nm for the second DSPC monolayer transferred on top of graphene.

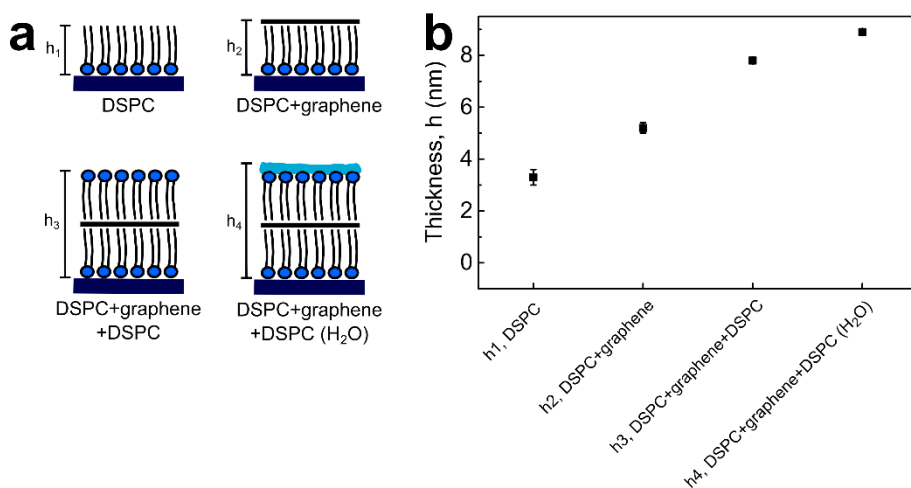


Figure 3.3. Illustration of the lipid-graphene assembly and the corresponding ellipsometry data. a) Stepwise assembly of lipids with graphene yielding the encapsulation of graphene in the hydrophobic core of a DSPC bilayer: DSPC monolayer on a Si/SiO₂ substrate, deposition of a graphene monolayer on top of the DSPC monolayer and transfer of the second DSPC monolayer (with and without water on top). b) Ellipsometry data thicknesses of DSPC monolayer (h_1), DSPC with graphene on top (h_2), and DSPC with graphene and the transfer of a second DSPC monolayer without (h_3) and with water (h_4) on top.

In addition to the IRRAS and ellipsometry studies, neutron reflectometry measurements were also performed. Neutron specular reflectivity is a non-destructive technique which provides information about the thickness, roughness, hydration and composition of the lipid layers at atomic scales.¹⁵⁻¹⁶ Similar to ellipsometry, it resolves several different layers each one with a specific scattering length density (SLD). For this purpose, instead of the standard Si/SiO₂ substrates, the samples were prepared on 5x5 cm² silicon blocks (see Appendix II for experimental methods). The silicon blocks were cleaned and measured with three different contrasts (H₂O, D₂O and silicon matched water, SMW). The silicon block had a SiO₂ layer thickness of 1 nm.¹⁵

The neutron reflectivity measurements of the DSPC in the absence and presence of graphene on the silicon blocks (5x5 cm²) were stored at all times in a liquid environment (hydrophilic lipid head groups of the second lipid monolayer were always facing water) by placing the sample inside a liquid cell for the duration of the measurements. The specular reflectivity profiles (Figure 3.4a) of DSPC lipids at two different contrasts, D₂O (green) and SMW (blue) and the corresponding SLD data (Figure 3.4c), revealed the formation of a lipid bilayer on top of the Si/SiO₂ block. Particularly, the specular reflectivity profiles of the DSPC bilayer with graphene at three different contrasts, H₂O (blue), SMW (green) and D₂O (red), demonstrated that the integrity of the lipid bilayer was preserved when graphene was present in between the lipid monolayers (Figure 3.4b). The comparison of SLD profiles for the lipid bilayer with graphene encapsulated (solid lines, Figure 3.4b and Figure 3.4d), and the SLD profiles of a lipid bilayer without graphene (dashed lines, Figure 3.4b and Figure 3.4d), showed similar profiles suggesting that graphene does not strongly affect the structure of the lipid bilayer (Figure 3.4b and Figure 3.4d), in line with the IRRAS measurements (Figure 3.2b). The results showed no off-specular signal even if the lateral coverage of graphene was not homogeneous and continuous all over the sample. The graphene monolayer does not significantly alter the reflectivity curve, most likely due to the inherent one carbon atom thickness and the low graphene surface coverage (<50%), resulting in a SLD value lower than expected (Figure 3.4d). Therefore, the neutron reflectivity results do not prove the presence of the graphene sheet in the lipid bilayer, but clearly demonstrate that the integrity of the bilayer is preserved. Nevertheless, the transfer of graphene on top of the lipid monolayer is confirmed with the

ellipsometry measurements and with the Raman spectroscopy measured in Chapter 2, Figure 2.4.

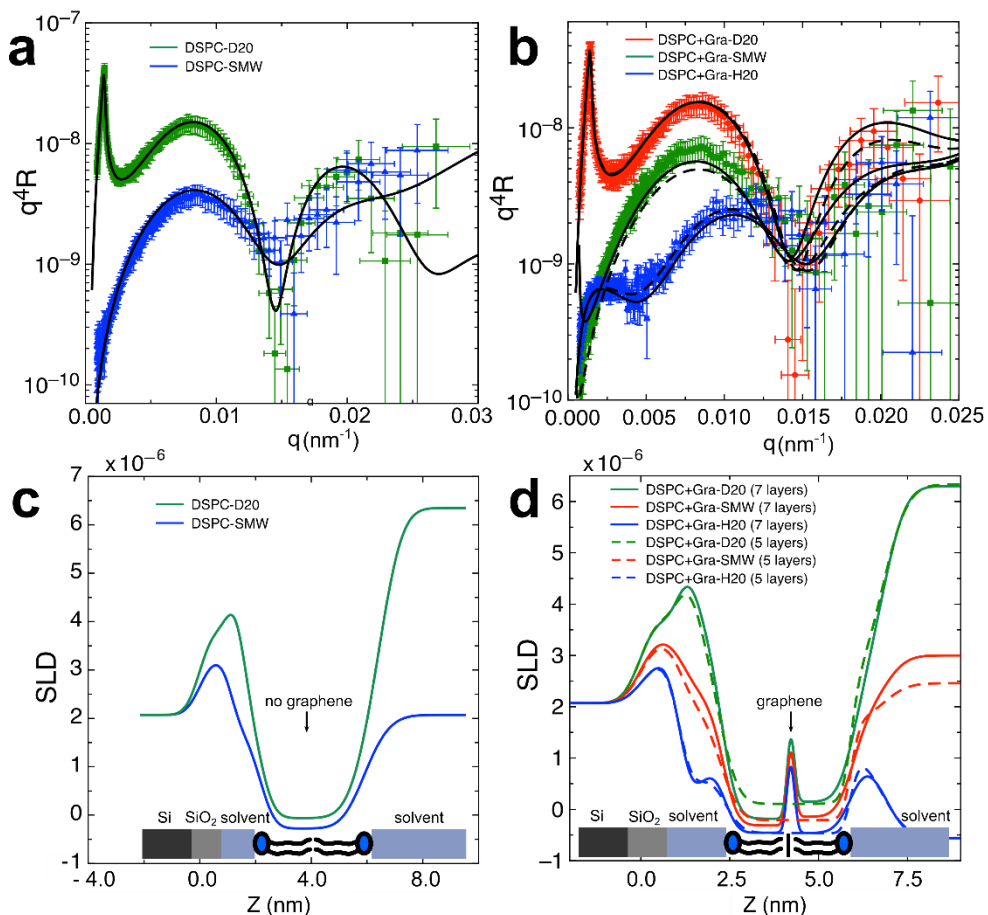


Figure 3.4. Neutron reflectivity (q^4R) characterization of a supported DSPC bilayer on a silicon block with and without graphene encapsulated in the hydrophobic core of the bilayer. a) DSPC bilayer at 25 °C with two different contrasts, D₂O (green line) and silicon matched water (SMW, blue line). b) DSPC bilayer at 25 °C with graphene in the hydrophobic core of the lipid bilayer with three different contrasts: H₂O (blue), SMW (green) and D₂O (red). The black lines correspond to the best fit and dashed black lines correspond to a fit without graphene (only the lipid bilayer). c) The corresponding SLD for the DSPC bilayer with two different contrasts, D₂O (green line) and SMW (blue line). d) The corresponding SLD for the DSPC-graphene-DSPC assembly with three different contrasts: H₂O (blue line), SMW (red line) and D₂O (green line). The dashed black lines correspond to a fit without graphene (only the lipid bilayer).

3.3 Conclusion

The successful assembly of graphene within the hydrophobic core of a DSPC bilayer was demonstrated and characterized in detail using IRRAS, ellipsometry and neutron reflectivity measurements. The characterization techniques are in agreement and confirmed the stable arrangement of lipids below and above graphene, with no significant perturbation compared to a plain lipid bilayer. The neutron reflectivity yielded data on the fine structure of the assembly, and concluded that the presence of graphene preserved the integrity of the lipid bilayer. The demonstration of placing graphene within the hydrophobic core of a lipid bilayer opens up a route of directly probing biological membrane related processes in situ using graphene as an electrical sensor.

3.4 References

1. Tristram-Nagle, S.; Nagle, J. F., Lipid bilayers: Thermodynamics, structure, fluctuations, and interactions. *Chem. Phys. Lipids* **2004**, *127* (1), 3-14.
2. M., E.; M., D., From biological membranes to biomimetic model membranes. *Biotechnol. Agron. Soc. Environ.* **2010**, *14* (4), 719-736.
3. Szoka, F.; Papahadjopoulos, D., Comparative properties and methods of preparation of lipid vesicles (liposomes). *Annu. Rev. Biophys. Bioeng.* **1980**, *9*, 467-508.
4. Eeman, M.; Deleu, M., From biological membranes to biomimetic model membranes. *Biotechnol. Agron. Soc. Environ.* **2010**, *14* (4), 719-736.
5. McConnell, H. M., Structures and transitions in lipid monolayers at the air-water interface. *Annu. Rev. Phys. Chem.* **1991**, *42*, 171-195.
6. Novoselov, K. S.; Geim, A. K.; Morozov, S. V.; Jiang, D.; Zhang, Y.; Dubonos, S. V.; Grigorieva, I. V.; Firsov, A. A., Electric field effect in atomically thin carbon films. *Science* **2004**, *306* (5696), 666-669.
7. Castro Neto, A. H.; Guinea, F.; Peres, N. M. R.; Novoselov, K. S.; Geim, A. K., The electronic properties of graphene. *Rev. Mod. Phys.* **2009**, *81* (1), 109-162.
8. Titov, A. V.; Kral, P.; Pearson, R., Sandwiched graphene-membrane superstructures. *ACS Nano* **2010**, *4* (1), 229-234.
9. Mao, J.; Guo, R.; Yan, L.-T., Simulation and analysis of cellular internalization pathways and membrane perturbation for graphene nanosheets. *Biomaterials* **2014**, *35* (23), 6069-6077.
10. Chen, J.; Zhou, G.; Chen, L.; Wang, Y.; Wang, X.; Zeng, S., Interaction of graphene and its oxide with lipid membrane: A molecular dynamics simulation study. *J. Phys. Chem. C* **2016**, *120* (11), 6225-6231.

11. Wang, J.; Wei, Y.; Shi, X.; Gao, H., Cellular entry of graphene nanosheets: The role of thickness, oxidation and surface adsorption. *RSC Adv.* **2013**, *3* (36), 15776-15782.
12. Bang, J. J.; Porter, A. G.; Davis, T. C.; Hayes, T. R.; Claridge, S. A., Spatially controlled noncovalent functionalization of 2D materials based on molecular architecture. *Langmuir* **2018**, *34* (19), 5454-5463.
13. Yu, Z.-W.; Jin, J.; Cao, Y., Characterization of the liquid-expanded to liquid-condensed phase transition of monolayers by means of compressibility. *Langmuir* **2002**, *18* (11), 4530-4531.
14. Lewis, R. N. A. H.; McElhaney, R. N., Membrane lipid phase transitions and phase organization studied by fourier transform infrared spectroscopy. *BBA-Biomembranes* **2013**, *1828* (10), 2347-2358.
15. Charitat, T.; Bellet-Amalric, E.; Fragneto, G.; Graner, F., Adsorbed and free lipid bilayers at the solid-liquid interface. *Eur. Phys. J. B Condens. Matter Compl. Syst.* **1999**, *8* (4), 583-593.
16. Lecuyer, S.; Fragneto, G.; Charitat, T., Effect of an electric field on a floating lipid bilayer: A neutron reflectivity study. *Eur. Phys. J. E* **2006**, *21* (2), 153-159.

CHAPTER 4

Effect of temperature on the structure of lipids in the presence of graphene

Understanding how lipids respond to changes in temperature is important to design stable and well-defined lipid-graphene assemblies. Here, the effect of temperature on the structure and stability of a lipid monolayer with and without graphene on top was studied. Above the phase transition temperature, lipids presented a fluidic phase resulting in a decrease in layer thickness and order as measured by atomic force microscopy (AFM) and infrared spectroscopy. Furthermore, graphene acts as a protecting layer preventing the lipids underneath graphene from being removed, after a washing step using the surfactant hexadecyltrimethylammonium bromide (CTAB). Infrared spectroscopy studies revealed that upon cooling the temperature from above to below the phase transition temperature, the lipids underwent the expected conformation changes from a more ordered to a less ordered structure. The changes in lipid conformation with graphene transferred on top, above and below the phase transition temperature, revealed a stable heterostructure enabling the design of well-defined biosensors with graphene.

Manuscript in preparation: Lia M. C. Lima, Hadi Arjmandi-Tash, Grégory F. Schneider.

4.1 Introduction

In Chapter 2 and 3 the formation of lipid-graphene assemblies were characterized, i.e. namely graphene on a lipid monolayer and graphene encapsulated within the hydrophobic core of a lipid bilayer. In this Chapter, the effect of temperature on the stability of lipid-graphene assemblies is investigated.

A lipid assembly can exist in different phases characterized by the conformational order and lateral diffusion of the lipids, depending on temperature, composition, concentration, pressure and pH.¹ More specifically, phospholipids undergo a gel-to-liquid phase transition temperature (T_m) which is dependent on the chemical composition of the lipid head group, lipid size, and structure of the hydrocarbon chain.² At very low temperatures, the phospholipids are typically packed in a sub-gel phase (L_c) with a well-organized and compact structure. Upon heating, a transition to a gel-phase ($L_{\beta'}$) occurs where the hydrocarbon chains start to present some degree of flexibility. After increasing the temperature further, the phospholipids undergo a pre-transition with a rippled arrangement ($P_{\beta'}$) in the structure and, above the T_m , a liquid-crystalline phase (L_{α}) is formed (Figure 4.1). The lipids display a *trans* to *gauche* conformation change in the acyl chain with a high increase on the mobility.³⁻⁴

The phospholipid 1,2-dipalmitoyl-*sn*-glycero-3-phosphocholine (DPPC) used in this study exhibits mainly two distinct phase transitions. At room temperature (RT), DPPC presents a $L_{\beta'}$ phase with a tilted arrangement. Upon increasing the temperature, the lipids undergo a $P_{\beta'}$ pre-transition at ~ 35 °C followed by the main phase transition T_m (gel-to-liquid crystal) at ~ 41 °C, resulting in a fluidic phase L_{α} .⁵⁻⁶

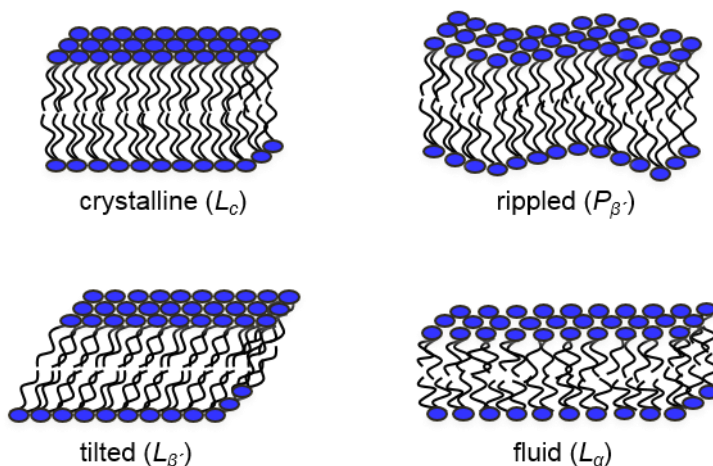


Figure 4.1. Schematic illustration of the molecular organization of lipid bilayers at different phase temperatures: crystalline (L_c), tilted ($L_{\beta'}$), rippled ($P_{\beta'}$) and fluid (L_{α}) phase.

Atomic force microscopy (AFM) was used here to image the surface of the lipid monolayer with and without graphene on top and study the morphology and lateral organization of the lipids at a nanometer resolution.⁷ Furthermore, AFM was performed to monitor the effect of temperature on the structure of the membrane.⁸ In fact, the temperature influences the packing and the lateral interactions between the lipid molecules, resulting in AFM images from which the step heights were extracted.⁹⁻¹¹ Increasing the temperature of the lipids destabilizes the lipid membrane with a concomitant decrease of the thickness of the lipid monolayer, suggesting a lateral expansion of the lipids on the surface.

Complementary to AFM, infrared reflection absorption spectroscopy (IRRAS) was used to study the structure of the lipid monolayer, particularly to monitor the phase transition temperatures.¹²⁻¹³ As already mentioned in Chapter 3, IRRAS also yields information on the vibrational frequency of the lipid hydrocarbon chains.¹² Depending on the temperature state of the lipids, i.e., the phase transition temperature T_m , a variation on the absorption bands can be observed and monitored by IRRAS spectroscopy. Above the T_m , the absorption bands show typically a broadening of the vibration peak and a decrease of the peak intensity.¹³

In this study, AFM and IRRAS measurements were dually performed to investigate the effect of temperature on the structure and stability of lipids with and without a graphene layer on top of the lipid monolayer. Lipids tend to decrease their thickness above the T_m and lipids covered with graphene cannot be removed even after a washing step involving organic solvents, such as chloroform or an aqueous solution of hexadecyltrimethylammonium bromide (CTAB). Additionally, IRRAS revealed a decrease in peak intensity and a shift to higher wavenumbers with increasing temperature, characteristic of a lower lipid molecular order. Remarkably, the lipids underneath graphene are less susceptible to phase transitions than lipids not covered with graphene.

4.2 Results and discussion

On the air-water interface of a Langmuir trough DPPC lipids were deposited, compressed to a surface pressure (π) of 30 mN/m and transferred to Si/SiO₂ substrates using the Langmuir-Blodgett method (Figure 4.2a). A chemical vapor deposition (CVD) graphene layer was then transferred on top of the DPPC monolayer (Figure 4.2b), as described previously in Chapter 2.

For AFM experiments, the samples were treated with one heating-cooling cycle (RT – 60 °C – RT, above the T_m of DPPC) and left at 60 °C for five minutes using a hot plate. Prior to imaging, the samples were cooled down to RT. Upon imaging, the samples were subsequently subjected to five heating-cooling cycles (RT – 60 °C – RT) and subsequently scanned by AFM. After that, a second heating-cooling cycle (RT – 100 °C – RT) was performed five times for five minutes each time and the topography of the samples was measured again.

Afterwards, a second DPPC lipid monolayer was transferred using the Langmuir-Schaefer (LS) method¹⁴ at $\pi = 30$ mN/m on top of the graphene layer, forming a lipid-graphene-lipid assembly (Figure 4.2c). The sample was characterized by AFM and subsequently cleaned with chloroform by dipping the sample into the chloroform several times and scanned again by AFM. As a control measurement, a plain DPPC monolayer ($\pi = 30$ mN/m) on Si/SiO₂ substrate was also characterized by AFM.

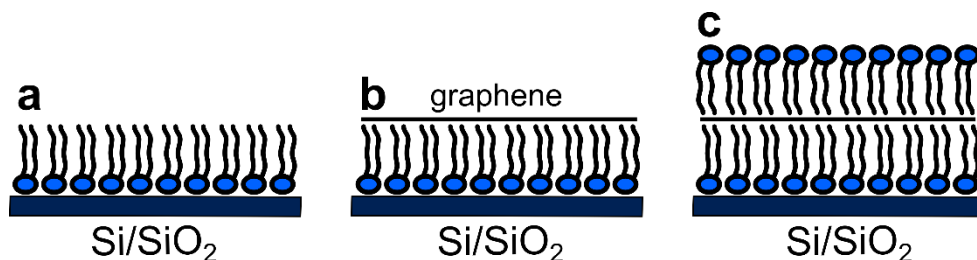


Figure 4.2. Schematic illustration of graphene-lipid constructs studied in this chapter. a) A DPPC lipid monolayer assembled on Si/SiO₂ substrate. b) The DPPC monolayer with a layer of graphene deposited on top. c) A graphene monolayer encapsulated in between two DPPC layers (tails facing towards the graphene).

A transfer ratio (T_{ratio}) of approximately one for the DPPC monolayer transferred on Si/SiO₂ substrate was obtained, indicative of complete transfer of a well-ordered lipid monolayer. Optical images of graphene transferred on top of the DPPC monolayer are shown in Figure 4.3. The graphene layer stayed intact on top of the lipids (in purple) during the heating cycles (Figure 4.3a, b, c). At 100 °C (Figure 4.3d), graphene became unstable and folded in some parts of the sample. Graphene remained intact after the transfer of a second DPPC monolayer on top (Figure 4.3e). When the sample was rinsed with chloroform, the graphene sheet was partially removed from the sample (Figure 4.3f).

To investigate whether the heating-cooling cycles and the transfer of a second lipid monolayer affected the morphology of the DPPC layer(s), AFM imaging was performed. Analysis of height step profiles in the AFM images of a DPPC monolayer transferred using the LB method at $\pi = 30$ mN/m on a Si/SiO₂ substrate (Figure 4.4a) revealed a thickness of 1.8 ± 0.2 nm, which is slightly smaller compared to literature data (i.e., 2.4 – 2.8 nm).¹⁵ The lower thickness could be associated to the hardness of the AFM tip (70 kHz nominal resonance frequency, due to the rigid graphene surface) used in this work compared to softer tips typically used for scanning lipid membranes.¹⁶

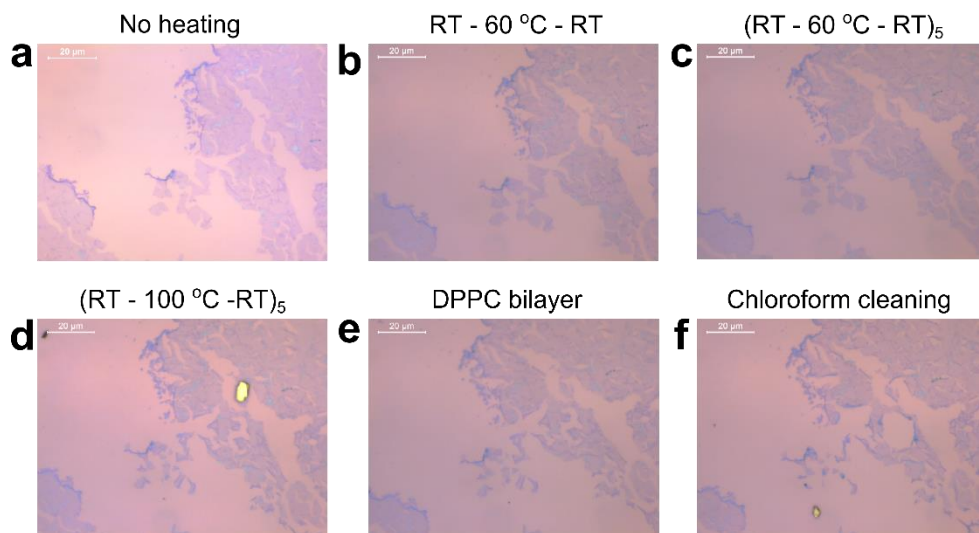


Figure 4.3. Optical bright field imaging of graphene on a lipid monolayer transferred on Si/SiO₂ substrate. a) Graphene transferred above a DPPC lipid monolayer. b) DPPC-graphene assembly after one cycle of heating-cooling (RT – 60 °C – RT). c) DPPC-graphene assembly after five cycles of heating-cooling (RT – 60 °C – RT)₅. d) DPPC-graphene assembly after five cycles of heating-cooling (RT – 100 °C – RT)₅. e) After transferring a second DPPC lipid monolayer on top of graphene. f) DPPC-graphene assembly after rinsing the sample with chloroform.

After one heating-cooling cycle the DPPC monolayer above the T_m , a decrease of the thickness to 1.2 ± 0.2 nm is observed, corresponding to a change from a gel $L_{\beta'}$ to a liquid L_{α} phase (Figure 4.4b). After five heating-cooling cycles (RT – 60 °C – RT), the lipid patches became more uniform and formed a continuous lipid monolayer on the surface of the substrate, rendering impossible to measure the lipids step height (Figure 4.4c). The roughness measured on flat sections of the image was 0.26 ± 0.10 nm. The same uniformity was observed after five heating-cooling cycles (RT – 100 °C – RT, Figure 4.4d), however the roughness decreased to 0.22 ± 0.10 nm.

After the transfer of a second lipid monolayer on top of the first DPPC monolayer assembly, the lipids tended to form small agglomerates instead of spreading evenly over the surface (Figure 4.4e). Indeed, the transfer ratio of the second lipid monolayer using the LS method was < 1 , indicative of an incomplete

lipid monolayer transfer. This lower transfer ratios is in agreement with the formation of lipid agglomerates with thicknesses ranging from 2.1 ± 0.3 to 4.9 ± 0.3 nm, as measured by AFM. In addition, the sample was not kept in a liquid environment, leading to a less stable lipid bilayer as the hydrophilic lipid head groups are forced to face the air in these dry samples, as observed previously.¹⁷ Next, the sample was rinsed with chloroform (Figure 4.4f) with a decrease of the roughness to 0.21 ± 0.10 nm. Surprisingly, the lipid agglomerates disappeared from the surface, probably due to the instability of the second lipid layer in air.

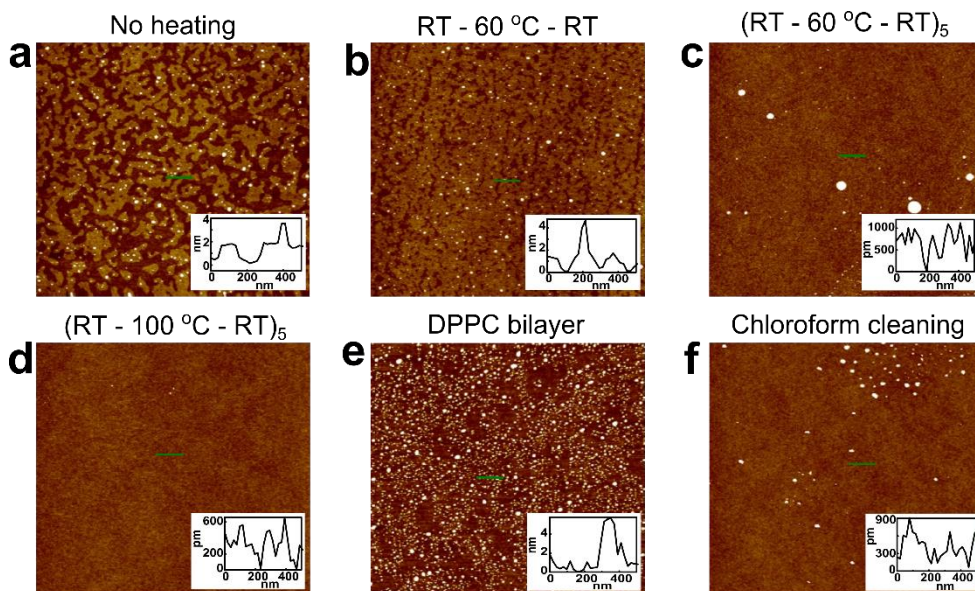


Figure 4.4. AFM intermittent contact mode images in air and the corresponding step heights of $5 \times 5 \mu\text{m}^2$ of DPPC on Si/SiO₂ substrate. a) DPPC monolayer transferred by the LB method at 30 mN/m on Si/SiO₂. b) DPPC monolayer after one cycle of heating-cooling (RT - 60 °C - RT). c) DPPC monolayer after five cycles of heating-cooling (RT - 60 °C - RT). d) DPPC monolayer after five cycles of heating-cooling (RT - 100 °C - RT). e) Second DPPC monolayer transferred on top of the first DPPC monolayer. f) DPPC lipids after rinsing the sample with chloroform.

Next, graphene was deposited on top of a DPPC monolayer on Si/SiO₂ and a heating-cooling cycle was performed. AFM was used to study whether the lipids underneath and surrounding graphene (i.e., lipids not covered with graphene, for example at cracks) change in morphology upon a temperature cycling and upon

rinsing the sample with chloroform and an aqueous solution of CTAB. Surprisingly, the lipid monolayer on the surroundings of graphene showed less lipid patches (Figure 4.5a) compared to the lipid monolayer on Si/SiO₂ (Figure 4.4a). The measured graphene thickness was 1.3 ± 0.1 nm. After a heating cooling cycle (RT – 60 °C – RT), the lipids on the surroundings of graphene rearranged in lipid patches and the graphene decreased slightly its thickness to 0.9 ± 0.1 nm (Figure 4.5b). After five heating-cooling cycles (RT – 60 °C – RT), the lipid patches spread more evenly over all the surface (Figure 4.5c) and a similar thickness for the graphene layer was measured, i.e., 1.0 ± 0.1 nm. After five more heating-cooling cycles (RT – 100 °C – RT), the lipids presented a more uniform and continuous layer with some parts of the graphene folded on itself or partially removed from the substrate (Figure 4.5d), as also confirmed by optical microscopy (Figure 4.3d). The graphene thickness measured on a monolayer remained unchanged, i.e. 1.0 ± 0.2 nm. Upon transferring the second lipid layer on top of DPPC coated with graphene, small lipid agglomerates formed (Figure 4.5e). The thickness of graphene increased to 1.5 ± 0.3 nm, as some lipid aggregates were also present on the graphene surface, yielding a thicker graphene. As also observed on the optical images, Figure 4.3f, rinsing the sample with chloroform also yielded the folding and the partial removal of the graphene from the surface (Figure 4.5f). The small lipid agglomerates were also removed from the sample, as observed for Si/SiO₂ (Figure 4.4f).

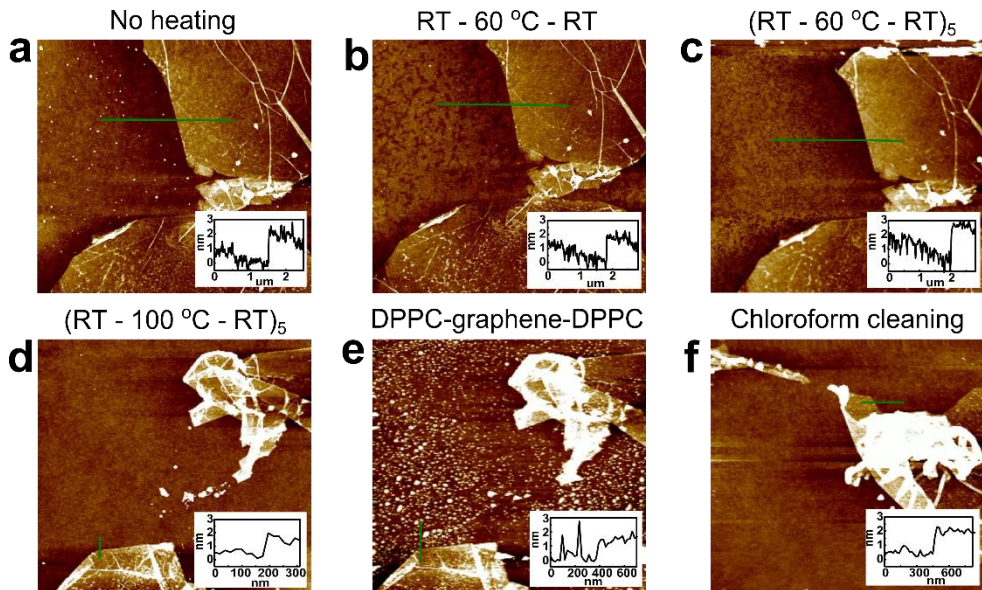


Figure 4.5. AFM intermittent contact mode images in air and the corresponding step heights of $5 \times 5 \mu\text{m}^2$ of graphene transferred on top of DPPC on a Si/SiO₂ substrate. a) Graphene transferred above a DPPC monolayer. b) Graphene on a DPPC monolayer after one cycle of heating-cooling (RT – 60 °C – RT). c) Graphene on DPPC monolayer after five cycles of heating-cooling (RT – 60 °C – RT)₅. d) Graphene folded on DPPC monolayer after five cycles of heating-cooling (RT – 100 °C – RT)₅. e) Second DPPC monolayer transferred on top of a monolayer of DPPC coated with graphene. f) DPPC-graphene-DPPC after rinsed with chloroform.

In order to confirm whether the lipids remained at the surface of the substrate after a chloroform washing step, fluorescence microscopy experiments were performed. For this, 1 mol% of 1,2-dipalmitoyl-*sn*-glycero-3-phosphoethanolamine-N-(lissamine rhodamine B sulfonyl) (Liss Rhod PE) was added to the DPPC lipids prior to compression. A lipid monolayer on Si/SiO₂ with a graphene layer on top was obtained and imaged with fluorescence microscopy before and after a washing step with chloroform (Figure 4.6a and b, respectively). The lipids (bright areas) underneath graphene (black areas) and on the surroundings of graphene, presented a continuous and uniform layer, but after being rinsed with chloroform, large lipid agglomerates formed on the surface (Figure 4.6b). Surprisingly, these large agglomerates were not observed on the AFM images (Figure 4.5f). Nevertheless, the chloroform does not completely

remove the lipids from the surface of the substrate. To test whether it is possible to completely remove the lipids, the substrate was rinsed with a 10 mM CTAB aqueous solution known to solubilize lipids efficiently.¹⁸ For this, the sample was dipped vertically up and down seven times in a CTAB solution and finally washed with ultrapure water to remove the excess of surfactant. The sample showed no traces of the fluorescent lipids anymore, confirming that CTAB successfully dissolved all the lipids from the surface (Figure 4.6c). However, it is not possible to conclude at this stage whether graphene was also removed by CTAB, as graphene quenches the fluorescence of the lipids underneath. AFM imaging was performed to investigate whether graphene was still present (Figure 4.6d, e, f).

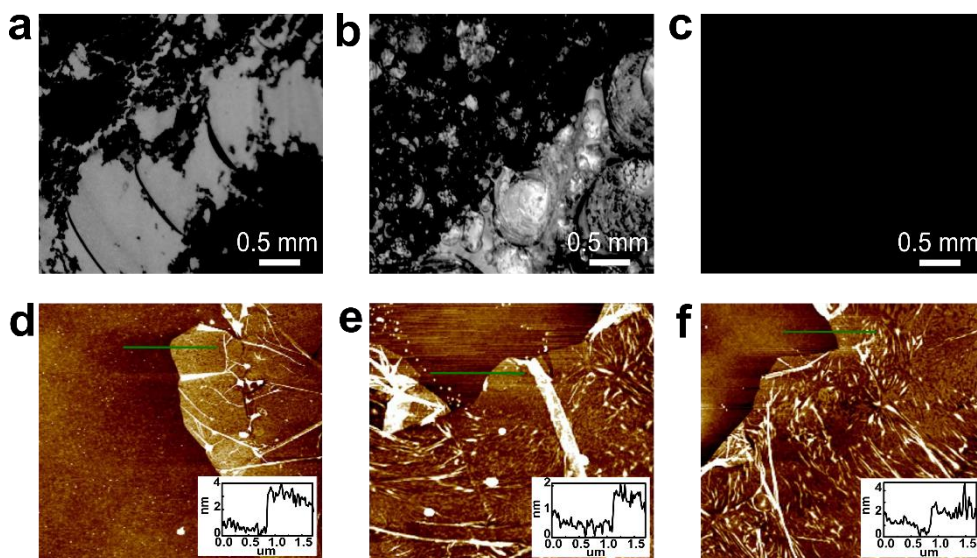


Figure 4.6. Fluorescence and AFM images ($5 \times 5 \mu\text{m}^2$) in air of graphene-lipid assemblies. a) Fluorescence image of graphene (black areas) transferred above a DPPC:Liss Rhod PE (99:1) monolayer (light areas). b) Fluorescence image of graphene (black areas) transferred above a DPPC:Liss Rhod PE (99:1) monolayer (light areas) after being rinsed with chloroform. c) Fluorescence image of a clean surface – no lipid fluorophores – after being rinsed with CTAB. d) AFM image of graphene transferred above a DPPC Liss Rhod PE (99:1) monolayer. e) AFM image of graphene transferred above a DPPC Liss Rhod PE (99:1) monolayer after being rinsed with chloroform. f) AFM image of graphene transferred above a DPPC Liss Rhod PE (99:1) monolayer after being rinsed with CTAB.

The AFM images of graphene deposited on a DPPC:Liss Rhod PE (99:1) monolayer revealed a graphene thickness of 1.4 ± 0.2 nm (Figure 4.6d), in agreement with the thickness of the previous sample with only DPPC lipids (Figure 4.5a). Again, after rinsing the sample with chloroform, some parts of the graphene folded and others were partly removed from the sample. However, graphene was present at different positions (Figure 4.6e) with an equivalent thickness of 1.3 ± 0.2 nm. After rinsing the sample with CTAB, the thickness of graphene (which was again partially removed from the surface) decreased to 0.8 ± 0.1 nm (Figure 4.5f). Such a lower height for graphene suggests that CTAB removed the lipids near the edges of graphene (as observed by the fluorescence image in Figure 4.6c). In addition, this lower step height indicates the presence of a shield-graphene layer where graphene is on top of the lipid monolayer until the edge where graphene is in direct contact with the Si/SiO₂ substrate with no lipids underneath, therefore resulting in a slight decrease of the measured thickness of graphene at the edge on the AFM step profiles (Figure 4.7c). AFM could not quantify how far from the edges the lipids underneath graphene were removed. The assumption here is that if all the lipids underneath graphene would have been removed by CTAB, graphene would have desorbed from the substrate. The step heights for all the samples analyzed are shown in Figure 4.7a and b.

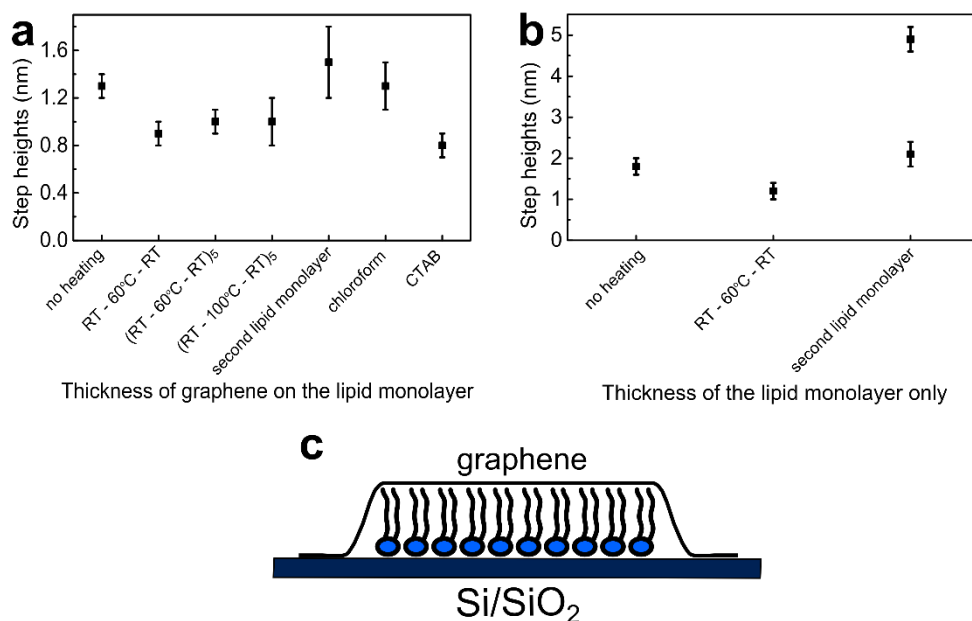


Figure 4.7. Step heights of graphene and lipids measured by AFM. a) Thickness of graphene on a DPPC monolayer before and after one cycle heating cooling (RT – 60 °C – RT); after five cycles of heating-cooling (RT – 60 °C – RT); after five cycles of heating-cooling (RT – 100 °C – RT); after the transfer of a second lipid monolayer on top of DPPC-graphene; after being rinsed with chloroform and; finally cleaned with an aqueous solution of 10 mM of CTAB. b) Thickness of the lipid monolayer before and after one cycle heating cooling (RT – 60 °C – RT); and after the transfer of a second lipid monolayer on top without graphene. c) Illustration of the shielded-graphene where graphene acts as a protective layer for the lipid monolayer underneath assembled on a Si/SiO₂ substrate.

For IRRAS experiments, temperature cycles were carried using a resistive heater positioned on the sample holder used for IRRAS. The sample (Si/SiO₂, DPPC monolayer and graphene on top) was mounted on the resistor using silver paste (see Figure III.1a, Appendix III). Direct current (DC) biasing the resistor heated up the sample. A commercially available probe thermometer including a thermocouple glued onto the sample was used to monitor the temperature. The sample was subjected to heating-cooling cycles (RT – 78 °C – RT) by slowly increasing or decreasing (respectively) the voltage applied to the sample step by step (see Appendix III for experimental details). The shifts on the absorption bands of the symmetric and asymmetric methylene stretching vibrations of the lipid

chains for different temperatures indicated a change in lipid conformation, from a gel $L_{\beta'}$ to a liquid L_{α} phase (Figure 4.8). The slow increase of the temperature step-by-step (see Figure III.1b, Appendix III) resulted in melting of the hydrocarbon lipid chains, as shown by the decreasing intensities of the symmetric and asymmetric CH_2 vibration peaks and the shift of the peak maximum to higher wavenumbers (Figure 4.8a). Decreasing the temperature to RT showed the same trend but in opposite directions (Figure 4.8b): the absorption bands showed increased intensities and shifted to lower wavenumbers upon cooling, characteristic of a higher molecular order of the lipids. Notably, around the T_m of DPPC (42 °C), the absorption peak revealed a slightly higher shift compared to lower temperatures (34 °C). This peculiar behavior was also observed in previous studies, suggesting an “atypical softening”, i.e. a sudden unexpected decrease in the ordering of the lipids around the T_m .¹⁰

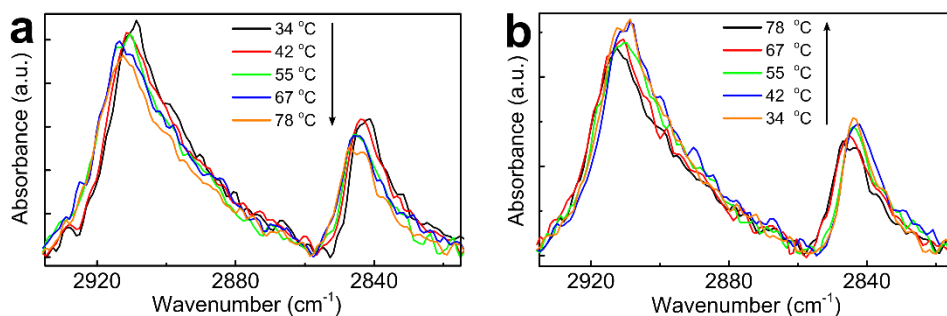


Figure 4.8. Infrared reflection absorption spectroscopy (IRRAS) spectra of a DPPC monolayer underneath graphene. a) Absorption bands of the symmetric and asymmetric methylene stretching vibrations of the lipid chains with increasing temperatures, 34, 42, 55, 67, 78 °C. b) Absorption bands of the symmetric and asymmetric stretching vibrations of the lipid chains with decreasing temperatures steps: 78, 67, 55, 42, 34 °C.

4.3 Conclusions

In this work the effect of temperature on the lipids structure and lateral organization was studied by AFM and IRRAS spectroscopy. By AFM, topographies and step heights of the supported DPPC monolayer with and without graphene on top were analyzed in detail. The lipids decreased their thickness upon increasing the temperature to 60 °C – above the T_m of DPPC, 41 °C – and laterally diffused on

the surface of the Si/SiO₂ substrate. Upon cycling the temperature five times between room temperature and 60 °C (respectively 100 °C), the lipids covered all the substrate surface forming a continuous lipid monolayer, characteristic of the L_α fluidic phase. Heating to 100 °C yielded graphene to fold, at best to be partially removed from the surface. The transfer of a second lipid monolayer yielded the formation of lipid agglomerates both on the lipid monolayer and on graphene which could be subsequently removed by rinsing the sample with chloroform.

Additionally, the surfactant solution (CTAB) removed all the lipids from underneath the edges of graphene, while minimally affecting the lipids underneath graphene. Furthermore, IRRAS experiments demonstrated that the lipid monolayer was re-organized upon temperature variations as evidenced from the shifts of the wavenumbers on the intensity of the symmetric and asymmetric CH₂ vibrations bands, attributed to a variation of the conformational order and organization of the lipids.

In conclusion, covering a lipid monolayer with graphene yields a graphene heterostructure that is stable upon temperature variations (here up to 100 °C), allowing the construction of temperature stable sensors based on graphene.

4.4 References

1. Jacobson, K.; Papahadjopoulos, D., Phase transitions and phase separations in phospholipid membranes induced by changes in temperature, pH, and concentration of bivalent cations. *Biochemistry* **1975**, *14* (1), 152-161.
2. Cevc, G., How membrane chain-melting phase-transition temperature is affected by the lipid chain asymmetry and degree of unsaturation: An effective chain-length model. *Biochemistry* **1991**, *30* (29), 7186-7193.
3. M., E.; M., D., From biological membranes to biomimetic model membranes. *Biotechnol. Agron. Soc. Environ.* **2010**, *14* (4), 719-736.
4. Kučerka, N.; Nieh, M.-P.; Katsaras, J., Fluid phase lipid areas and bilayer thicknesses of commonly used phosphatidylcholines as a function of temperature. *BBA - Biomembranes* **2011**, *1808* (11), 2761-2771.
5. Tristram-Nagle, S.; Nagle, J. F., Lipid bilayers: Thermodynamics, structure, fluctuations, and interactions. *Chem. Phys. Lipids* **2004**, *127* (1), 3-14.
6. Chatzigeorgiou, P.; Mourelatou, A.; Pollatos, E.; Margari, D.; Zogzas, N.; Viras, K.; Mavromoustakos, T.; Semidalas, C. E., Comparison of the thermal behavior and conformational changes in partially and fully hydrated dipalmitoylphosphatidylcholine systems. *J. Therm. Anal. Calorim.* **2018**, *131* (2), 887-898.
7. El Kirat, K.; Morandat, S.; Dufrene, Y. F., Nanoscale analysis of supported lipid bilayers using atomic force microscopy. *BBA-Biomembranes* **2010**, *1798* (4), 750-765.
8. Zhong, J., From simple to complex: Investigating the effects of lipid composition and phase on the membrane interactions of biomolecules using in situ atomic force microscopy. *Integr. Biol.* **2011**, *3* (6), 632-644.
9. Alessandrini, A.; Facci, P., Phase transitions in supported lipid bilayers studied by afm. *Soft Matter* **2014**, *10* (37), 7145-7164.

10. Garcia-Manyes, S.; Oncins, G.; Sanz, F., Effect of temperature on the nanomechanics of lipid bilayers studied by force spectroscopy. *Biophys. J.* **2005**, *89* (6), 4261-4274.
11. Ramkaran, M.; Badia, A., Gel-to-fluid phase transformations in solid-supported phospholipid bilayers assembled by the langmuir–blodgett technique: Effect of the langmuir monolayer phase state and molecular density. *J. Phys. Chem. B* **2014**, *118* (32), 9708-9721.
12. Tamm, L. K.; Tatulian, S. A., Infrared spectroscopy of proteins and peptides in lipid bilayers. *Q. Rev. Biophys.* **1997**, *30* (4), 365-429.
13. Lewis, R. N. A. H.; McElhaney, R. N., Membrane lipid phase transitions and phase organization studied by fourier transform infrared spectroscopy. *BBA-Biomembranes* **2013**, *1828* (10), 2347-2358.
14. Bang, J. J.; Porter, A. G.; Davis, T. C.; Hayes, T. R.; Claridge, S. A., Spatially controlled noncovalent functionalization of 2d materials based on molecular architecture. *Langmuir* **2018**, *34* (19), 5454-5463.
15. Yang, X. M.; Xiao, D.; Xiao, S. J.; Wei, Y., Domain structures of phospholipid monolayer langmuir-blodgett films determined by atomic force microscopy. *Appl. Phys. A* **1994**, *59* (2), 139-143.
16. Richter, R. P.; Brisson, A. R., Following the formation of supported lipid bilayers on mica: A study combining afm, qcm-d, and ellipsometry. *Biophys. J.* **2005**, *88* (5), 3422-3433.
17. Scomparin, C.; Lecuyer, S.; Ferreira, M.; Charitat, T.; Tinland, B., Diffusion in supported lipid bilayers: Influence of substrate and preparation technique on the internal dynamics. *Eur. Phys. J. E* **2009**, *28* (2), 211-220.
18. Lichtenberg, D.; Ahyayauch, H.; Goñi, Félix M., The mechanism of detergent solubilization of lipid bilayers. *Biophys. J.* **2013**, *105* (2), 289-299.

CHAPTER 5

Assembly and structural characterization of lipids on graphite and on graphene

Lipids organize in distinct molecular assemblies on graphene, depending on their chemical structure, the substrate underneath graphene and the experimental conditions used for lipid deposition. Using infrared (IR) spectroscopy and quartz crystal microbalance with dissipation monitoring (QCM-D), the formation and structure of lipids with different charges, saturations and chains lengths deposited on graphene was studied systematically. The IR study revealed that saturated lipids exhibited a higher molecular order structure on the graphene surfaces compare to unsaturated lipids, where cationic unsaturated lipids yielded a more organized lipid assembly in comparison to the zwitterionic and anionic unsaturated lipids. QCM-D measurements revealed the wetting transparency effect on the assembly of zwitterionic lipids on graphene with different supporting materials: the formation of a lipid bilayer on graphene transferred on SiO₂ and the adsorption of intact liposomes on graphene transferred on gold. Understanding how a set of different lipids interact and assemble on the surface of graphene transferred on different substrates revealed that the wetting transparency phenomena also impact how lipids interact with graphene.

Publication in preparation: Lia M. C. Lima, Xiaoyan Zhang and Grégory F. Schneider.

5.1 Introduction

Several discrepancies exist regarding how lipids of different molecular composition assemble on the basal plane of graphene.¹⁻⁸ Some papers claim the formation of lipid bilayers,^{1-2, 4, 6} whereas others report the formation of a lipid monolayer^{3, 5, 7-8} with hydrophobic chains facing graphene. Moreover, very few lipids were studied, limiting the scope of understanding of what chemical building blocks in lipids drive their assembly on graphene. So far, lipids were typically assembled on graphene using the vesicle fusion (VF) method¹⁻⁶ or using the so-called dip-pen nanolithography technique,⁷⁻⁸ where lipids such as 1-palmitoyl-2-oleoyl-*sn*-glycero-3-phosphocholine (POPC) or 1,2-diphytanoyl-*sn*-glycero-3-phosphocholine (DPhPC) tend to form a lipid bilayer, while 1,2-dioleoyl-*sn*-glycero-3-phosphocholine (DOPC) and 1,2-dioleoyl-3-trimethylammonium-propane (DOTAP) lead to the formation of a lipid monolayer. Notably, the wetting transparency of graphene⁹ was suggested to play a role on the formation of a lipid bilayer on graphene particularly in the case where graphene has been transferred on hydrophilic substrates.² In addition, the typical characterization methods used to characterize the lipid-graphene structures only comprise fluorescence microscopy and atomic force microscopy (AFM) techniques.

Here, four different lipids were incubated on graphite and graphene using the VF and the Langmuir-Schaefer (LS) methods and were characterized by infrared (IR) spectroscopy and quartz crystal microbalance with dissipation monitoring (QCM-D).¹⁰ In the VF method,¹¹ liposomes are formed, deposited and adsorbed on solid substrates until the lipid vesicles rupture and form a stable layer on the surface of the substrates.¹² The formation and rupture of the lipids on a surface depends on several parameters such as temperature,¹³ vesicle size,¹⁴ buffer solution,¹⁵ vesicle-vesicle interactions¹⁶ and the interactions between the vesicles and the substrate.¹¹ In the LS technique however, the lipids are compressed on a Langmuir trough until a desired surface pressure is reached, and then transferred onto a solid substrate by contacting the substrate horizontally with the lipid monolayer floating at the surface of the Langmuir trough (see Appendix IV for experimental details). IR spectroscopy was used to analyze the structure, order and stability of the lipids assembled using LS and VF methods on chemical vapor deposition (CVD) graphene-on-copper, and on highly oriented pyrolytic graphite (HOPG) substrates.

QCM-D is a unique technique that allows to study dynamic processes at the interface between a solid and a liquid. Over the past two decades, QCM was largely used to study, for instance the formation of lipid monolayers and bilayers on metals, SiO₂ or gold substrates.¹⁰ QCM-D has however not yet been systematically used to study lipid-graphene interactions.^{3,17} As described in Chapter 2 and 3, lipids can form stable structures using the Langmuir-Blodgett technique if graphene is assembled on top, particularly graphene on monolayers of lipids and graphene encapsulated in the hydrophobic core of a lipid bilayer. Dynamic studies (i.e., the kinetics of lipids interacting with graphene, for example with the VF method) are best accessible using QCM-D. In addition, the effect of the wetting transparency on how lipids – from liposomes – rupture on graphene transferred onto different substrates was investigated systematically. CVD graphene was transferred on SiO₂ and on gold QCM crystal sensors using the standard PMMA assisted transfer method.¹⁸ Distinct lipids presented different assemblies on graphene and the wetting transparency also played a role on how lipids arranged on the surface of graphene.

5.2 Results and discussion

In a Langmuir trough, 1,2-dipalmitoyl-*sn*-glycero-3-phosphocholine (DPPC), 1,2-dioleoyl-*sn*-glycero-3-phosphocholine (DOPC), 1,2-dioleoyl-3-trimethylammonium-propane (DOTAP) and 1,2-dioleoyl-*sn*-glycero-3-phospho-L-serine (DOPS) lipids were dropwise deposited at the air-water interface from a chloroform-methanol solution, and compressed to a surface pressure (π) of 30 mN/m and transferred using the LS method to different substrates (Figure 5.1a), namely HOPG and graphene-on-copper. DPPC is in a gel phase at room temperature and presents characteristic phase states upon compression: a gaseous state for π close to 0 mN/m, a solid state for $\pi \sim 30$ mN/m, passing through a plateau – $\pi \sim 10$ mN/m – where the lipid molecules undergo a transition from a fluidic to a condensed phase (Figure 5.1a, solid line).¹⁹ DPPC has a phase transition temperature of 41 °C, DOPC of -20 °C, DOTAP of 0 °C and DOPS of -11 °C all with chains composed of 18 carbons, except for DPPC (16 chains composed of carbon).²⁰⁻²² In the VF method, the liposomes are deposited and ruptured (or adsorbed) on the surface of different substrates forming e.g., supported lipid bilayers (Figure 5.1b, top) or supported lipid monolayers (Figure 5.1b, bottom), depending on the properties of the substrates (for instance, gold vs SiO₂).¹⁷

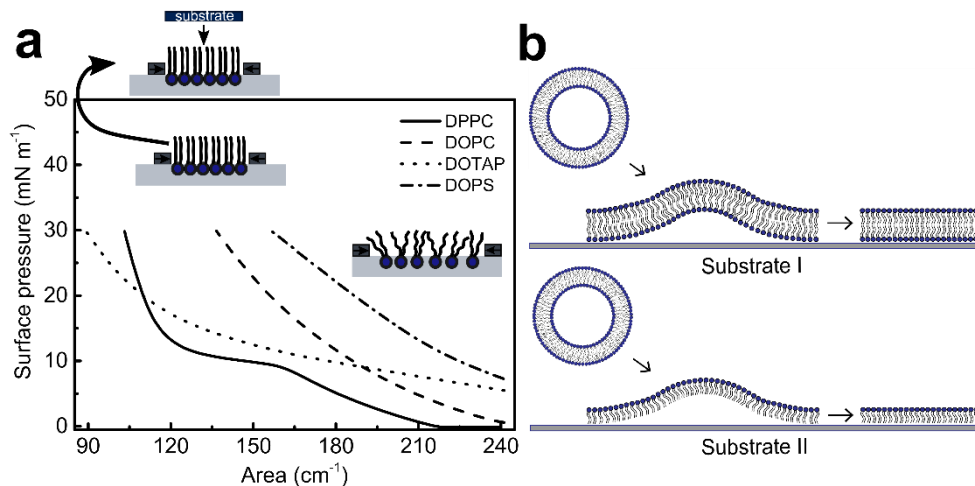


Figure 5.1. Different experimental protocols, namely Langmuir-Schaefer (LS) and vesicle fusion (VF) yielding the formation of a lipid monolayer and bilayer on solid substrates. a) Surface pressure-area isotherms of DPPC, DOPC, DOTAP and DOPS lipids and the subsequent transfer of the compressed lipids to a substrate by the LS method. b) Schematic representation of the possible formation of supported lipid bilayers (top) or supported lipid monolayers (bottom) by VF on substrates.

To study the lipid assembly, different parameters were investigated. The chemical structure of the lipids (Figure 5.2a), the influence of the hydrophobicity of four different substrates (graphene-on-copper, HOPG, graphene-on-SiO₂ and graphene-on-gold), and the difference on the experimental protocol to deposit the lipids (LS or VF).

To assess the structural information and organization of the four types of lipids on graphene-on-copper and HOPG, attenuated total reflectance infrared spectroscopy (ATR-IR) was performed. ATR-IR data was collected for the four different lipids transferred on graphene-on-copper, and on HOPG by the LS and VF methods (black and red respectively, Figure 5.2b). The absorbance peaks of the symmetric and asymmetric CH₂ stretching vibration band were fitted with a Gaussian model and the wavenumbers of the maximum were plotted against the experimental conditions (for at least seven different samples for each condition, see Appendix IV and Figure IV.1 for details). All the samples were measured in a dry state. The absorption bands of the lipid acyl chains are known to vary if the

physical properties of the lipids change.²³ An upward wavenumber shift of the absorption bands corresponds to an increase in disorder of the hydrocarbon chains, and consequently an increase of the lipid mobility within the monolayer/bilayer.²⁴ As expected, the saturated DPPC presented a more ordered structure in comparison with the other three unsaturated lipids independently of their charge (zwitterionic, cationic or anionic), due to the well-organized lipid chains all in a *trans* configuration.²⁵ Unsaturated alkene bonds in the lipid chains promoted a higher degree of disorder due to an increase of the *gauche* conformers in the lipid chains²⁶ and therefore an upward shift of the wavenumbers (Figure 5.2b). Notably, the cationic unsaturated DOTAP lipid presented a higher molecular stability in comparison with the zwitterionic unsaturated DOPC and the anionic DOPS. The unsaturated lipids studied here possess the same chains length and two unsaturated alkene bonds, thus the difference can only be attributed to the composition of the head groups and particularly their charges. A previous study⁵ highlighted that the cationic DOTAP lipid forms a continuous and stable lipid layer on graphene on Si/SiO₂ using the VF method, whereas negatively charged lipids did not interact (i.e. no assembly) on graphene. In fact, in this work the anionic DOPS showed in general a lower structural order compared to the other lipids studied, independently of the substrate or the experimental assembly protocol, as revealed by the shift of the CH₂ stretching bands to higher wavenumbers (Figure 5.2b).

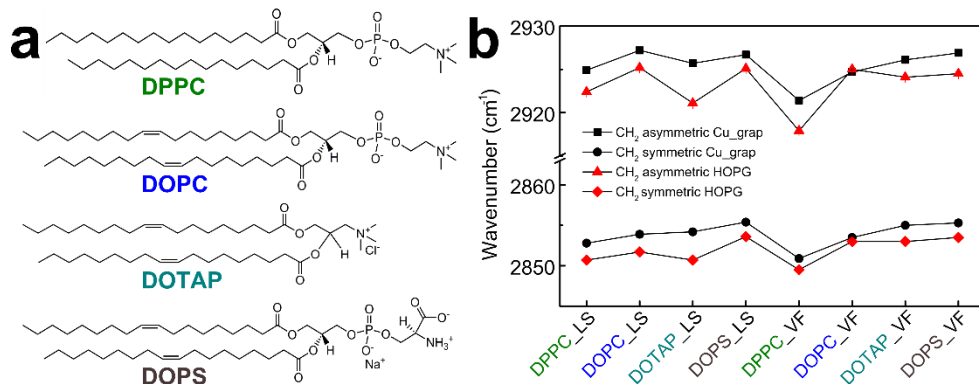


Figure 5.2. Lipid structures and wavenumbers of the CH₂ vibrations infrared absorbance peaks for the four lipid studied and deposited on graphene-on-copper and on highly oriented pyrolytic graphite (HOPG) using vesicle fusion (VF) and Langmuir-Schaefer (LS). a) Molecular structure of DPPC, DOPC, DOTAP and DOPS. b) Mean distribution of the ATR-IR wavenumbers of the symmetric and asymmetric CH₂ vibration peaks for DPPC, DOPC, DOTAP and DOPS lipids transferred by the Langmuir-Schaefer (LS) and the vesicle fusion (VF) methods on graphene-on-copper and HOPG.

The lipids deposited on HOPG presented a higher molecular packing compared to the lipids on graphene-on-copper, independently of the experimental method used (i.e. LS or VF, Figure 5.2b). This is attributed to the disparity in roughness between the supporting substrates.²⁷⁻²⁸ In fact, graphene grown on a copper foil has a considerable high roughness²⁹ in comparison with HOPG, which is atomically flat although constituted of small different layered terraces.³⁰ The AFM topography image of graphene-on-copper presented a roughness of 28.3 nm with folds and pleats (Figure 5.3a), whereas HOPG showed a roughness of 2.3 nm with very flat and continuous flakes (Figure 5.3b). The solid support, particularly the roughness,^{11, 31-32} the surface charge of the substrate and consequently also the ions and pH of the buffer solution,³³⁻³⁴ among others,³⁵⁻³⁶ influence the morphology of the resulting lipid layer. Additionally, the wetting properties, i.e. hydrophobic/hydrophilic^{12, 37} have also a very important role on the formation of a lipid layer.

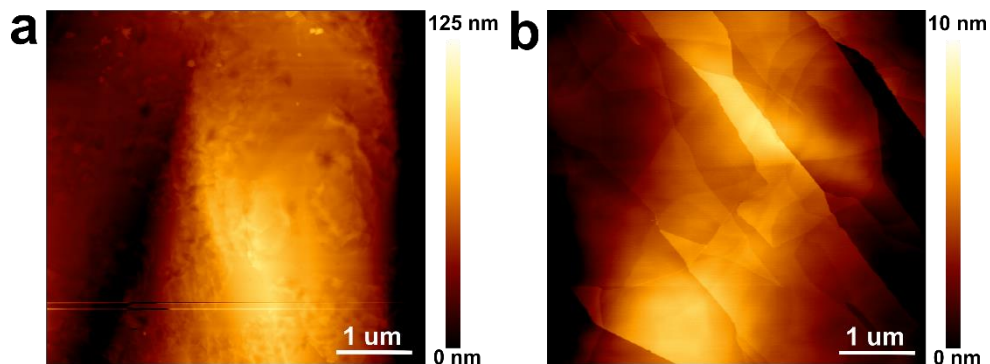


Figure 5.3. AFM intermittent contact mode images in air at room temperature. a) Graphene on a copper foil. b) Highly oriented pyrolytic graphite (HOPG) freshly exfoliated.

In order to investigate and understand the dynamics of vesicle fusion at the interface of a graphene layer, QCM-D experiments were performed. SiO₂-coated and gold-coated QCM crystals were used as substrates for the measurements. CVD graphene was transferred on top of both QCM crystals to investigate the interactions between the different liposomes and graphene. The influence of the substrates underneath graphene were also studied.

Liposomes in a phosphate buffer solution (PBS) were injected 20 minutes (Figure 5.4i) after preparation and were in contact with the substrate using a continuous flow (60 μL/minute) of liposomes for ~1 hour. After, the assembly on graphene was rinsed with PBS (Figure 5.4ii). The change in the resonance frequency of the quartz crystal (Δf) was used to quantify the amount of lipids adsorbed on the graphene.

The zwitterionic saturated DPPC liposomes showed a drop of the resonance frequency, indicating the adsorption of the liposomes on the surface which ruptured to form a lipid bilayer (based on Sauerbrey fitting the layer thickness was 3-4 nm, see appendix for details) on top of graphene-on-SiO₂ (Figure 5.4a). The lipid bilayer was stable for ~6 minutes but at ~26 minutes a sudden drop to a lower frequency (-70 Hz) was observed, indicating that other liposomes or even small air bubbles adsorbed on the surface, also creating a high increase on the energy dissipation values (in red). In contrast, liposomes composed of the cationic unsaturated DOTAP, showed an instant frequency drop to ~-220 Hz with the exact

opposite direction of the energy dissipation values. This indicates that the liposomes did not rupture on top of graphene-on-SiO₂, but rather remained as intact vesicles adsorbed on the graphene surface (Figure 5.4b). The anionic DOPS liposomes showed an increase in frequency and a decrease of the energy dissipation values, indicating that the liposomes did not interact with the surface of graphene (Figure 5.4c). The non-adsorption of DOPS liposomes was also observed in previous studies, where negatively charged liposomes could not deposit on the surface of graphene.⁵

Surprisingly, the QCM-D data showed different results compared to the ATR-IR experiments primarily due to the differences of the solid supports (graphene-on-copper and HOPG are not available as substrates for the QCM measurements), and additionally, the samples for ATR-IR experiments were measured in air (and not in liquid as for QCM-D), likely changing the conformation structure of the lipids.

Finally, the wetting transparency of graphene was investigated using DOPC liposomes deposited on graphene transferred on SiO₂ and on gold substrates. As control experiments, DOPC liposomes were first tested on plain SiO₂ and on plain gold, without the transfer of graphene on top. Liposome rupture resulted in the formation a lipid bilayer on the surface of SiO₂, with a layer thickness of around 4 nm based on Sauerbrey fit. In contrast, DOPC liposomes adsorbed and remained intact on the surface of gold without rupturing (Appendix IV, Figure IV.2). These results are in agreement with literature.¹⁷ For a graphene transferred on a SiO₂ substrate, the liposomes ruptured and formed a lipid bilayer with a layer thickness of 3-4 nm based on Sauerbrey fit (Figure 5.4d), on a graphene-on-gold substrate, the liposomes adsorbed on the surface of graphene without rupturing (Figure 5.4e). The results are similar for graphene-on-SiO₂ and graphene-on-gold compared to SiO₂ and gold alone, suggesting the wetting transparency of graphene, where graphene is transparent to the wetting properties of the substrate underneath.

All graphene sheets transferred on the sensors were characterized by Raman spectroscopy, before and after the QCM-D measurements in order to confirm the transfer of a single layer graphene and the integrity of graphene after the measurements (see plots on Appendix IV, Figure IV.3).

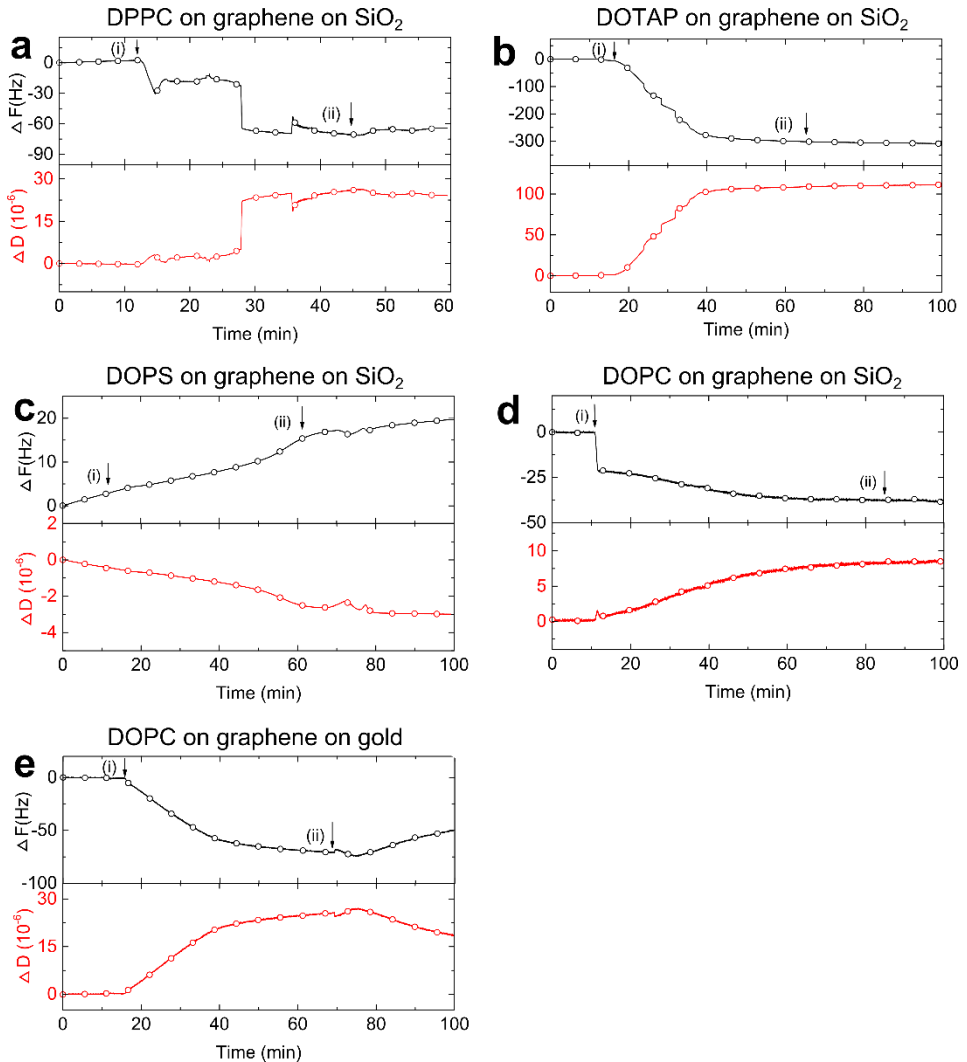


Figure 5.4. Dynamics of liposomes interactions with graphene monitored by quartz crystal microbalance with dissipation monitoring (QCM-D). a) Assembly of the zwitterionic saturated DPPC lipids on graphene-on- SiO_2 . b) Assembly of the cationic unsaturated DOTAP lipids on graphene-on- SiO_2 . c) Assembly of the anionic unsaturated DOPS lipids on graphene-on- SiO_2 . d) Assembly of the zwitterionic unsaturated DOPC lipids on graphene-on- SiO_2 . e) Assembly of the zwitterionic unsaturated DOPC lipids on graphene-on-gold.

5.3 Conclusions

This study elucidates how distinct lipids (DPPC, DOPC, DOTAP and DOPS) assemble on graphite (in the form of HOPG), graphene-on-copper, graphene-on-SiO₂ and graphene-on-gold. ATR-IR results showed that saturated DPPC lipids presented a more ordered structure on the surface of graphene compared to unsaturated lipids, due to a higher rigidity of the lipid acyl chains. For the unsaturated lipids, the cationic DOTAP yielded a higher packed assembly in comparison with the other two unsaturated lipids, i.e. DOPC and DOPS. The anionic DOPS showed a higher fluidity compared to the other lipids. Nevertheless, all the samples were dried in air before the measurements, possibly changing the molecular conformation of the lipids.

Using QCM-D the interactions of the same lipids from liposome solutions were studied for graphene-on-SiO₂ and graphene-on-gold substrates. DPPC liposomes ruptured on the surface of graphene-on-SiO₂ primarily forming a lipid bilayer (similarly to control experiments with plain SiO₂). The cationic DOTAP liposomes adsorbed and remained intact on the surface of graphene whereas the anionic DOPS liposomes did not interact nor adsorbed on graphene-on-SiO₂. The wetting transparency of graphene therefore played a role on the conformational structure of DOPC liposomes, forming a lipid bilayer on graphene transferred on SiO₂ (i.e. hydrophilic), and adsorbed without rupturing on graphene transferred on hydrophobic gold substrate.

In conclusion, distinct lipids interact differently with graphene materials depending on their charge, saturation, structure, on the experimental method used, and on the wetting properties of the solid supports. This work now unifies all the studies reported so far for lipids interacting with graphene transferred on different substrates.

5.4 References

1. Ang, P. K.; Jaiswal, M.; Lim, C. H. Y. X.; Wang, Y.; Sankaran, J.; Li, A.; Lim, C. T.; Wohland, T.; Barbaros, Ö.; Loh, K. P., A bioelectronic platform using a graphene–lipid bilayer interface. *ACS Nano* **2010**, *4* (12), 7387-7394.
2. Wang, Y. Y.; Pham, T. D.; Zand, K.; Li, J.; Burke, P. J., Charging the quantum capacitance of graphene with a single biological ion channel. *ACS Nano* **2014**, *8* (5), 4228–4238.
3. Tabaei, S. R.; Ng, W. B.; Cho, S.-J.; Cho, N.-J., Controlling the formation of phospholipid monolayer, bilayer, and intact vesicle layer on graphene. *ACS Appl. Mater. Interf.* **2016**, *8* (18), 11875-11880.
4. Kuo, C.-J.; Chiang, H.-C.; Tseng, C.-A.; Chang, C.-F.; Ulaganathan, R. K.; Ling, T.-T.; Chang, Y.-J.; Chen, C.-C.; Chen, Y.-R.; Chen, Y.-T., Lipid-modified graphene-transistor biosensor for monitoring amyloid- β aggregation. *ACS Appl. Mater. Interf.* **2018**, *10* (15), 12311-12316.
5. Blaschke, B. M.; Böhm, P.; Drieschner, S.; Nickel, B.; Garrido, J. A., Lipid monolayer formation and lipid exchange monitored by a graphene field-effect transistor. *Langmuir* **2018**, *34* (14), 4224-4233.
6. Connelly, L. S.; Meckes, B.; Larkin, J.; Gillman, A. L.; Wanunu, M.; Lal, R., Graphene nanopore support system for simultaneous high-resolution afm imaging and conductance measurements. *ACS Appl. Mater. Interf.* **2014**, *6* (7), 5290-5296.
7. Hirtz, M.; Oikonomou, A.; Georgiou, T.; Fuchs, H.; Vijayaraghavan, A., Multiplexed biomimetic lipid membranes on graphene by dip-pen nanolithography. *Nat. Commun.* **2013**, *4*, 2591.
8. Hirtz, M.; Oikonomou, A.; Clark, N.; Kim, Y.-J.; Fuchs, H.; Vijayaraghavan, A., Self-limiting multiplexed assembly of lipid membranes on large-area graphene sensor arrays. *Nanoscale* **2016**, *8* (33), 15147-15151.

9. Rafiee, J.; Mi, X.; Gullapalli, H.; Thomas, A. V.; Yavari, F.; Shi, Y.; Ajayan, P. M.; Koratkar, N. A., Wetting transparency of graphene. *Nat. Mater.* **2012**, *11*, 217–222.
10. Cho, N.-J.; Frank, C. W.; Kasemo, B.; Höök, F., Quartz crystal microbalance with dissipation monitoring of supported lipid bilayers on various substrates. *Nat. Protoc.* **2010**, *5*, 1096-1106.
11. Richter, R. P.; Bérat, R.; Brisson, A. R., Formation of solid-supported lipid bilayers: An integrated view. *Langmuir* **2006**, *22* (8), 3497-3505.
12. Jass, J.; Tjärnhage, T.; Puu, G., From liposomes to supported, planar bilayer structures on hydrophilic and hydrophobic surfaces: An atomic force microscopy study. *Biophys. J.* **2000**, *79* (6), 3153-3163.
13. Puu, G.; Gustafson, I., Planar lipid bilayers on solid supports from liposomes – factors of importance for kinetics and stability. *BBA - Biomembranes* **1997**, *1327* (2), 149-161.
14. Jing, Y.; Trefna, H.; Persson, M.; Kasemo, B.; Svedhem, S., Formation of supported lipid bilayers on silica: Relation to lipid phase transition temperature and liposome size. *Soft Matter* **2014**, *10* (1), 187-195.
15. Dacic, M.; Jackman, J. A.; Yorulmaz, S.; Zhdanov, V. P.; Kasemo, B.; Cho, N.-J., Influence of divalent cations on deformation and rupture of adsorbed lipid vesicles. *Langmuir* **2016**, *32* (25), 6486-6495.
16. Zhdanov, V. P.; Dimitrievski, K.; Kasemo, B., Adsorption and spontaneous rupture of vesicles composed of two types of lipids. *Langmuir* **2006**, *22* (8), 3477-3480.
17. Melendrez, D.; Jowitt, T.; Iliut, M.; Verre, A. F.; Goodwin, S.; Vijayaraghavan, A., Adsorption and binding dynamics of graphene-supported phospholipid membranes using the qcm-d technique. *Nanoscale* **2018**, *10* (5), 2555-2567.

18. Li, X.; Zhu, Y.; Cai, W.; Borysiak, M.; Han, B.; Chen, D.; Piner, R. D.; Colombo, L.; Ruoff, R. S., Transfer of large-area graphene films for high-performance transparent conductive electrodes. *Nano Lett.* **2009**, *9* (12), 4359-4363.
19. Lima, L. M. C.; Fu, W.; Jiang, L.; Kros, A.; Schneider, G. F., Graphene-stabilized lipid monolayer heterostructures: A novel biomembrane superstructure. *Nanoscale* **2016**, *8* (44), 18646-18653.
20. Lima, L. M. C.; Giannotti, M. I.; Redondo-Morata, L.; Vale, M. L. C.; Marques, E. F.; Sanz, F., Morphological and nanomechanical behavior of supported lipid bilayers on addition of cationic surfactants. *Langmuir* **2013**, *29* (30), 9352-9361.
21. Picas, L.; Rico, F.; Scheuring, S., Direct measurement of the mechanical properties of lipid phases in supported bilayers. *Biophys. J.* **2012**, *102* (1), L01-L03.
22. Cinelli, S.; Onori, G.; Zuzzi, S.; Bordi, F.; Cametti, C.; Sennato, S.; Diociaiuti, M., Properties of mixed dotap-dppc bilayer membranes as reported by differential scanning calorimetry and dynamic light scattering measurements. *J. Phys. Chem. B* **2007**, *111* (33), 10032-10039.
23. Mitchell, M. L.; Dluhy, R. A., In situ ft-ir investigation of phospholipid monolayer phase transitions at the air water interface. *J. Am. Chem. Soc.* **1988**, *110* (3), 712-718.
24. Lewis, R. N. A. H.; McElhaney, R. N., Membrane lipid phase transitions and phase organization studied by fourier transform infrared spectroscopy. *BBA-Biomembranes* **2013**, *1828* (10), 2347-2358.
25. Garcia-Manyes, S.; Sanz, F., Nanomechanics of lipid bilayers by force spectroscopy with afm: A perspective. *BBA - Biomembranes* **2010**, *1798* (4), 741-749.
26. Tatulian, S. A., Attenuated total reflection fourier transform infrared spectroscopy: A method of choice for studying membrane proteins and lipids. *Biochemistry* **2003**, *42* (41), 11898-11907.

27. Raedler, J.; Strey, H.; Sackmann, E., Phenomenology and kinetics of lipid bilayer spreading on hydrophilic surfaces. *Langmuir* **1995**, *11* (11), 4539-4548.
28. Tero, R., Substrate effects on the formation process, structure and physicochemical properties of supported lipid bilayers. *Materials* **2012**, *5* (12), 2658-2680.
29. Kwon, G. D.; Moyon, E.; Lee, Y. J.; Kim, Y. W.; Baik, S. H.; Pribat, D., Influence of the copper substrate roughness on the electrical quality of graphene. *Mater. Res. Express* **2017**, *4* (1), 015604.
30. Vincent, H.; Bendiab, N.; Rosman, N.; Ebbesen, T.; Delacour, C.; Bouchiat, V., Large and flat graphene flakes produced by epoxy bonding and reverse exfoliation of highly oriented pyrolytic graphite. *Nanotechnology* **2008**, *19* (45), 455601.
31. Cremer, P. S.; Boxer, S. G., Formation and spreading of lipid bilayers on planar glass supports. *J. Phys. Chem. B* **1999**, *103* (13), 2554-2559.
32. Scomparin, C.; Lecuyer, S.; Ferreira, M.; Charitat, T.; Tinland, B., Diffusion in supported lipid bilayers: Influence of substrate and preparation technique on the internal dynamics. *Eur. Phys. J. E* **2009**, *28* (2), 211-220.
33. Richter, R.; Mukhopadhyay, A.; Brisson, A., Pathways of lipid vesicle deposition on solid surfaces: A combined qcm-d and afm study. *Biophys. J.* **2003**, *85* (5), 3035-3047.
34. Redondo-Morata, L.; Oncins, G.; Sanz, F., Force spectroscopy reveals the effect of different ions in the nanomechanical behavior of phospholipid model membranes: The case of potassium cation. *J. Biophys.* **2012**, *102*(1), 66-74.
35. Czolkos, I.; Jesorka, A.; Orwar, O., Molecular phospholipid films on solid supports. *Soft Matter* **2011**, *7* (10), 4562-4576.

36. Reimhult, E.; Höök, F.; Kasemo, B., Intact vesicle adsorption and supported biomembrane formation from vesicles in solution: Influence of surface chemistry, vesicle size, temperature, and osmotic pressure. *Langmuir* **2003**, *19* (5), 1681-1691.
37. González, C. M.; Pizarro-Guerra, G.; Droguett, F.; Sarabia, M., Artificial biomembrane based on dppc — investigation into phase transition and thermal behavior through ellipsometric techniques. *BBA - Biomembranes* **2015**, *1848* (10), 2295-2307.

CHAPTER 6

Lateral non-covalent clamping of graphene at the edges using a lipid scaffold

Developing a clean handling and transfer process, capable to preserve the integrity of two-dimensional materials, is still a challenge. Here, a flexible, dynamic and molecular lipid-based scaffold clamps graphene at the edges providing a practical, simple and clean graphene manipulation and transfer method. Lipid films with different surface pressures of lipids are deposited at the air/copper-etchant interface immediately after placing the graphene samples. At surface pressures above 30 mN/m, the lateral support prevents the movement and cracking of graphene during all etching and transfer. The method provides new insights into the critical handling of graphene and can yield efficient, sensitive and clean graphene-based devices.

This chapter was published as a full article: Lia M. C. Lima, Hadi Arjmandi-Tash and Grégory F. Schneider, *ACS Applied Materials & Interfaces*, **2018**, 10, 11328-11332

6.1 Introduction

Over the last years, a growing interest in graphene led to the development of novel sensing devices.¹⁻⁵ However, for the achievement of such devices, graphene has to pass through several fabrication steps.⁶⁻⁹ Large scale graphene sheets are typically synthesized on metallic catalysts¹⁰⁻¹¹ and then transferred to target substrates such as Si/SiO₂.¹²⁻¹³ The transfer process can highly degrade the properties of graphene and its performance in the final applications.¹⁴ The immobilization of two-dimensional (2D) materials (e.g. graphene) by Langmuir films is a strategy to controllably manipulate graphene directly in an aqueous environment, without using polymeric scaffolds.¹⁵ Langmuir films of amphiphilic lipid molecules are insoluble at an air-liquid interface generating a lateral pressure profile due to the intermolecular forces in the lipid monolayer. The film is stable and 2D, guaranteeing a strictly lateral compression (no perpendicular component which may cause out-of-plane deformation) of graphene. The molecules act to decrease the surface tension of the subphase, therefore creating a dynamic clamp which adjust itself according to the geometry of graphene. For the first time, lipids are introduced as molecular springs clamping graphene from the side at an air-liquid interface. The flexible lipid-based scaffold prevents graphene movement and cracking during copper etching and later on, during transfer onto a target substrate. The reliability of lipid clamps compared to existing polymer-free transfer methods was also investigated.¹⁶⁻¹⁸

In a Langmuir-Blodgett (LB),¹⁵ the lipids are deposited on an air-water interface and compressed passing through different characteristic phases, namely the gaseous (G) state, the liquid expanded (LE) state, the liquid condensed (LC) state and the solid (S) state (Figure 6.1a).¹⁹⁻²¹ In the presence of graphene, as the intermolecular distance between the lipid molecules decreases during compression, the force exerted by both the hydrophobic acyl chains and the hydrophilic polar groups induces a pressure on the graphene edges; the increase in the surface pressure (π) is directly linked to how closely the lipids are packed. Therefore, the dynamic pressure of the lipid monolayer can keep the domains of graphene together and intact, preventing the growth of already existing cracks (e.g. through grain boundaries).²²

The most common transferring method includes a temporarily coating of graphene with a polymer while etching the metal substrate in an etchant solution. The coating acts as a mechanical support and prevents graphene cracking. The coating is thereafter removed by suitable chemicals once graphene is transferred onto the target substrate. Leftovers of polymer residuals are the important limitation of the technique which may degrade the ultimate quality of the graphene.²³⁻²⁶ Therefore, in the recent years, novel polymer-free transfer methods have been developed most of which, use physical supports such as graphite holders¹⁶ or TEM grids,¹⁷ limiting the flexibility of the process. Alternatively, graphene is also covered with organic solvents such as cyclohexane⁹ or hexane,¹⁸ avoiding polymer contaminations.

In this work, as the surface of graphene is not in contact with any physical support, the basal plane remains uncontaminated allowing the realization of clean devices directly on water. With this non-covalent bonding, graphene can be manipulated from the edges, leading additionally to an optimal transfer to arbitrary substrates. Increasing the lateral pressure of the lipids decreases the number of cracks and further preserves the quality of the transfer. The development of a lateral support damps vibrations on the surface of the etchant (happening during etching or transfer) which may induce cracks. This immobilization by Langmuir films establishes a novel strategy for fundamental studies of graphene and also for transfer purposes.

6.2 Results and discussion

The 1,2-dipalmitoyl-*sn*-glycero-3-phosphocholine (DPPC) monolayer was compressed up to $\pi = 50$ mN/m in a Langmuir trough (Figure 6.1a). The recorded isotherms were used to reproduce the same lipids π /area conditions in six different Petri dishes (see Appendix V). All the experiments were carried out at room temperature ($\sim 25^\circ\text{C}$) where DPPC is in the gel phase. Note that DPPC has a main phase transition temperature (T_m) of 41°C . Below the T_m , the DPPC monolayer presents different phases during compression, as observed in Figure 6.1a. Figure 6.1b illustrates the concept of the molecular edge clamp. Sufficiently high π prevents any noticeable movement of graphene during all the etching procedure and forms a well-ordered and compact layer that holds the graphene in place through all the processes. Figure 6.1c and d shows overlapped snapshots at

different copper etching stages of two samples with and without the lipid clamp at the edges. Clearly, the graphene without any lateral support moves randomly, which may eventually promote its cracking. Instead, lipids on the surroundings of graphene hold the graphene in place during all the etching and transfer, preserving its integrity.

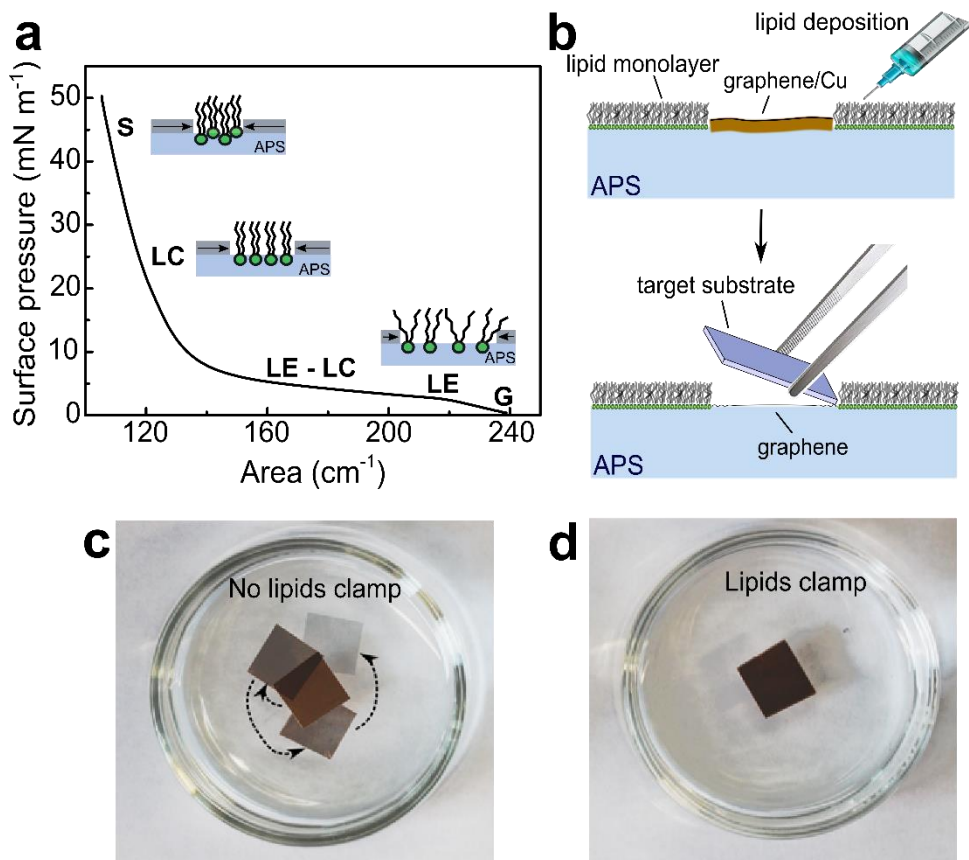


Figure 6.1. Lipidic molecular edge-clamping of graphene. a) Surface pressure-area compression isotherm of 1,2-dipalmitoyl-*sn*-glycero-3-phosphocholine (DPPC) lipid monolayer on ammonium persulfate solution (APS) at 25 °C showing different phase separations. G: gaseous state; LE: liquid expanded state; LC: liquid condensed state; S: solid state. b) Illustration of the molecular edge clamp concept. c-d) Time-lapse photographs of a piece of graphene-on-copper floating on a solution of 0.5 M APS in water without (c) and with (d) the lipid clamp.

Figure 6.2 shows the optical images of graphene samples transferred onto Si/SiO₂ substrates with different lateral pressures. In fact, the sample without any lipid lateral support is unsteady and dramatically loses its integrity. The low-amplitude vibrations of the surface of the etchant and the transfer could be responsible for such damages. The graphene sheets transferred in the presence of the lipid edge clamp, however, are continuous to a large extent: increasing the π prevents the formation of the cracks, showing the advantage of the lateral clamp support. Particularly, at the LC state ($\pi > 30$ mN/m), the interaction between the lipid molecules at the interface is large enough to induce a high pressure on the edges of graphene and promotes a stable clamp while transferring to the Si/SiO₂ substrates.

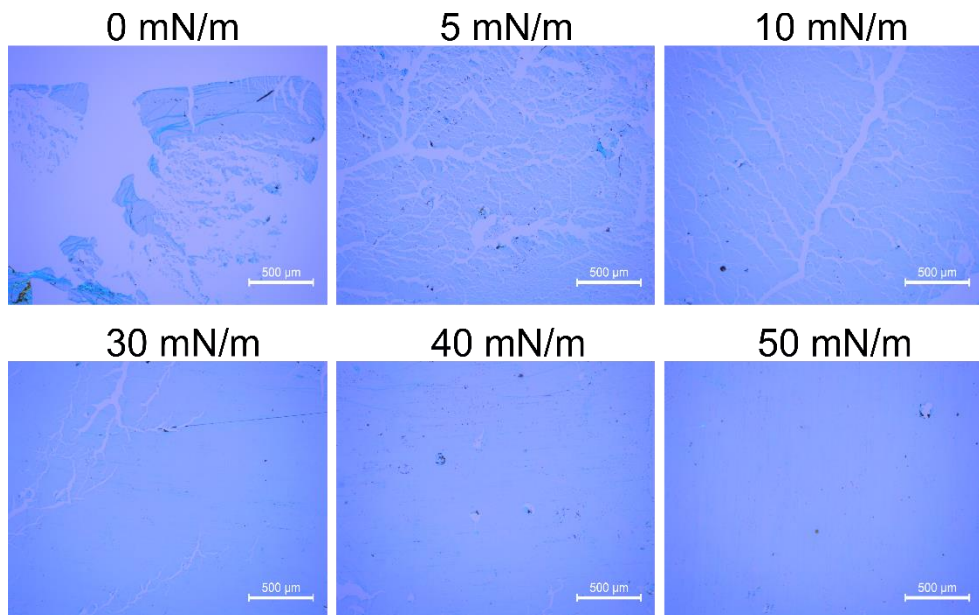


Figure 6.2. Integrity of graphene as a function of the lipid clamping pressure. Optical micrographs of graphene on Si/SiO₂ substrates transferred at different clamp pressures (0, 5, 10, 30, 40 and 50 mN/m). Scale bars are 500 μ m.

The rupture index (RI) provides a quantitative measure of the integrity of graphene samples.²⁷ The emission of the fluorophore molecules in close vicinity to graphene is quenched via a peculiar energy transfer mechanism, leading to an outstanding contrast between cracked and continuous graphene areas in

fluorescence microscopy (see the images in the top row in Figure 6.3). The RI is determined by counting the number of pixels localized at the border of the cracks (white pixels visible in the bottom row in Figure 6.3) and divided by the total number of pixels corresponding to graphene multiplied by one thousand. In application, the median of different RI values measured at several spots on the sample is reported to exclude the effect of any local inhomogeneities (see Figure 6.4). Remarkably, increasing the surface pressure using the lipid-edge clamp has a direct effect on the integrity of graphene. Particularly, $\pi \geq 40$ mN/m provides a negligible RI, comparable to graphene transferred with a PMMA coating. The RI results are in line with the optical microscopy studies. At higher π , the lipid monolayer becomes more compact with smaller intermolecular areas reflecting on a more confined lipid clamp, therefore preserving the original state of graphene upon transfer to the Si/SiO₂ substrate.

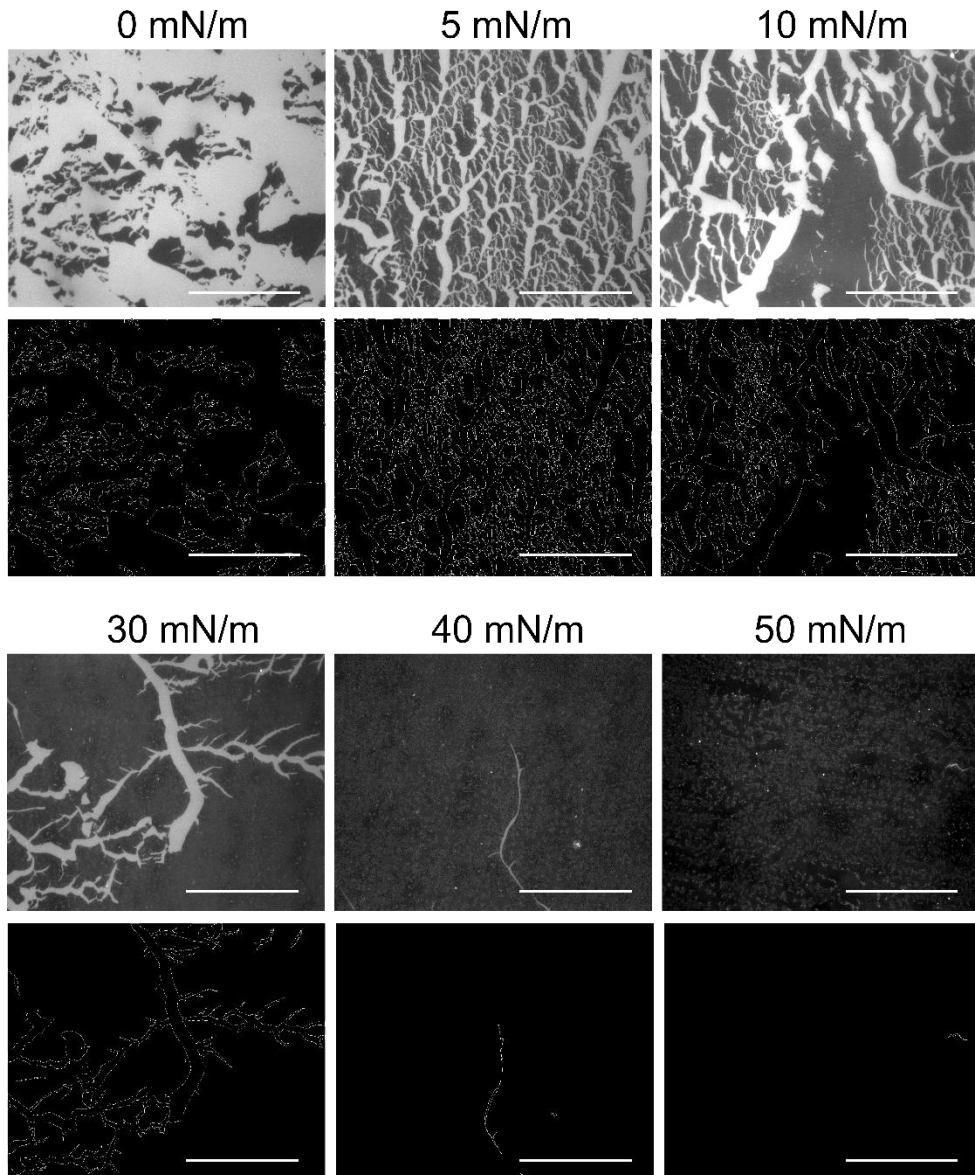


Figure 6.3. Quantification of crack in graphene transferred using a lipid clamp by fluorescence quenching microscopy. Fluorescence quenching microscopy images of graphene on Si/SiO₂ substrates with different surface pressures of the lipids (top row) and the corresponding images after processing (bottom row). All the scale bars correspond to 50 μm .

The π also affects the duration of the copper foil etching (t_{etch}). Figure 6.5a plots the estimated etching time (t_{etch}) as the function of π : we use the time span between the moment some parts of the foil started to be transparent up to the moment the foil turns to be fully invisible. Generally, increasing the π increases t_{etch} . Indeed, the very high intermolecular interactions between lipid molecules most probably drives lipids towards the foil/etchant interface resulting in delays of the etching as migrated lipids may form a layer between the copper and the etchant. The delay depends on the concentration of the intercalated lipid molecules, the latter being proportional to the π . At the highest π (50 mN/m), presumably a considerable amount of the lipids collapsed (reducing the effective π), in line with what is observed in Figure V.2, Appendix V.

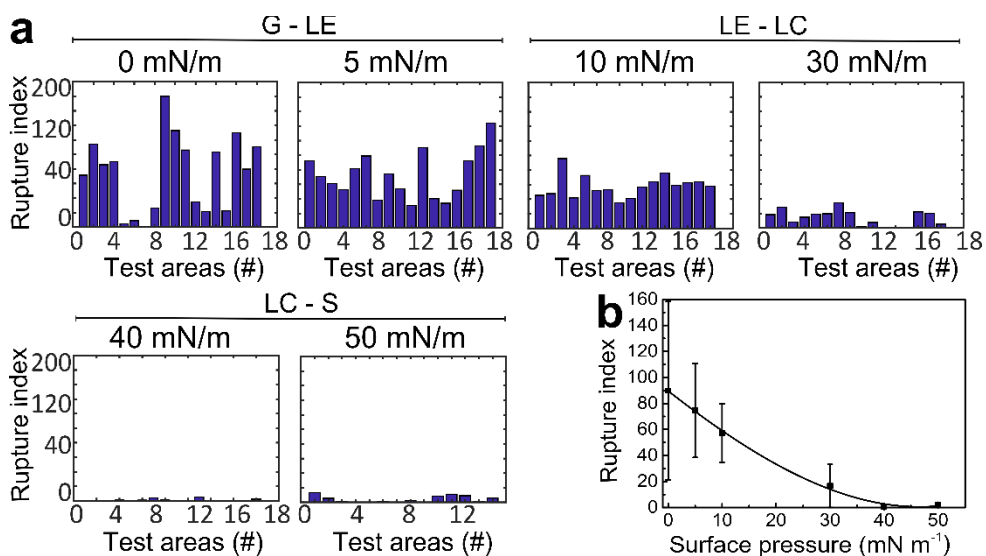


Figure 6.4. Characterization of graphene samples using the rupture index method. a) Quantitative characterization of crack formation at different lateral clamping strengths for surface pressures ranging from 0 to 50 mN/m. G-LE: gaseous to liquid expanded state; LE-LC: liquid expanded to liquid condensed state; LC-S: liquid condensed to solid state. Dimensionless rupture index estimated for a maximum of 18 different arbitrarily selected windows (test areas, x axis) on the sample. b) Median rupture index values in (a) as a function of the surface pressure; the solid line is the fit using a polynomial function.

Infrared absorption reflection spectroscopy (IRRAS) was used to probe the lipid-graphene interactions after the transfer onto Si/SiO₂ substrates. As showed in Figure 6.5b, no significant absorption bands characteristic for the stretching vibrations of the lipid acyl chains were detected. The lack of lipid traces suggests that during the transfer, the affinity between the lipid molecules intercalated underneath graphene and the water is stronger than the lipids-graphene interaction, allowing the molecules to remain at the interface. Alternatively, the step of rinsing with ultrapure water after the transfer of graphene – to remove the remaining etchant residues – could have rinsed the lipids away. For the purpose of comparison, we measured the infrared spectra of a well-organized lipid monolayer transferred onto a Si/SiO₂ substrate using Langmuir trough at $\pi = 30$ mN/m with a graphene sheet above (Figure 6.5b, orange line – LB DPPC).²⁸ The results show an intense absorbance for the symmetric (~ 2844 cm⁻¹) and asymmetric (~ 2912 cm⁻¹) methylene vibrations of the lipid acyl chains even for a single layer of lipids, further confirming the assumption that the lipids from the clamp were not transferred. Additionally, the black line corresponding to the graphene without any lipids at the interface is comparable to any other spectra of graphene transferred with different surface pressures, further emphasizing that the lipids were indeed not transferred with the graphene to the Si/SiO₂ substrates. Such observations further confirm that the molecular edge clamp provides a clean transfer to realize sensitive graphene-based devices.

Separately, the quality of the graphene transferred at different π was analyzed by Raman spectroscopy after transfer on Si/SiO₂ substrates (Figure 6.5c). Remarkably, Raman spectra are insensitive to π and feature a 2D peak (~ 2680 cm⁻¹) characteristic of a single layer graphene, a weak D peak at ~ 1350 cm⁻¹ and a sharp G peak (~ 1590 cm⁻¹), confirming the outstanding quality of graphene after transfer. Similarly, Figure 6.5d shows an AFM image of continuous graphene on Si/SiO₂ substrate transferred with a $\pi = 30$ mN/m. In line with what was mentioned above, graphene is fully immobilized by the lipid molecules when the lipids are in the LC state or above, because of the increasing intermolecular interactions in the monolayer that reduces the surface tension and creates a flexible scaffold on the edges of graphene. This prevents graphene from cracking during all etching time prevents also graphene to crack during its transfer onto Si/SiO₂ substrates.

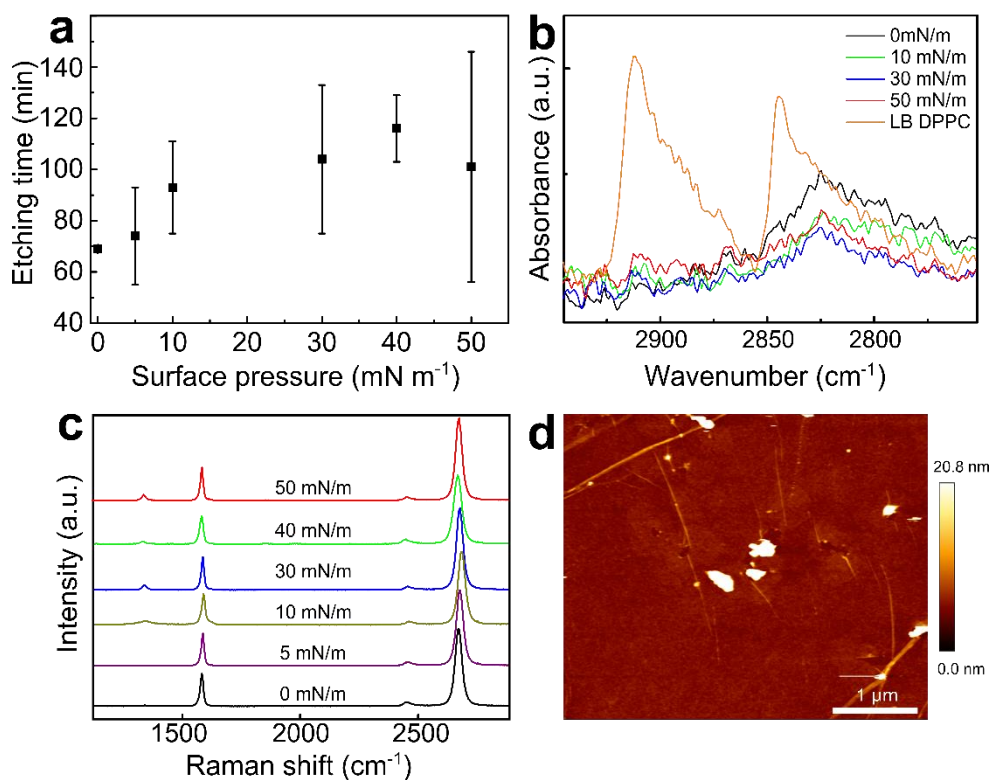


Figure 6.5. Characterization of graphene with different surface pressures of lipids. a) Etching time of the copper foil as a function of the lipid surface pressure. b) IRRAS spectra of graphene transferred at different surface pressures. A control spectra corresponding to the transfer of a DPPC lipid monolayer by Langmuir-Blodgett with graphene sheet above is also presented. c) Raman spectra of different graphene samples on Si/SiO₂ substrates transferred with different surface pressures (0, 5, 10, 30, 40 and 50 mN/m). d) AFM intermittent contact mode image in air at room temperature for graphene transferred to a Si/SiO₂ substrate with a surface pressure of 30 mN/m.

6.3 Conclusions

A molecular lipid-based scaffold that laterally clamps graphene from the edges was developed leading to an optimal manipulation and transfer of graphene to solid substrates, preventing polymeric contamination and cracking of graphene. The

method is based on laterally supporting graphene with a lipid monolayer on the surface of an etchant.

The uniformity of the graphene was investigated by means of optical images and RI. The integrity of graphene increases by increasing the lipid lateral pressure. The surface of graphene is clean without process residuals. Compared to other existing polymer-free transfer methods, this process benefits from the fact that the surface of graphene is not in contact with any physical support during transfer and etching, the process is flexible and straightforward. One immediate possible application would be to study the electrical and mechanical properties of graphene with lateral compression of the lipid scaffold.

6.4 References

1. Fu, W.; Jiang, L.; Geest, E. P. v.; Lima, L. M. C.; Schneider, G. F., Sensing at the surface of graphene field-effect transistors. *Adv. Mater.* **2017**, *29* (6), 1603610.
2. Arjmandi-Tash, H.; Belyaeva, L. A.; Schneider, G. F., Single molecule detection with graphene and other two-dimensional materials: Nanopores and beyond. *Chem. Soc. Rev.* **2016**, *45* (3), 476-493.
3. Gobbi, M.; Orgiu, E.; Samori, P., When 2d materials meet molecules: Opportunities and challenges of hybrid organic/inorganic van der waals heterostructures. *Adv. Mater.* **2018**, *30*, 1706103.
4. Tabaei, S. R.; Ng, W. B.; Cho, S.-J.; Cho, N.-J., Controlling the formation of phospholipid monolayer, bilayer, and intact vesicle layer on graphene. *ACS Appl. Mater. Interf.* **2016**, *8* (18), 11875-11880.
5. Willems, N.; Urtizberea, A.; Verre, A. F.; Iliut, M.; Lelimosin, M.; Hirtz, M.; Vijayaraghavan, A.; Sansom, M. S. P., Biomimetic phospholipid membrane organization on graphene and graphene oxide surfaces: A molecular dynamics simulation study. *ACS Nano* **2017**, *11* (2), 1613-1625.
6. Gao, L.; Ni, G.-X.; Liu, Y.; Liu, B.; Castro Neto, A. H.; Loh, K. P., Face-to-face transfer of wafer-scale graphene films. *Nature* **2014**, *505* (7482), 190-194.
7. Joshua, D. W.; Gregory, P. D.; Enrique, A. C.; Justin, C. K.; Joshua, A. K.; Isha, D.; Ashkan, B.; Jayan, H.; Basil, A.; Yaofeng, C.; Hefei, D.; Richard, T. H.; Joseph, W. L.; Eric, P., Annealing free, clean graphene transfer using alternative polymer scaffolds. *Nanotechnology* **2015**, *26* (5), 055302.
8. Arjmandi-Tash, H.; Adrien, A.; Zheng, H.; Vincent, B., Large scale integration of cvd-graphene based nems with narrow distribution of resonance parameters. *2D Materials* **2017**, *4* (2), 025023.

9. Belyaeva, L. A.; Fu, W. Y.; Arjmandi-Tash, H.; Schneider, G. F., Molecular caging of graphene with cyclohexane: Transfer and electrical transport. *ACS Cent. Sci.* **2016**, *2* (12), 904-909.
10. Mattevi, C.; Kim, H.; Chhowalla, M., A review of chemical vapour deposition of graphene on copper. *J. Mater. Chem.* **2011**, *21*, 3324-3334.
11. Arjmandi-Tash, H.; Lebedev, N.; van Deursen, P. M. G.; Aarts, J.; Schneider, G. F., Hybrid cold and hot-wall reaction chamber for the rapid synthesis of uniform graphene. *Carbon* **2017**, *118*, 438-442.
12. Li, X.; Cai, W.; An, J.; Kim, S.; Nah, J.; Yang, D.; Piner, R.; Velamakanni, A.; Jung, I.; Tutuc, E.; Banerjee, S. K.; Colombo, L.; Ruoff, R. S., Large-area synthesis of high-quality and uniform graphene films on copper foils. *Science* **2009**, *324* (5932), 1312-1314.
13. Suk, J. W.; Kitt, A.; Magnuson, C. W.; Hao, Y.; Ahmed, S.; An, J.; Swan, A. K.; Goldberg, B. B.; Ruoff, R. S., Transfer of cvd-grown monolayer graphene onto arbitrary substrates. *ACS Nano* **2011**, *5* (9), 6916-6924.
14. Chen, Y.; Gong, X.-L.; Gai, J.-G., Progress and challenges in transfer of large-area graphene films. *Adv. Sci.* **2016**, *3* (8), 1500343.
15. Kaganer, V. M.; Mohwald, H.; Dutta, P., Structure and phase transitions in langmuir monolayers. *Rev. Mod. Phys.* **1999**, *71* (3), 779.
16. Lin, W.-H.; Chen, T.-H.; Chang, J.-K.; Taur, J.-I.; Lo, Y.-Y.; Lee, W.-L.; Chang, C.-S.; Su, W.-B.; Wu, C.-I., A direct and polymer-free method for transferring graphene grown by chemical vapor deposition to any substrate. *ACS Nano* **2014**, *8* (2), 1784-1791.
17. Regan, W.; Alem, N.; Aleman, B.; Geng, B. S.; Girit, C.; Maserati, L.; Wang, F.; Crommie, M.; Zettl, A., A direct transfer of layer-area graphene. *Appl. Phys. Lett.* **2010**, *96* (11), 113102.

18. Zhang, G.; Güell, A. G.; Kirkman, P. M.; Lazenby, R. A.; Miller, T. S.; Unwin, P. R., Versatile polymer-free graphene transfer method and applications. *ACS Appl. Mater. Interf.* **2016**, *8* (12), 8008-8016.
19. Girard-Egrot, A. P., Blum, L. J., *Nanobiotechnology of biomimetic membranes* 2007; Vol. 1.
20. Klopfer, K. J.; Vanderlick, T. K., Isotherms of dipalmitoylphosphatidylcholine (dppc) monolayers: Features revealed and features obscured. *J. Colloid Interf. Sci.* **1996**, *182* (1), 220-229.
21. Baoukina, S.; Monticelli, L.; Marrink, S. J.; Tieleman, D. P., Pressure–area isotherm of a lipid monolayer from molecular dynamics simulations. *Langmuir* **2007**, *23* (25), 12617-12623.
22. Huang, P. Y.; Ruiz-Vargas, C. S.; van der Zande, A. M.; Whitney, W. S.; Levendorf, M. P.; Kevek, J. W.; Garg, S.; Alden, J. S.; Hustedt, C. J.; Zhu, Y.; Park, J.; McEuen, P. L.; Muller, D. A., Grains and grain boundaries in single-layer graphene atomic patchwork quilts. *Nature* **2011**, *469* (7330), 389-392.
23. Li, X.; Zhu, Y.; Cai, W.; Borysiak, M.; Han, B.; Chen, D.; Piner, R. D.; Colombo, L.; Ruoff, R. S., Transfer of large-area graphene films for high-performance transparent conductive electrodes. *Nano Lett.* **2009**, *9* (12), 4359-4363.
24. Su, Y.; Han, H.-L.; Cai, Q.; Wu, Q.; Xie, M.; Chen, D.; Geng, B.; Zhang, Y.; Wang, F.; Shen, Y. R.; Tian, C., Polymer adsorption on graphite and cvd graphene surfaces studied by surface-specific vibrational spectroscopy. *Nano Lett.* **2015**, *15* (10), 6501-6505.
25. Pirkle, A.; Chan, J.; Venugopal, A.; Hinojos, D.; Magnuson, C. W., The effect of chemical residues on the physical and electrical properties of chemical vapor deposited graphene transferred to sio₂. *Appl. Phys. Lett.* *99*, 122108.
26. Kumar, K.; Kim, Y.-S.; Yang, E.-H., The influence of thermal annealing to remove polymeric residue on the electronic doping and morphological characteristics of graphene. *Carbon* **2013**, *65*, 35-45.

27. Arjmandi-Tash, H.; Jiang, L.; Schneider, G. F., Rupture index: A quantitative measure of sub-micrometer cracks in graphene. *Carbon* **2017**, *118*, 556-560.
28. Lima, L. M. C.; Fu, W.; Jiang, L.; Kros, A.; Schneider, G. F., Graphene-stabilized lipid monolayer heterostructures: A novel biomembrane superstructure. *Nanoscale* **2016**, *8* (44), 18646-18653.

CHAPTER 7

Conclusions, Challenges and Outlook

7.1 Summary and general conclusions

The main focus of this thesis was to understand how amphiphilic lipid molecules interact with the hydrophobic surface of graphene. Lipid bilayers have a hydrophobic core, so the first thought was to encapsulate graphene in the center of a lipid bilayer. Thus, the electrical properties of graphene could be used to monitor any environmental change on its surroundings through lipid interactions with proteins, DNA or any specific biomolecule. Furthermore, the functionalization of graphene with lipids renders graphene more hydrophilic and more compatible with a biological environment, particularly if graphene is inserted within the hydrophobic core of a lipid bilayer. Graphene is atomically flat with sp^2 hybridized carbon atoms with conjugated p_z orbitals, where the electrons are directly exposed to the environment in which graphene is exposed, therefore very sensitive to any perturbation or variations, particularly changes in dielectric properties. Lipids, as the main constituents of cell membranes, participate in numerous biological processes, thus graphene can be used as a sensor to monitor those processes.

This project work started by characterizing the structure of a lipid monolayer with graphene transferred on top, as described in Chapter 2. A lipid monolayer was assembled on a Si/SiO₂ substrate using the Langmuir-Blodgett (LB) method and a graphene layer was transferred on top. The lipids were characterized by infrared (IR) spectroscopy and ellipsometry in the absence and in the presence of graphene. The monolayer adopted a more compact and organized structure with a graphene layer deposited on top and the presence of the lipid monolayer underneath graphene improved the electrical performances of graphene which were measured with a graphene field-effect transistor (GFET).

The re-ordering of the lipids upon the transfer of graphene represented the first step towards encapsulating graphene within a lipid bilayer. In Chapter 3, a second lipid monolayer of lipids was transferred on top of graphene – lipid acyl chains facing the graphene. The lipid-graphene-lipid assembly presented a well-defined and stable structure similar to a lipid bilayer without graphene; i.e. graphene in the hydrophobic core of the lipid bilayer did not disturb the integrity of the lipid bilayer. In addition, neutron reflectometry experiments provided information on the thickness, structure, roughness and stability of the lipid-graphene assemblies. IR spectroscopy and ellipsometry measurements complemented and confirmed

the same results as neutron reflectometry: the successful assembly of a stable lipid-graphene-lipid construct, never achieved experimentally.

Lipids can exhibit different phases which influence the mobility, molecular order and lateral organization of the lipids assembly. In Chapter 4, temperature variations were applied to a lipid monolayer assembled using the LB technique with a graphene monolayer transferred on top, below and above the phase transition temperature of the lipids. Atomic force microscopy (AFM) studies showed that the lipid monolayer decreased its thickness and formed a continuous monolayer after increasing the temperature above the phase transition of the lipids. Additionally, graphene acted as a protective layer, shielding the lipids from environmental variations. The lipid monolayer underneath graphene remained intact after rinsing the assembly with chloroform or with an aqueous solution of the surfactant CTAB.

Lipid assemblies depend on the chemical structure like charge, acyl chain length and degree of unsaturation, and parameters such as temperature and solid support used. In Chapter 5, zwitterionic, cationic and anionic lipids with different chain lengths and degree of saturation were investigated by IR spectroscopy on HOPG and graphene. The lipids were assembled on top of a chemical vapor deposition (CVD) graphene-on-copper and on graphite (in the form of HOPG) supports using the Langmuir-Schaefer (LS) and vesicle fusion (VF) methods. IR spectroscopy showed that saturated lipids presented a higher structural order on the substrates in comparison with the unsaturated lipids. For a range of unsaturated lipids with the same chain length, cationic lipids yielded a more organized lipid structure on graphene and graphite. Separately, liposomes of the different lipids were prepared for quartz crystal microbalance dissipation monitoring (QCM-D) measurements. Lipids were deposited using the VF method on CVD graphene transferred on SiO_2 and on gold-coated QCM sensors, respectively. Depending on the lipid charge, saturation and chain length, lipids assembled differently on graphene-on- SiO_2 and on graphene-on-gold. Importantly, the results suggested that graphene is transparent to the wetting properties of the substrates on which it has been transferred and thereby on how lipids (from liposomes) interact with the graphene surface. In fact, the results showed that a lipid bilayer was formed on graphene transferred to a SiO_2 substrate, i.e. graphene-

on-SiO₂ is hydrophilic, and that instead liposomes remained intact on graphene-on-gold (hydrophobic).

After studying the lipids-graphene interactions in assemblies where graphene was positioned on top or deposited underneath a lipid layer, in Chapter 6, the interactions of lipids with graphene edges were investigated. Remarkably, a compressed lipid monolayer in a Langmuir trough prevented graphene to crack during etching and transfer, therefore acting as molecular clamps on the edges of the 2D material. For applications such as biosensors, graphene has to be pristine, thus, without contaminants. Using this approach, lipids were only interacting with the edges of graphene, therefore promoting a basal plane free of contaminants.

7.2 Challenges and outlook

Despite all the promising potential applications of lipid-graphene assemblies, studying the interactions between pristine graphene and lipids encountered several difficulties. Lipids are dynamic systems while graphene is static and very difficult to handle when is not supported by a polymer/substrate. As mentioned in Chapter 6, the surface of graphene has to be pristine and without contaminants to preserve its electrical properties. We successfully managed to transfer a very clean graphene surface of $\sim 1 \times 1 \text{ cm}^2$ to a Si/SiO₂ substrate, but for large graphene sheets ($> 3 \times 3 \text{ cm}^2$), the method was less efficient, facing a variety of issues. For instance, to assemble the samples for the neutron reflectometry experiments in Chapter 3 where $5 \times 5 \text{ cm}^2$ samples were needed. Graphene transfer (without a polymer) to the $5 \times 5 \text{ cm}^2$ silicon blocks typically induced the folding and cracking of graphene, making the handling and consequently the transfer of graphene very difficult. In general, using graphene without a polymer yields very clean graphene surfaces but still remains a big challenge to overcome for large graphene sheets, a major technical problem to still overcome in the future.

Additionally, amphiphilic lipids are comprised of a hydrophilic head group and hydrophobic acyl chains which interact with the hydrophobic basal plane of graphene. When graphene is used as a substrate for the lipids assembly, the hydrophilic lipid head groups will face the outer environment (the hydrophobic tails will face graphene) which tend to be very unstable thermodynamically (most probably changing their conformation after drying) if they are not constantly kept in a liquid environment, as depicted in Chapter 5. The continuous exposure to

liquid environments therefore limits the handling, reproducibility and the characterization methods that can be used to study the structure and monitor how lipids and graphene interact.

Nevertheless, we successfully encapsulated graphene in the hydrophobic core of a lipid bilayer. The characterization by neutron reflectometry allowed to measure and estimate the thickness, structure and stability of the lipid bilayer with graphene encapsulated in its hydrophobic core which was never realized experimentally so far. As mentioned above, although the handling of such a large graphene monolayer ($5 \times 5 \text{ cm}^2$) still induced cracks on the graphene surface after transfer, the structure could be well characterized by neutron reflectometry.

Now would be interesting to study whether lipid-graphene assemblies are a useful platform to study the formation of molecular imprints of (bio)molecules (Lei Ye, *Molecular Imprinting*, Pan Stanford Publishing, 2013) or a lipid film (with graphene underneath or sandwiched in the hydrophobic core of the lipid bilayer). In addition, removing the Si/SiO₂ substrate from the lipid-graphene-lipid assembly in a liquid environment (hydrophilic lipid head groups facing the liquid and graphene in the hydrophobic core) could also provide a new concept of sensing device where graphene would be circulating inside of the body – stabilized by the lipids – acting as a in situ sensor of any environmental modification or binding to the lipids. Such a platform could yield potential biosensing applications taking advantage of the excellent electrical properties of graphene and the affinity of lipids with other biomolecules. The major challenge lies in how to sense the graphene: remote sensing using radio frequency or Raman for in vitro experiments.

Another challenge would be to fabricate graphene liquid cells functionalized with lipids. Graphene liquid cells are very small pockets of liquid sandwiched between two graphene sheets deposited on TEM grids. Graphene is one atom thick, and ultimately allows a better contrast on the TEM images compared to currently used SiN cells (which are at least two orders of magnitude thicker). Imaging dynamic biological processes with nanometer resolution, in liquid, in situ for instance, lipid interactions with other biomolecules, vesicle fusion and/or rupture and ultimately membrane fusion in biomimetic graphene liquid pockets, is a challenge that may overcome a reality based on the first results of this thesis.

Appendix I

Supporting Information to Chapter 2

I. Materials and Methods

Langmuir-Blodgett technique

1,2-dipalmitoyl-*sn*-glycero-3-phosphocholine (DPPC) and 1% of 1,2-dipalmitoyl-*sn*-glycero-3-phosphoethanolamine-N-(lissamine rhodamine B sulfonyl) (Liss Rhod PE) (99:1) lipids (Avanti Polar Lipids Inc.) with a concentration of 1 mg/mL were prepared in CHCl₃/CH₃OH 3:1 vol %. The lipid solution was deposited dropwise at the interface of air-ultrapure water in a Langmuir trough at 25 °C using a glass microliter syringe, and the organic solvent was left to evaporate for 15 min. The measurements were performed in a Minitrough 2, KSV Instruments using the KSV Research Lab v2.01 software. The Teflon trough was equipped with hydrophilic barriers made of Delrin. The surface pressure (π) was measured with a microbalance platinum plate, with the lipids passing through different phases upon compression. The Si/SiO₂ substrate was primarily inserted in the ultrapure water and after compressing the lipids to $\pi = 30$ mN/m, the substrate was slowly retracted from the trough while simultaneously keeping the surface pressure of the lipids constant. Consequently, the lipid monolayer was transferred onto the Si/SiO₂ substrate and the lipids transfer ratio was determined. The transfer ratio is defined by the ratio between the change on the barriers area and consequently the drop in the monolayer area during the transfer to the substrate, and the area of the substrate. In all the samples prepared, the transfer ratio was 1.0 ± 0.1 , in agreement with the transfer of a homogeneous lipid film. Multiple (> 10) measurements confirmed the reproducibility of the experiments.

Lipid-assisted transfer method

A monolayer of graphene was grown on a copper foil (chemical vapor deposition (CVD) graphene from Graphenea) and placed on an ammonium persulfate solution (0.5 M) (APS) – copper etchant – and after etching, the graphene was transferred above the lipid monolayer on a Si/SiO₂ substrate by bringing both into contact. Subsequently, the sample was rinsed with ultrapure water to remove the etchant residues. A Si/SiO₂-lipid-graphene assembly was obtained.

Imaging set-up

Optical images were obtained using a Leica DM 2700 M microscope. Bright field fluorescence images were obtained using a Zeiss Axiovert 200 with a 5x objective. For the fluorescence microscopy studies, a fluorescent 1,2-dipalmitoyl-*sn*-glycero-3-phosphoethanolamine-N-(lissamine rhodamine B sulfonyl) (1 mol %) lipid was mixed with DPPC, to characterize the lipid monolayer assembly and the fluorescence quenching of graphene after the transfer on top of the lipid monolayer.

Attenuated total reflectance infrared spectroscopy (ATR-IR)

Infrared spectroscopy determines the conformation and orientation of lipid molecules by measuring the frequency of the absorbed molecules and recording the difference before and after the physical perturbations induced by graphene on the molecules. The chemical bonds of lipid molecules present mainly different vibrational modes: symmetric and asymmetric stretching, scissoring and rocking. The frequency of the methylene (CH₂) stretching vibrations is responsible for conformational changes in the lipid acyl chains. A shift of the symmetric and asymmetric CH₂ stretching vibrations (~2850 cm⁻¹ and ~2920 cm⁻¹, respectively) to higher wavenumbers is observed if a transition of the lipids from a gel to a fluidic phase occurs (i.e. typically *gauche* to *trans* conformational change).¹⁻³

Spectra were collected with a BIO-RAD Excalibur Series spectroscopy apparatus using a silicon ATR crystal 25 reflections (4x2 cm) with an angle of incidence of 45° (Specac) and a spectra range of 6000-400 cm⁻¹. For each spectrum 128 scans with a resolution of 2 cm⁻¹ were averaged and the chamber was continuously purged with dry air. The data was processed with Origin-Pro software. The spectrum of a clean silicon ATR crystal was subtracted as background. The sample preparation on the ATR crystal was the same as on the Si/SiO₂ substrate, using a larger piece of CVD monolayer graphene on copper (60x40 mm from Graphenea). All lipid spectra were measured before and after the transfer of the graphene layer on top of the lipid monolayer.

Ellipsometry

The thicknesses of the lipid monolayer before and after graphene transfer were determined using a WVASE ellipsometer M-2000F EC-400 from J.A. Woollam Co.

Inc. The data were collected using the WVase32 software. Each sample was measured at least in three different positions with five angles of incidence (65°, 70°, 75°, 80° and 85°), at a wavelength ranging between 250 and 1000 nm. The thicknesses values were measured step-by-step, using layer-by-layer models: i) the SiO₂ layer on the Si/SiO₂ substrate, ii) the transferred Langmuir DPPC monolayer and, iii) the graphene layer transferred on top. The collected data were fitted with models specific for each material. Each material has a set of optical constants containing the refractive index n and the extinction coefficient k . Plain SiO₂ substrate data were fitted with SiO₂.JAW model ($n = 1.4554-1.5157$; $k = 0$) and the lipid monolayer with a CAUCHY model.⁴ The CAUCHY optical constants were $n = 1.46-1.615$ and k were set at 0. A_n , B_n and C_n (constants determined for the material, i.e. the lipids) were 1.45, 0.01 and 0, respectively. A_n , B_n and C_n were kept constant. The model for graphene was taken from the literature.⁵

Atomic force microscopy (AFM)

AFM images were obtained with a JPK NanoWizard Ultra Speed apparatus and the images were processed using JPK SPM Data Processing software. AFM images were recorded by scanning the sample with a silicon probe (AC240TS, Asylum Research) with 70 kHz nominal resonance frequency. The images were scanned in an intermittent contact mode in air at room temperature with 512x512 pixels.

Raman spectroscopy

Raman spectra and imaging were measured using a WITec confocal spectrometer with a 532 nm laser and a 100x objective with a lateral resolution of 200-300 nm. The laser power was finely tuned to be below 1 mW to avoid damages to the graphene and the lipid monolayer.

Electrical measurements

The transistor characteristics of the graphene field-effect transistor devices on a Si/SiO₂ substrate and on a lipid monolayer were tested using a home-made setup. A SR830 DSP lock-in amplifier with narrow filters was used to recover weak signal from a noisy background. The back gate voltage V_g (up to 200 V) was applied using a Keithley 2400 multimeter. The defective lipid monolayer yielded a transfer ratio of 0.5 on the Langmuir-Blodgett technique, meaning that the surface of the Si/SiO₂ substrate was not fully covered with the lipid monolayer.

References

1. Lewis, R. N. A. H.; McElhaney, R. N., Membrane lipid phase transitions and phase organization studied by fourier transform infrared spectroscopy. *BBA-Biomembranes* **2013**, *1828* (10), 2347-2358.
2. Tamm, L. K.; Tatulian, S. A., Infrared spectroscopy of proteins and peptides in lipid bilayers. *Q. Rev. Biophys.* **1997**, *30* (4), 365-429.
3. Blume, A.; Kerth, A., Peptide and protein binding to lipid monolayers studied by ft-irra spectroscopy. *BBA-Biomembranes* **2013**, *1828* (10), 2294-2305.
4. Mora, M. F.; Wehmeyer, J. L.; Synowicki, R.; Garcia, C. D., Investigating protein adsorption via spectroscopic ellipsometry In *Biol. Inter. Mater. Surf.*, Puleo, D. A.; Bizios, R., Eds. Springer Science, 2009.
5. Nelson, F. J.; Kamineni, V. K.; Zhang, T.; Comfort, E. S.; Lee, J. U.; Diebold, A. C., Optical properties of large-area polycrystalline chemical vapor deposited graphene by spectroscopic ellipsometry. *Appl. Phys. Lett.* **2010**, *97* (25), 253110.

Appendix II

Supporting Information to Chapter 3

II. Materials and Methods

Langmuir-Blodgett and Langmuir-Schaefer techniques

The measurements were performed in a Minitrough 2, KSV Instruments equipped with hydrophilic barriers made of Delrin. The 1,2-distearoyl-*sn*-glycero-3-phosphocholine (DSPC) lipids (Avanti Polar Lipids Inc.) were first dissolved in a $\text{CHCl}_3/\text{CH}_3\text{OH}$ mixture (3:1 vol%) with a concentration of 1 mg/mL in lipids. Next, the lipids were deposited at the air-ultrapure water interface in a Langmuir trough at 25 °C and compressed to a surface pressure (π) of 40 mN/m. The lipid monolayer was transferred to a Si/SiO₂ substrate at a constant lipid compression of $\pi = 40$ mN/m. Subsequently, a chemical vapor deposition (CVD) graphene on copper (1x1 cm², Graphenea) was transferred on top of the lipid monolayer by bringing the graphene into contact with the substrate coated with the lipid monolayer, as described in detail in Appendix I. The Langmuir-Schaefer¹ method was used to transfer a second DSPC monolayer on top of graphene. The lipids were compressed in a Langmuir trough to $\pi = 40$ mN/m and the Si/SiO₂-lipid monolayer-graphene sample was horizontally lowered into contact with the lipid monolayer at the air-ultrapure water interface and immediately retracted from the interface, encapsulating graphene in the hydrophobic core of a DSPC lipid bilayer. The sample preparation for the neutron reflectometry experiments is described below.

Infrared reflection absorption spectroscopy (IRRAS)

IR spectra were collected with a BIO-RAD Excalibur Series infrared spectrometer in external reflectance mode. The chamber was continuously purged with dry air and a sample of plain Si/SiO₂ substrate was taken as reference. The angle of incidence was measured at 45° with a spectra range of 6000-400 cm⁻¹. Each spectrum was collected for an average of 128 scans with a resolution of 2 cm⁻¹. The data were processed using Origin-Pro software. All samples were dried in air before the measurements.

Ellipsometry

The thicknesses of the lipid monolayer before and after graphene transfer were determined using a WVASE ellipsometer M-2000F EC-400 from J.A. Woollam Co. Inc. The data were collected using the WVase32 software. Each sample was measured at least in three different positions with five angles of incidence (65°, 70°, 75°, 80° and 85°), at a wavelength ranging between 250 and 1000 nm. The thicknesses values were measured step-by-step, using layer-by-layer models: i) the SiO₂ layer on the Si/SiO₂ substrate, ii) the transferred Langmuir DSPC monolayer, iii) the graphene layer transferred on top and, iv) the second DSPC monolayer transferred above graphene. The collected data were fitted with models specific for each material. Each material has a set of optical constants containing the refractive index n and the extinction coefficient k . Plain SiO₂ substrate data were fitted with SiO2.JAW model ($n = 1.4554-1.5157$; $k = 0$) and the lipid monolayer with a CAUCHY model.² The CAUCHY optical constants were $n = 1.46-1.615$ and k were set at 0. A_n , B_n and C_n (constants determined for the material, i.e. the lipids) were 1.45, 0.01 and 0, respectively. A_n , B_n and C_n were kept constant. The model for graphene was taken from the literature.³ All samples were dried in air before the measurements.

Neutron reflectometry

Neutron reflectivity measurements were performed at the Institut Laue-Langevin (ILL, Grenoble, France) at the D17 reflectometer,⁴ in Time-of-Flight (TOF) mode, with wavelengths between 2 and 20 Å at two incident angles (0.8 and 3.2°). Different water contrasts were used to measure the silicon blocks and the lipid layers with graphene – H₂O, silicon matched water (SMW), and D₂O. SMW is a mixture of H₂O and D₂O to give different scattering length density (SLD, Table II.1). The samples were prepared with different freshly polished silicon blocks (5x5 cm²), cleaned with solvents (chloroform, acetone and ethanol) and then with five minutes of oxygen plasma. DSPC lipids were prepared, deposited and compressed on a Langmuir trough to $\pi = 40$ mN/m, at ILL (NIMA, Warwick, UK) at 19 °C and transferred to the silicon blocks as described above. For the deposition of the second DSPC monolayer by the Langmuir-Schaefer method, the silicon block (with the graphene on the lipid monolayer) was horizontally moved downwards and pushed through the lipids at the air-ultrapure water interface onto a Teflon cell

placed primarily inside the trough. The sample was then sealed in a liquid cell with a small volume of enclosed water inside to keep the second lipid monolayer hydrated, as described previously.⁵ The reflectivity data was fit by dividing each sample into different layers with distinct SLD, thickness and roughness (Table II.1). The SLD profiles were modeled using MOTOFIT,⁶ where the specular reflectivity was calculated with the Abeles matrix method for stratified interfaces.⁷ For example, for the lipid-graphene-lipid assembly, the layers were divided as following: 1) SiO₂, 2) solvent, 3) inner lipid head groups, 4) inner lipid tails, 5) graphene, 6) outer lipid tails, and 7) outer lipid head groups. Large sheets of CVD graphene on copper were transferred above the silicon blocks (with the lipid monolayer) after the copper was etched in a solution of ammonium persulfate (0.1 M). The graphene (without any support) floating on water was transferred from the top inducing some cracks and folding of the graphene surface due to the very large piece of graphene transferred. The coverage of the graphene on the silicon block was ~31%, as observed in Figure II.1.

Table II.1. Parameters obtained from the fits for the lipid-graphene-lipid assembly at 25 °C. The SLD, thickness, roughness and percentage of water of the different layers.

Layers	SLD x10 ⁻⁶ (Å ⁻²)			Thickness (Å)	Roughness (Å)	% of water
Si	2.07			-	4	-
SiO ₂	3.47			11	3	15
Solvents	H ₂ O	SMW	D ₂ O	4.5	-	100
	-0.56	2.07	6.35			
Lipid head groups	1.5			8	3	15
Lipid tails	-0.45			18	4	4
Graphene	7.3*0.31			1.5	3	10
Lipid tails	-0.4			17	4	8
Lipid head groups	1.5			8.8	5	17
Solvents	H ₂ O	SMW	D ₂ O	-	-	-
	-0.56	2.07	6.35			

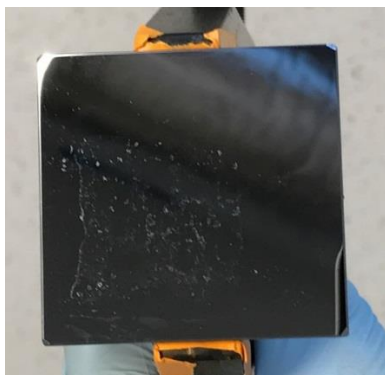


Figure II.1. Image of the 5x5 cm² silicon block showing the graphene transferred on top with a coverage of ~31%.

References

1. Bang, J. J.; Porter, A. G.; Davis, T. C.; Hayes, T. R.; Claridge, S. A., spatially controlled noncovalent functionalization of 2D materials based on molecular architecture. *Langmuir* **2018**, *34* (19), 5454-5463.
2. Mora, M. F.; Wehmeyer, J. L.; Synowicki, R.; Garcia, C. D., Investigating protein adsorption via spectroscopic ellipsometry In *Biol. Inter. Mater. Surf.*, Puleo, D. A.; Bizios, R., Eds. Springer Science, 2009.
3. Nelson, F. J.; Kamineni, V. K.; Zhang, T.; Comfort, E. S.; Lee, J. U.; Diebold, A. C., Optical properties of large-Area polycrystalline chemical vapor deposited graphene by spectroscopic ellipsometry. *Appl. Phys. Lett.* **2010**, *97* (25), 253110.
4. Cubitt, R.; Fragneto, G., D17: the new reflectometer at the ILL. *Appl. Phys. A* **2002**, *74* (1), s329-s331.
5. Charitat, T.; Bellet-Amalric, E.; Fragneto, G.; Graner, F., Adsorbed and free lipid bilayers at the solid-liquid interface. *Eur. Phys. J. B Condens. Matter Compl. Syst.* **1999**, *8* (4), 583-593.
6. Nelson, A., Co-refinement of multiple-contrast neutron/X-ray reflectivity data using MOTOFIT. *J. Appl. Crystallogr.* **2006**, *39* (2), 273-276.
7. Heavens, O. S., *Optical Properties of Thin Solid Films*. Butterworth 1955.

Appendix III

Supporting Information to Chapter 4

III. Materials and Methods

Langmuir-Blodgett and Langmuir-Schaefer techniques

As described in detail in Appendix I, 1,2-dipalmitoyl-*sn*-glycero-3-phosphocholine (DPPC) lipids were deposited at the interface of a Langmuir trough with ultrapure water, compressed until a surface pressure (π) of 30 mN/m and transferred to a Si/SiO₂ substrate. Next, a chemical vapor deposition (CVD) graphene layer on copper (Graphenea) was transferred on top. The Langmuir-Schaefer method was used to transfer the second DPPC monolayer on top of graphene deposited on the first DPPC monolayer. The transfer ratio of the first DPPC monolayer was ~ 1 , obtaining an uniform and continuous lipid monolayer on the Si/SiO₂ substrate, but the transfer ratio of the second DPPC monolayer was incomplete (0.5), suggesting that the transfer of a second lipid monolayer did not yield a continuous and intact layer.

Atomic force microscopy (AFM)

AFM images were obtained using a JPK NanoWizard Ultra Speed instrument apparatus, and the images were processed with a JPK SPM Data Processing software. The experiments were performed using a silicon probe (AC240TS, Asylum Research) with 70 kHz nominal resonance frequency. The images of 5x5 μm^2 were scanned in an intermittent contact mode in air at room temperature with 512x512 pixels.

Temperature-controlled AFM measurements

For the AFM experiments, heating-cooling cycles were performed. First the sample was heated at 60 °C on a hot plate (IKA® RCT basic), stabilized for 5 min, and then cooled down to room temperature (RT). After AFM scanning, the sample was subjected to five heating-cooling cycles (RT – 60 °C – RT) and scanned again by AFM. Afterwards, the sample was cycled five times to 100 °C (RT – 100 °C – RT) and measured again by AFM.

Rinsing with solvents

The Si/SiO₂-lipid-graphene assemblies were carefully rinsed with chloroform and then with a 10 mM of hexadecyltrimethylammonium bromide (CTAB) solution in water. For that, the samples were dipped into the solutions vertically upon and down seven times. For the CTAB rinsing, the sample was afterwards rinsed with ultrapure water before the measurements, to remove residual CTAB from the sample.

Optical images

Optical images were acquired using a Leica DM 2700 M microscope and the fluorescence images were performed using a Zeiss Axiovert 200 inverted microscope with 5x objective. For the fluorescence microscopy experiments, 1 mol% of 1,2-dipalmitoyl-*sn*-glycero-3-phosphoethanolamine-N-(lissamine rhodamine B sulfonyl) (Liss Rhod PE) was added to the DPPC stock solution (1 mg/mL) before depositing the lipids in the Langmuir trough.

Infrared reflection absorption spectroscopy (IRRAS)

Measurements were performed with a BIO-RAD Excalibur Series infrared spectrometer in an external reflectance mode. The chamber was continuously purged with dry air and a sample of plain Si/SiO₂ substrate was taken as reference. The angle of incidence was measured at 45° with a spectra range of 6000-400 cm⁻¹. Each spectrum was obtained with an average of 20 scans and with a resolution of 2 cm⁻¹.

A home-made temperature controller – resistive heater – was positioned inside of the infrared spectrometer holder (resistance of few hundreds of kΩ), as observed in Figure III.1a. The sample was placed on top of the resistive heater using silver paste and a digital probe thermometer (Amprobe, AM-530-EUR) equipped with a thermocouple glued on the sample to monitor the temperature. A potential was applied using a Keithley 2400 multimeter. For example, applying a potential of 28 V, corresponding to electrical current of 49.8 mA allowed to reach a maximum temperature of 78 °C in our experiments (Figure III.1b).

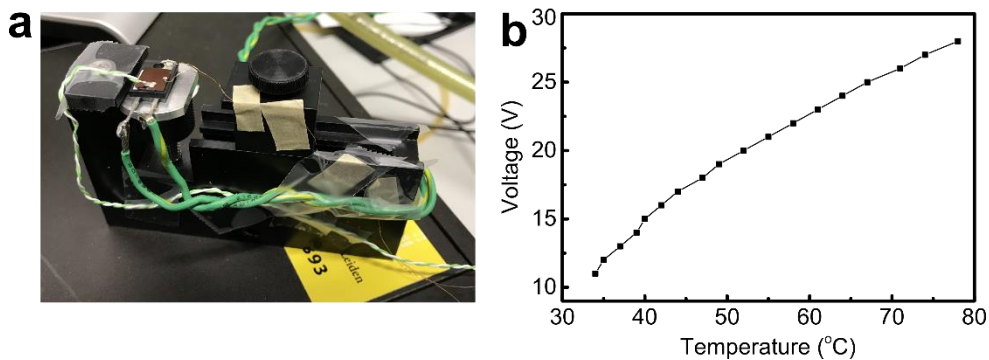


Figure III.1. a) Image of the home-made setup mounted on the spectrometer holder. The sample (blue, Si/SiO₂ substrate) is mounted on a resistive heater that is placed on top of the metal holder. A thermocouple is glued to the sample with silver paste. b) Temperature vs voltage plot applied to the sample step-by-step.

Appendix IV

Supporting Information to Chapter 5

IV. Materials and Methods

Samples preparation

Four different lipids were used in this work: the zwitterionic saturated 1,2-dipalmitoyl-*sn*-glycero-3-phosphocholine (DPPC), the zwitterionic unsaturated 1,2-dioleoyl-*sn*-glycero-3-phosphocholine (DOPC), the anionic unsaturated 1,2-dioleoyl-*sn*-glycero-3-phospho-L-serine (DOPS), and the cationic unsaturated 1,2-dioleoyl-3-trimethylammonium-propane (DOTAP), all purchased from Avanti Polar Lipids Inc. The lipids were transferred to distinct substrates with two different methods: the Langmuir-Schaefer (LS) and the vesicle fusion (VF). The LS technique was performed using a Minitrough 2, KSV Instruments at 25 °C with ultrapure water and the lipids were compressed until a surface pressure (π) of 30 mN/m, as described in detail in Appendix I. Then, the substrate was approached horizontally downwards contacting the lipid chains at the interface, and thereafter immediately retracted under a constant lipid compression ($\pi = 30$ mN/m). For the VF method, each individual lipid was first dissolved in a mixture of CHCl₃/CH₃OH 3:1 vol% to yield a 3 mM concentration. The solutions were evaporated under nitrogen flow for 30 minutes and then resuspended with ultrapure water (or phosphate buffer for the QCM experiments) to obtain a final concentration of 0.5 mM. Subsequently, the lipids were subjected five times to 40 seconds cycles of vortex and thereafter, 30 minutes of sonication (VWR, Ultrasonic Cleaner USC-TH) in order to obtain unilamellar vesicles. 100 μ l of the lipid suspensions were added to the different substrates for a duration time of 30 minutes and then rinsed several times with ultrapure water (or phosphate buffer, PBS), to remove the vesicles in excess. For DPPC lipids, the liposomes assembly were performed above the phase transition temperature of 41°C.

The substrates used for attenuated total reflectance infrared spectroscopy (ATR-IR) characterization were: chemical vapor deposition (CVD) graphene-on-copper and highly oriented pyrolytic graphite (HOPG). The graphene-on-copper was grown in our group using a Planar Tech tube oven and the HOPG was purchased from SPI supplies.

Attenuated total reflectance infrared spectroscopy (ATR-IR)

The spectra were collected with a PerkinElmer FT-IR Spectrometer Spectrum Two apparatus with a diamond attenuated total reflection (ATR) crystal. Typically 16 scans were collected and averaged with a resolution of 2 cm^{-1} . The CVD graphene-on-copper and the HOPG samples with the different lipids deposited on top were scanned at room temperature after the samples were dried in air. The data were processed using Origin-Pro software. The ATR-IR spectra collected for the mean distribution of wavenumbers of the symmetric and asymmetric stretching CH_2 vibrations of the different lipids are observed in Figure IV.1. The lipids were transferred to CVD graphene-on-copper and HOPG by two different methods – Langmuir-Schaefer and vesicle fusion.

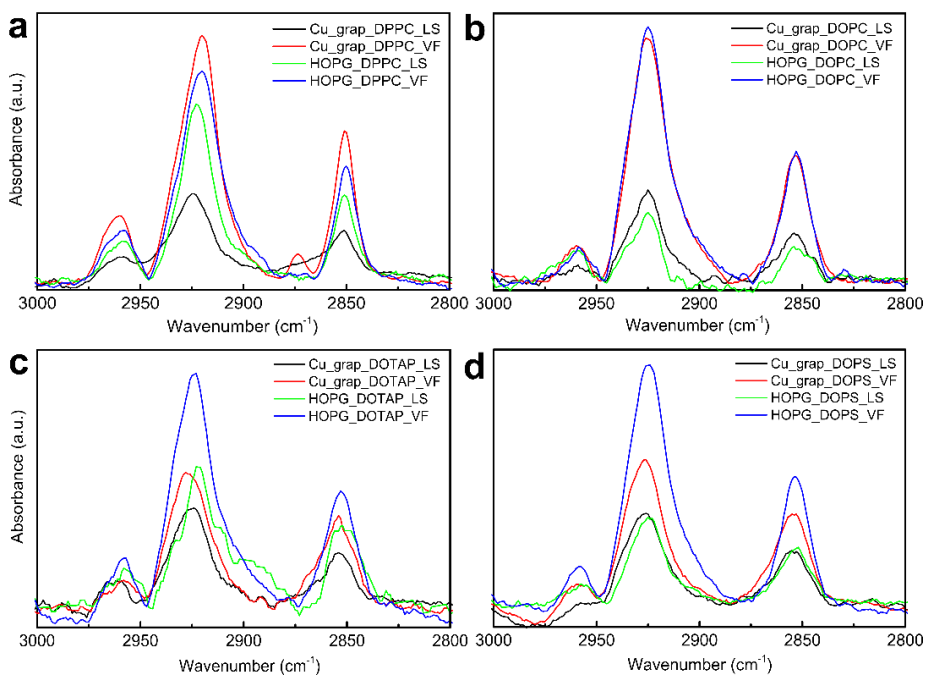


Figure IV.1 a) ATR-IR spectra of DPPC assembled with the Langmuir-Schaefer and the vesicle fusion methods on graphene-on-copper and HOPG. b) ATR-IR spectra of DOPC assembled with the Langmuir-Schaefer and the vesicle fusion methods on graphene-on-copper and HOPG. c) ATR-IR spectra of DOTAP assembled with the Langmuir-Schaefer and the vesicle fusion methods on graphene-on-copper and HOPG. d) ATR-IR spectra of DOPS assembled with the Langmuir-Schaefer and the vesicle fusion methods on graphene-on-copper and HOPG.

Atomic force microscopy (AFM)

AFM images with 512x512 pixels were scanned in an intermittent mode in air at room temperature and performed with a JPK NanoWizard Ultraspeed instrument. The experiments were acquired using a silicon probe (AC240TS, Asylum Research) with a 70 kHz nominal resonance frequency. The HOPG samples were freshly exfoliated before the measurements.

Quartz crystal microbalance with dissipation monitoring (QCM-D)

The QCM-D technique is used to monitor the assembly and formation of lipid monolayers or bilayers by the VF method on quartz crystal substrates.¹ The substrates are equipped with two electrodes which activate the piezoelectric effect of the quartz crystal sandwiched between the electrodes upon applying an alternating voltage (AC) to the crystal resulting in an oscillation of the quartz crystal. If a lipid layer adsorbs on the crystal substrate, the resonance frequency of the crystal decreases, yielding a change in frequency (Δf) that is proportional to the mass adsorbed. The exponential decay of the oscillation frequency after a discontinuity of the applied AC voltage is associated to the energy dissipation factor (D), i.e., the loss of energy per oscillation, and is proportional to the viscoelastic property of the adsorbed layer.² The adsorption of liposomes on a QCM crystal typically results in a large decrease of frequency of oscillation and an increase of the energy dissipation. The subsequent rupture of the liposomes and the formation of a SLB, however leads to an increase of the frequency change (solvent loss inside the vesicles) and an abrupt decrease of the energy dissipation values to almost 0, due to the formation of a “rigid” SLB.² Liposomes tend to rupture and form a lipid bilayer on SiO₂-coated QCM crystals, due to the hydrophilicity of both the substrate and the lipid head groups.³⁻⁴ However, for gold-coated QCM crystals the hydrophobicity of gold leads to the adsorption of intact liposomes.^{1, 5}

QCM-D experiments were performed with a Q-sense Explorer, Biolin Scientific AB. The normalized frequency and the changes in dissipation were measured simultaneously, at room temperature (~22 °C) for DOTAP, DOPS and DOPC lipids and above the phase transition temperature of DPPC lipid (~55 °C). The data were presented for the third overtone and the Sauerbrey equation (valid for thin and soft lipid layers) was used to calculate the adsorbed masses on the crystal sensors.¹

The lipid samples were all prepared in PBS solution. The PBS solution was first injected in the chamber and after ~ 20 minutes of stabilization, a volume of ~ 0.5 mL of liposomes of the different lipids was injected in the chamber with the QCM sensors. After ~ 1 hour, pure PBS solution was again injected into the QCM chamber in order to check the stability of the layer deposited on the QCM sensors.

The QCM-sensors used for the measurements were the SiO_2 and gold. The CVD graphene was transferred on top of the sensors using the PMMA assisted transfer method.⁶ The plain SiO_2 and gold QCM sensors were also measured with DOPC lipids as a control. Figure IV.2 shows the QCM data for DOPC liposomes deposited on SiO_2 (Figure IV.2a) and on gold (Figure IV.2b).

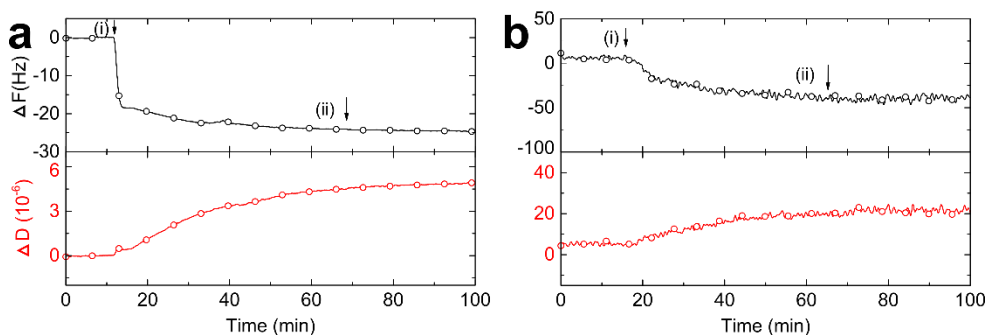


Figure IV.2. a) Quartz crystal microbalance monitoring the assembly of the zwitterionic unsaturated DOPC lipids on SiO_2 . e) Quartz crystal microbalance monitoring the assembly of the zwitterionic unsaturated DOPC lipids on gold.

Raman spectroscopy

Raman spectra were measured on a WITec confocal spectrometer with a 532 nm laser and a 100x objective with the lateral resolution of 200-300 nm. The SiO_2 QCM crystals with a CVD graphene transferred on top were scanned before and after the QCM-D measurements, in order to confirm the integrity of graphene on the surface of the crystal during all the QCM-D measurements. Figure IV.3 shows the Raman spectra of CVD graphene transferred on the SiO_2 sensor crystal before and after performing the QCM-D experiments.

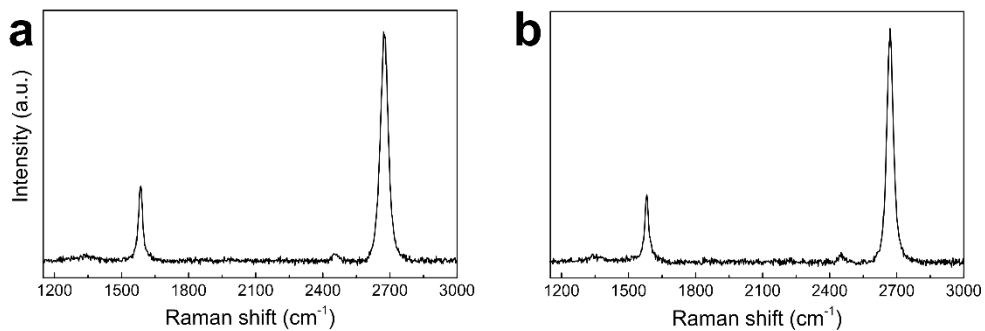


Figure IV.3. Raman spectroscopy of graphene transferred on the SiO₂ sensor crystal before (a) and after (b) the QCM-D measurements.

References

1. Keller, C. A.; Kasemo, B., Surface specific kinetics of lipid vesicle adsorption measured with a quartz crystal microbalance. *Biophys. J.* **1998**, *75* (3), 1397-1402.
2. Cho, N.-J.; Frank, C. W.; Kasemo, B.; Höök, F., Quartz crystal microbalance with dissipation monitoring of supported lipid bilayers on various substrates. *Nat. Protoc.* **2010**, *5*, 1096-1106.
3. Tabaei, S. R.; Ng, W. B.; Cho, S.-J.; Cho, N.-J., Controlling the formation of phospholipid monolayer, bilayer, and intact vesicle layer on graphene. *ACS Appl. Mater. Interf.* **2016**, *8* (18), 11875-11880.
4. Frost, R.; Jonsson, G. E.; Chakarov, D.; Svedhem, S.; Kasemo, B., Graphene oxide and lipid membranes: Interactions and nanocomposite structures. *Nano Lett.* **2012**, *12* (7), 3356-3362.
5. Melendrez, D.; Jowitt, T.; Iliut, M.; Verre, A. F.; Goodwin, S.; Vijayaraghavan, A., Adsorption and binding dynamics of graphene-supported phospholipid membranes using the qcm-d technique. *Nanoscale* **2018**, *10* (5), 2555-2567.
6. Li, X.; Zhu, Y.; Cai, W.; Borysiak, M.; Han, B.; Chen, D.; Piner, R. D.; Colombo, L.; Ruoff, R. S., Transfer of large-area graphene films for high-performance transparent conductive electrodes. *Nano Lett.* **2009**, *9* (12), 4359-4363.

Appendix V

Supporting Information to Chapter 6

V. Materials and Methods

Langmuir-Blodgett technique

The measurements were performed in a Minitrough 2, KSV Instruments using KSV Research Lab v2.01 software. 1,2-dipalmitoyl-*sn*-glycero-3-phosphocholine (DPPC) lipids (Avanti Polar Lipids Inc.) with a concentration of 1 mg/mL were prepared in $\text{CHCl}_3/\text{CH}_3\text{OH}$ 3:1 vol %. The lipid solution was deposited dropwise on an ammonium persulfate solution (APS, 0.5 mM) at 25 °C using a microliter syringe, and the solvent was allowed to evaporate for 15 min. The lipids were compressed until a surface pressure (π) of 50 mN/m. The isotherm (π -area) obtained was used to calculate the amount of lipids deposited on each Petri dish.

Graphene transfer

Six Petri dishes filled with APS were prepared prior to the experiments. Copper foils with chemical vapor deposition (CVD) graphene on copper (all with approximate size of $\sim 10 \times 10 \text{ mm}^2$) were placed on the surface of the etchant (Figure V.1). Immediately afterwards, the DPPC lipids were added to the air-etchant interface with different π (0 – 50 mN/m) in separate Petri dishes. After copper was etched, the graphene floating at the interface, was transferred to Si/SiO₂ substrates by gently placing the substrate in contact with graphene. APS residues remaining on the surface of graphene were rinsed with a continuous flow of ultrapure water. π below 10 mN/m was insufficient to prevent the lateral movements of the graphene or preserve its integrity during etching (see Figure V.1a and b). Instead, for $\pi \geq 30$ mN/m, the foil (graphene) remained immobilized. Higher π , fixed the foils in position throughout the etching. However, at the π of 40 mN/m the graphene sheet was slightly contracted probably due to the force induced by the lipids on the graphene edges. Importantly, we did not observe any remarkable contraction of graphene at 50 mN/m, which suggests that the lipids collapsed¹ (i.e. overlapped or sank) reducing the overall π .

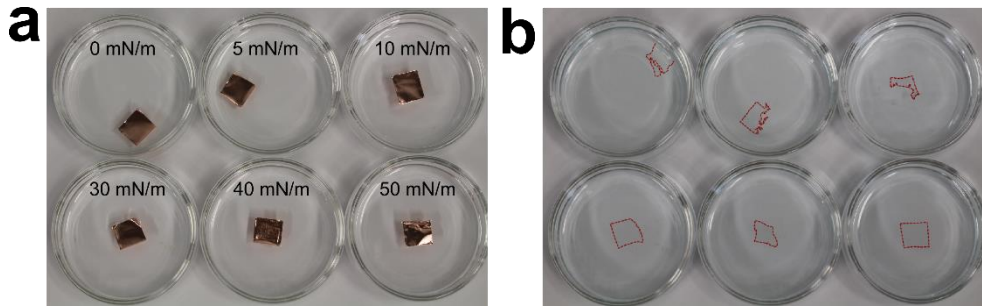


Figure V.1. a) Photographs of a sequence of six Petri dishes with CVD graphene on copper foil floating in ammonium persulfate solution (0.5M) with different surface pressure (0, 5, 10, 30, 40 and 50 mN/m): a) initial state; b) after the etching of the copper. The red dashed lines represent the area of graphene after the etching of the copper.

An alternative transfer approach was to dip the Si/SiO₂ substrate in the liquid etchant (Figure V.2a). After the etching of the copper, the APS was replaced by ultrapure water with a continuous flow of water in and APS out. Eventually, the surface of the water was lowered to gently position the graphene onto the substrate. This method also allowed the transfer of a continuous graphene sheet, as observed by the optical image micrograph in Figure V.2b.

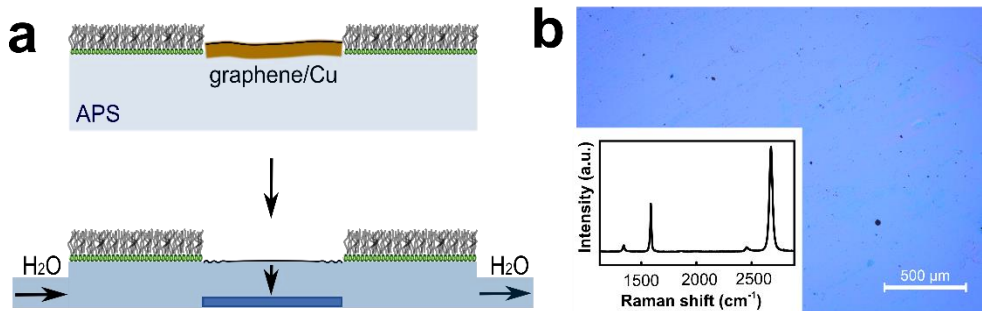


Figure V.2. a) Illustration of the molecular edge clamp concept with the substrate on the bottom of the Petri dish. b) Optical image of the transfer of graphene to a Si/SiO₂ substrate with a surface pressure of 30 mN/m. Inset: Raman spectrum of graphene transferred to a Si/SiO₂ substrate with a surface pressure of 30 mN/m.

Imaging set-up

Optical images were obtained with a Leica DM 2700 M microscope with a 5x objective. Fluorescence quenching microscopy was performed with a 20x objective mounted on an Axiovert 200 ZEISS inverted fluorescence microscope equipped with a monochrome AxioCam MRm ZEISS camera, to quantify the amount of cracks on graphene. To perform the measurement, the surface of graphene was spin-coated with poly(methyl methacrylate) (PMMA) layer pre-mixed with 2–6 μL solution of Rhodamine B, 4 mM (dissolved in acetone). The images were post processed according to the protocol published earlier² to estimate the surface rupture index (RI).

Infrared reflection absorption spectroscopy (IRRAS)

Spectra were collected with a BIO-RAD Excalibur Series infrared spectrometer in external reflectance mode. The chamber was continuously purged with dry air and a sample of plain Si/SiO₂ substrate was taken as reference. The angle of incidence was measured at 45° with a spectra range of 6000-400 cm^{-1} . Each spectrum was collected for an average of 128 scans with a resolution of 2 cm^{-1} .

Raman spectroscopy

Raman spectra were measured on a WiTec alpha 3000 confocal spectrometer with a 532 nm laser and a 100x objective. Each sample was measured at least on three different locations to obtain an average spectrum.

Atomic force microscopy (AFM)

AFM images were obtained with a JPK NanoWizard Ultra Speed instrument, and the images were processed with a JPK SPM Data Processing software. The experiments were performed using a silicon probe (AC160TS, Asylum Research) with 300 kHz nominal resonance frequency. The images were scanned in an intermittent contact mode at room temperature with 512x512 pixels.

References

1. Baoukina, S.; Monticelli, L.; Risselada, H. J.; Marrink, S. J.; Tieleman, D. P., The molecular mechanism of lipid monolayer collapse. *Proc. Natl. Acad. Sci.* **2008**, *105* (31), 10803-10808.
2. Arjmandi-Tash, H.; Jiang, L.; Schneider, G. F., Rupture index: A quantitative measure of sub-micrometer cracks in graphene. *Carbon* **2017**, *118*, 556-560.

Summary

In this PhD work, I investigated the interactions of lipid molecules with the basal plane and edges of graphene. As it is well known that the surface of graphene is hydrophobic, I studied whether lipids could form a stable layer on the graphene basal plane. Lipids are main constituents of cell membranes and thus – through hydrophobic interactions – I aimed to sandwich graphene directly in the hydrophobic core of a lipid bilayer, with the long term goal of developing a graphene-based sensor within a bilayer. In fact, the outstanding electrical properties of graphene allow to monitor subtle changes in the dielectric properties of the environment of graphene. However, a major challenge remain ways to integrate graphene within such a lipid bilayer.

Chapter 1 is a literature review on lipid interactions with graphene, graphene oxide and reduced graphene oxide. Surprisingly, at the start of my PhD study, there was no general consensus or trend in systematically understanding which were the driving forces yielding stable lipid-graphene assemblies. Surprisingly, the most basic characterization methods used to study lipids on surfaces (namely infrared spectroscopy, quartz crystal microbalance and ellipsometry) were not used to study lipid-graphene interactions.

In Chapter 2, the packing and organization of a lipid monolayer interacting with graphene was therefore investigated using infrared spectroscopy. For this, a lipid monolayer was transferred by the Langmuir-Blodgett technique on a Si/SiO₂ substrate. Remarkably, the lipid monolayer changed its conformation when graphene was placed on top, resulting in a more ordered, compact and well-organized structure. The lipid-graphene assembly also suppressed the Si/SiO₂ p-doping effect, reducing graphene hysteresis loop and the average charge neutrality point when a voltage was applied. The obtained superstructure – a lipid monolayer with hydrophilic heads facing the Si/SiO₂ substrate and tails facing the graphene monolayer transferred on top – increased our understanding of the interaction between lipids and graphene and paved the way towards a graphene sheet sandwiched within the core of a lipid bilayer.

In Chapter 3, graphene was encapsulated within the hydrophobic core of a lipid bilayer. The Langmuir-Schaefer method was used to transfer a second lipid

monolayer on top of graphene, thereby forming a lipid-graphene-lipid assembly which was characterized by infrared spectroscopy, ellipsometry and neutron reflectometry. The assembly showed to be a very stable and organized structure as compared to a single lipid bilayer. Surprisingly, the encapsulation of graphene within the lipid bilayer did not alter the intrinsic structure of the bilayer membrane.

In Chapter 4, the influence of temperature on the stability of lipid-graphene assemblies was investigated. The temperature-dependence on the lipid monolayer structure with and without graphene on top was studied by atomic force microscopy and infrared spectroscopy. This study revealed that a graphene monolayer deposited on top of the lipid constructs protects the lipids from the removal by solvents like chloroform or a surfactant solution (i.e. CTAB).

The properties of a lipid assembly on graphene depends on the number of unsaturated bonds, chain lengths, and charges. In Chapter 5, the assembly and structural organization of distinct lipids on different graphene materials was investigated by infrared spectroscopy and quartz crystal microbalance with dissipation monitoring. Here, zwitterionic, cationic and anionic lipids were deposited on graphene using the Langmuir-Schaefer and a vesicle fusion method. Depending on the substrate and the assembly method used, the resulted lipid layers adopted a distinct molecular structure. Infrared spectroscopy studies revealed that the saturated lipid DPPC exhibited higher molecular order than unsaturated lipids, both on a graphene-on-copper or a graphite substrate. The unsaturated DOTAP lipid carries a positive charge and a smaller head group and assembled into a more organized lipid structure as compared to the unsaturated zwitterionic DOPC and anionic DOPS lipids. Quartz crystal microbalance studies showed that with the vesicle fusion method, liposomes of zwitterionic unsaturated lipids yielded a lipid bilayer on graphene-on-SiO₂ and adsorbed without rupturing on graphene-on-gold. This suggests that the wetting transparency of graphene (*i.e.*, the substrate on which graphene is deposited on) plays an important role in governing the interaction of lipids (in the form of vesicles) with the graphene basal plane.

In Chapter 6, lipids were used as a flexible and molecular scaffold to clamp graphene at the edges while floating at the air-water interface, enabling the transfer of a continuous and clean graphene monolayer to a Si/SiO₂ substrate.

Langmuir films were deposited at the edges of graphene floating on an air-etchant interface, preventing the movement and cracking of graphene during all the etching and transfer procedures. This method yielded graphene without contaminants and is a step towards the fabrication of clean and therefore sensitive graphene based sensors.

In conclusion, this study provides new insights on the interactions between lipids and graphene. Lipids were assembled by Langmuir-Blodgett or by vesicle fusion and characterized by infrared spectroscopy, ellipsometry, neutron reflectivity, atomic force microscopy and quartz crystal microbalance. Additionally, lipids were introduced as a molecular-based scaffold yielding the controllable manipulation of graphene at the edges which could be used as an alternative clean graphene transfer method. Importantly, graphene demonstrated to be stable within the hydrophobic core of a lipid bilayer, i.e., not disturbing the intrinsic properties of the lipid bilayer. This result yields potential applications for designing well-defined interfaces for biosensing devices.

Samenvatting

Mijn promotieonderzoek is gericht op de interactie tussen lipiden met grafeen. Omdat bekend is dat het oppervlak van grafeen hydrofoob is, heb ik onderzocht of lipiden op gecontroleerde wijze een stabiele laag op het oppervlak van grafeen (*i.e.* basal plane) kunnen vormen. Lipiden zijn het hoofdbestanddeel van celmembranen en ik heb ernaar gestreefd om via hydrofobe interacties grafeen rechtstreeks in de hydrofobe kern van een lipide dubbellaag te incorporeren. Het doel van dit onderzoek was om in de toekomst grafeen te gebruiken als sensor binnen een lipide dubbellaag. De uitstekende elektrische eigenschappen van grafeen maken het mogelijk om elektrisch subtiele veranderingen in de diëlektrische eigenschappen van de omgeving van grafeen te meten. Tevens blijft het een grote uitdaging een methode te vinden om grafeen in een dergelijke dubbele lipidenlaag in te bouwen als onderdeel van een sensor.

Hoofdstuk 1 van dit proefschrift geeft een overzicht van de bestaande literatuur over de interactie tussen lipiden en grafeen, grafeenoxide en gereduceerd grafeenoxide. Verrassend genoeg was er aan het begin van dit promotieonderzoek geen consensus met betrekking tot de onderliggende krachten van stabiele lipide-grafeenassemblages. De meest gebruikelijke karakterisatiemethoden om lipiden op oppervlakken te bestuderen, zoals infraroodspectroscopie, kwartskristal microbalansmetingen en ellipsometrie, werden eerder niet toegepast voor het bestuderen van lipide-grafeen interacties.

Daarom werd in hoofdstuk 2 de pakking en de organisatie van een lipide-monolaag in interactie met grafeen met behulp van infrarood spectroscopie bestudeerd. Hiervoor werd een Langmuir-Blodgett lipide monolaag op een Si/SiO₂-substraat aangebracht. Opmerkelijk was dat de conformatie in de lipide monolaag veranderde in de aanwezigheid van grafeen bovenop de monolaag, met als resultaat een meer geordende, compacte en goed georganiseerde structuur. De gevormde grafeen-lipide monolaag assemblage verminderde ook het Si/SiO₂-p-doteringseffect. Hierdoor werd de hystereselus van grafeen en het gemiddelde neutraliteitspunt van de lading verminderd wanneer een spanning werd aangelegd. De gebruikte superstructuur, een lipide monolaag met hydrofiele kopgroepen in contact met het Si/SiO₂-substraat en de acyl ketens in contact met

de grafeen monolaag, resulteerde in een beter inzicht over de interactie tussen lipide monolagen en grafeen.

Voortbouwend op dit inzicht werd in hoofdstuk 3 onderzocht of grafeen in de hydrofobe kern van een lipide dubbellaag kon worden ingebouwd. De Langmuir-Schäfer-methode werd toegepast om een tweede lipide monolaag bovenop grafeen aan te brengen, resulterend in een lipide-grafeen-lipide-sandwich. De constructie werd gekarakteriseerd met behulp van infraroodspectroscopie, ellipsometrie en neutronenreflectometrie. De assemblage heeft een zeer stabiele en georganiseerde structuur in vergelijking met een enkele lipide dubbellaag. Opvallend genoeg veranderde de introductie van grafeen in een lipide dubbellaag niet de intrinsieke structuur van de dubbellaag.

Hoofdstuk 4 beschrijft het onderzoek naar de invloed van temperatuur op de stabiliteit van lipide-grafeenassemblages. De temperatuurafhankelijkheid van de lipide monolaagstructuur met en zonder grafeen aan de bovenzijde werd bestudeerd met atoomkrachtmicroscopie en infraroodspectroscopie. Hieruit bleek dat grafeen gepositioneerd op een lipide monolaag, de lipiden beschermt tegen oplosmiddelen zoals chloroform en een waterige surfactantenoplossing.

Zelfassemblage van lipiden op grafeen is afhankelijk van de lipide structuur, zoals bijvoorbeeld lading, ketenlengte en verzadiging. Hoofdstuk 5 beschrijft het onderzoek naar de assemblage en structurele organisatie van verschillende lipiden op verschillende grafeenmaterialen door middel van infraroodspectroscopie en kwartskristal microbalansmetingen. Zwitterionische, kationische en anionische lipide monolagen op grafeen werden gemaakt met de Langmuir-Schäfer en vesikelfusie methode. Afhankelijk van het substraat en de gebruikte assemblagemethode, lieten lipiden verschillende moleculaire structuren zien. De infraroodspectroscopiestudie toonde aan dat een monolaag van de verzadigde lipide DPPC een hogere moleculaire orde bezit in vergelijking met onverzadigde lipiden. Vanwege de positieve lading en de kleinere kopgroep, gaf het onverzadigde DOTAP een meer georganiseerde lipidestructuur. Uit de kwartskristal microbalansstudies bleek dat de vesikelfusie methode, met zwitterionische onverzadigde vesikels een lipide dubbellaag opleverde op grafeen-op-SiO₂ en op grafeen-op-goud substraten. Dit resultaat suggereert dat de

zogenaamde “*wetting transparency*” van grafeen een belangrijke rol speelt bij de interactie van lipiden met grafeen.

In hoofdstuk 6 werden lipide monolagen gebruikt om grafeen op het grensvlak van water en lucht in te klemmen, waardoor de overdracht van een continue en schone grafeenmonolaag op een Si/SiO₂-substraat mogelijk was. De lipide monolaag op dit grensvlak voorkomt beweging en scheuren van grafeen tijdens het etsen van het kopersubstraat en het transport op het Si/SiO₂-substraat. Deze methode resulteerde in grafeen zonder verontreinigingen op Si/SiO₂, welke een cruciale stap is voor de fabricage van schone (en dus gevoelige) grafeen sensoren in de toekomst.

Samenvattend, dit proefschrift biedt nieuwe inzichten in de interacties tussen lipiden en grafeen. Lipiden werden geassembleerd door Langmuir-Blodgett of door vesikelfusie methodes en gekarakteriseerd met behulp van infrarood spectroscopie, ellipsometrie, neutronenreflectie, atoomkrachtmicroscopie en kwartskristal microbalans. Daarnaast werden lipiden geïntroduceerd als een scaffold die manipulatie van grafeen op het water-luchtgrensvlak mogelijk maakt, resulterend in een alternatieve schone grafeenoverdrachtsmethode. Een belangrijke conclusie van dit onderzoek is dat grafeen binnen de hydrofobe kern van een lipidedubbellaag stabiel bleek te zijn en dat de intrinsieke eigenschappen van de lipidedubbellaag niet verstoord werd. Dit resultaat maakt potentiële toepassingen mogelijk voor het ontwerpen van goed gedefinieerde interfaces voor biosensoren gebaseerd op grafeen.

Curriculum Vitae

Lia Macedo Coelho Lima was born in Manchester, United Kingdom on June 2nd 1987. She graduated from a high school in Braga, Portugal in 2005 and enrolled in a bachelor degree in Chemistry at the Faculty of Science of the University of Porto. During her studies, she was admitted to the Erasmus Exchange Bachelor Program in Turin, Italy at the Università degli Studi di Torino for six months. She graduated in 2009 after a research internship about studies of films deposition containing nanoparticles.

Lia continued her studies with a master degree in Chemistry at the Faculty of Science of the University of Porto. She spent her Erasmus Exchange Master Program in Barcelona, Spain at the Institute of Bioengineering of Catalonia, Nanoprobes and Nanoswitches group. During this one year program, Lia completed her final master research internship. Graduating at the end of 2011 in Chemistry, her master project was published as first author in 2013 with the title: *“Morphological and nanomechanical behavior of supported lipid bilayers on addition of cationic surfactants”*.

After working in business development for a short time (2012-2014), she started her PhD research in 2014 at the Leiden Institute of Chemistry (Leiden University) in the research group of Dr. Grégory F. Schneider, department of Supramolecular and Biomaterials Chemistry. During her PhD studies, she collaborated with several research groups in Leiden (Prof. dr. Alexander Kros, the Leiden Institute of Physics, particularly for the atomic force microscopy facilities with Dr. Federica Galli), in Strasbourg with Prof. dr. Thierry Charitat and, in Grenoble with Prof. dr. Giovanna Fragneto for the Neutron reflectometry experiments. She supervised several bachelor students and first year practical courses. She participated in a number of conferences as a speaker (e.g., CHAINS 2016, Veldhoven, The Netherlands), and by presenting a poster (e.g., CHAINS 2015, 2016, 2017, and Chem2DMat 2017, Strasbourg, France). At this last conference, Lia was awarded with a poster prize.

List of publications

- 1. Sensing at the surface of graphene field-effect transistors.**
Wangyang Fu, Lin Jiang, Erik P. van Geest, [Lia M. C. Lima](#), Grégory F. Schneider. *Advanced Materials*, 2017, 29, 1603610.
- 2. Graphene-stabilized lipid monolayer heterostructures: a novel biomembrane superstructure.**
[Lia M. C. Lima](#), Wangyang Fu, Lin Jiang, Alexander Kros, Grégory F. Schneider. *Nanoscale*, 2016, 8, 18646.
- 3. Encapsulation of graphene in the hydrophobic core of a lipid bilayer.**
[Lia M. C. Lima](#), Liubov A. Belyaeva, Hadi Arjmandi-Tash, Tetiana Mukhina, Giovanna Fragneto, Alexander Kros, Thierry Charitat, Grégory F. Schneider. In preparation.
- 4. Effect of temperature on the structure of lipids in the presence of graphene.**
[Lia M. C. Lima](#), Hadi Arjmandi-Tash, Grégory F. Schneider. In preparation.
- 5. Assembly and structural characterization of lipids on graphite and on graphene.**
[Lia M. C. Lima](#), Xiaoyang Zhang, Grégory F. Schneider. In preparation.
- 6. Lateral non-covalent clamping of graphene at the edge using a lipid scaffold.**
[Lia M. C. Lima](#), Hadi Arjmandi-Tash, Grégory F. Schneider. *ACS Applied Materials & Interfaces*, 2018, 10 (13), 11328-11332.
- 7. Biaxial compression of centimeter-scale graphene.**
Hadi Arjmandi-Tash, Hessam Sokooti, Khosrow Shakouri, Lin Jiang, Alexander Kloosterman, Marius Staring, [Lia M. C. Lima](#), Grégory F. Schneider. Submitted.
- 8. Contact angle measurement of free-standing square-millimeter single-layer graphene.**
Ana V. Prydatko, Liubov A. Belyaeva, Lin Jiang, [Lia M. C. Lima](#), Grégory F. Schneider. *Nature Communications*, 2018, 9, 4185.

9. **Ultrasensitive ethene detector based on a graphene–copper(I) hybrid material.**

Wangyang Fu, Thomas F. van Dijkman, Lia M. C. Lima, Feng Jiang, Grégory F. Schneider, Elisabeth Bouwman. *Nano Letters*, 2017, 17 (12), 7980-7988.

10. **Morphological and nanomechanical behavior of supported lipid bilayers on addition of cationic surfactants.**

Lia M. C. Lima, Marina I. Giannotti, Lorena Redondo-Morata, M. Luísa C. Vale, Eduardo F. Marques, Fausto Sanz. *Langmuir*, 2013, 29 (30), 9352-9361.